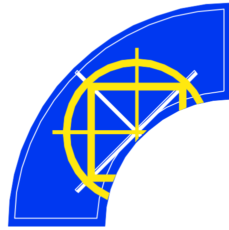

TEKNISKA HÖGSKOLAN

HÖGSKOLAN I JÖNKÖPING

WET ETCHING OF OPTICAL THIN FILMS

Curt Edström

THESIS WORK 2010

CHEMICAL ENGINEERING

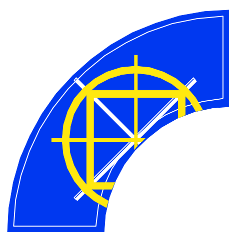

TEKNISKA HÖGSKOLAN
HÖGSKOLAN I JÖNKÖPING

WET ETCHING OF OPTICAL THIN FILMS

Curt Edström

This thesis work is performed at Jönköping Institute of Technology within the subject area Chemistry. The author is responsible for the given opinions, conclusions and results.

Supervisors: Peter Leisner and Maarten Rymenans
Examiner: Bo Nordström

Credit points: 30 hp

Date: 101203

Postal Address:	Visiting Address:	Telephone:
Box 1026	Gjuterigatan 5	036-10 10 00
551 11 Jönköping		

Abstract

Evaluation of the wet etching properties of several different thin film oxides grown by physical vapour deposition was performed in this work. MgO, Al_2O_3, SiO_2, TiO_2, HfO_2 ZrO_2 and Y_2O_3 were coated on two types of substrates; Si and borosilicate glass and etching tests were performed in different etching solutions. MgF_2 thin films have also been evaluated.

Important aspects of the choice of the thin films was taken into account in order to match to good optical properties such as refractive index (n), extinction coefficient (k) and optical thickness (T_P) as well as good chemical properties in the wet etching process.

A description is made of the physics of optical filters and how a combination of different oxides stacked onto each other can create interference filters.

A description of the manufacturing process of the thin films where physical vapour deposition (PVD) was used is presented.

Thermal shift of the optical spectra caused by porous coatings was investigated and analyses of the thin films by ellipsometry, surface profilometry and transmission spectrophotometry have been performed.

The wet etching properties were evaluated by monitoring the transmission in-situ on transparent borosilicate glass substrates. A method of how to measure the wet etching rate for different thin films is described.

A computer software was used to calculate the Pourbaix diagrams in order to understand the chemical behaviour of the etching solutions. The pH can have a significant impact on the etching behaviour.

In case of TiO_2, it can be dissolved in an alkaline solution of H_2O_2. The catalytically process behind this is evaluated. Etching rate for both Y_2O_3 and SiO_2 were matched by adjusting the etchant concentration as a case example.

The group IVB oxides are difficult to etch. The catalytic etching of TiO_2 with peroxide is slow but detectable. Al_2O_3, Y_2O_3 and MgO are reasonably easy to etch but have too low refractive indices to be useful in multilayer optical filters.

The In-situ etching instrument was found to be very useful for measuring etching rates.

Sammanfattning

Utvärdering av våtkemiska egenskaper för flera olika oxidtunnfilmer utfördes i detta arbete på tunnfilmer av MgO, Al_2O_3, SiO_2, TiO_2, HfO_2 ZrO_2 and Y_2O_3 vakuumdeponerade på både kiselwafers och borosilikatglas. Etstester gjordes med ett flertal etslösningar. Även MgF_2-tunnfilmer utvärderades .

Både optiska och kemiska egenskaper togs i beaktande vid utvärderingen av tunnfilmerna. De optiska lagar som gäller för tunnfilmer redovisas, bl a hur kombinationer av olika oxider kan skapa interferrensfilter.

En beskrivning av tillverkningsprocessen varvid PVD användes presenteras.

Termiskt skift av det optiska transmissionsspektrat orsakat av porositet undersöktes. Analyser av tunnfilmerna med ellipsometri, profilometri och transmissions spektroskopi utfördes.

Våtetsningsegenskaperna utvärderades genom att mäta in-situ vid etsprocessen på transparenta borosilikatglassubstrat. Metoden för att mäta etshastigheten för olika oxider är beskriven.

Datorberäkningar av pourbaixdiagram användes för att skapa en förståelse av de kemiska egenskaperna för etslösningarna.Etsegenskaperna påverkas till stor del av lösningens pH.

TiO_2 kan etsas i basisk lösning av peroxid. Denna process utvärderades, likaså utvärderades etshasigheten för Y_2O_3 och SiO_2 för att erhålla matchande par av oxider som en fallstudie.

Grupp IVB oxiderna är mycket svåra att etsa. Katalytisk etsning av TiO_2 med peroxid är detekterbar men långsam. Al_2O_3, Y_2O_3 and MgO är förhållandevis enkla att etsa men har för låga brytningsindex för att var praktiskt använbara i optiska multilagerfilter.

In-situ etsinstrumentet befanns vara ett utmärkt verktyg för att mäta etshastigheten för tunnfilmer.

Key Words

Thin film

Wet etching

Optical coating

Physical vapour deposition

Primary goals

- To evaluate the etching properties of the selected oxides
- To find a replacement for TiO_2 in etchable multilayer filters
- To find matching etching rate for the system Y_2O_3/SiO_2 as a case example

Abbreviations

PVD Physical Vapour Deposition

CVD Chemical Vapour Deposition

MOCVD Metal Organic Chemical Vapour Deposition

IBAD Ion Beam Assisted Deposition

RIE Reactive Ion Etching

Table of Contents

1 Introduction 6
1.1 BACKGROUND 6
1.2 DELIMITS 6
2 Theoretical background 7
2.1 OPTICAL FILTERS 7
2.1.1 *Absorption filters* 7
2.1.2 *Filters based on interference* 7
2.1.3 *Colour interference filters* 11
2.1.4 *Filter thickness* 12
2.1.5 *Computer simulations* 12
2.2 THIN FILM PROCESSES 13
2.2.1 *Sol-gel* 13
2.2.2 *Chemical vapour deposition* 13
2.2.3 *Physical vapour deposition* 13
2.2.4 *Thin film growth and nucleation* 17
2.3 LITHOGRAPHY 19
2.3.1 *Photoresist* 20
2.3.2 *Exposure* 23
2.3.3 *Developer* 24
2.3.4 *Etching methods* 24
2.4 WET ETCHING CHEMISTRY 27
2.4.1 *Acid etching* 28
2.4.2 *HF-etching* 28
2.4.3 *Alkaline etching* 29
2.4.4 *Catalytic etching of* TiO_2 29
2.4.5 *Redox etching* 30
2.4.6 *Photochemical etching* 30
2.4.7 *Electrochemical etching* 30
2.5 ETCHING ANISOTROPY 31
2.6 POURBAIX DIAGRAMS, PH AND REDOX ENVIRONMENT 32
2.6.1 *Nernst relation* 32
2.6.2 *Case example manganese system* 33
2.6.3 *Pourbaix simulations* 34
2.7 ETCHING RATE DETERMINATION 34
2.7.2 *Tolansky method* 35
2.7.3 *Stylus profilometry* 35
2.7.4 *Optical in-situ etching rate measurement* 35
2.8 THERMAL SHIFT 36
2.9 THIN FILM STRESS 37
2.10 OPTICAL CHARACTERISATION OF THE THIN FILMS 37
2.10.1 *Ellipsometry* 38
2.10.2 *Optical spectroscopy* 38
2.11 THE SELECTION OF DIELECTRICS 38
2.11.1 *MgO* 40
2.11.2 Al_2O_3 41
2.11.3 TiO_2 42
2.11.4 ZrO_2 43
2.11.5 HfO_2 45
2.11.6 Y_2O_3 46
2.11.7 SiO_2 47

2.11.8 MgF_2 ... 48

3 Experiment ... 49

3.1 PRODUCTION OF THE THIN FILMS ... 49
3.2 PHYSICAL CHARACTERIZATION OF THE THIN FILMS ... 50
3.2.1 Ellipsometric measurements ... 50
3.2.2 Transmission spectra ... 50
3.2.3 Surface profilometry ... 51
3.2.4 Thin film stress ... 51
3.2.5 Thermal shift ... 51
3.3 THE IN-SITU ETCHING INSTRUMENT ... 53
3.4 ETCHING TESTS ... 54
3.4.1 Etching tests of multilayer coatings ... 54
3.4.2 Etching test of single layer oxides ... 54
3.5 ETCH MATCHING OF Y_2O_3/SiO_2 ... 58
3.6 ETCHING RATE OF PHOTORESIST ... 58

4 Results and discussion ... 59

4.1 CHARACTERISATION OF THE THIN FILMS ... 59
4.1.1 Ellipsometric measurements ... 59
4.1.2 Transmission spectral fitting ... 59
4.1.3 Surface profilometry ... 60
4.1.4 Thin film stress ... 60
4.1.5 Thermal shift ... 61
4.2 ETCH TESTS ... 63
4.2.1 HF etching of M225-M325 magenta filters ... 63
4.2.2 In-situ etching measurements of the N250 magenta filter ... 64
4.2.3 Single oxides etching results ... 67
4.2.4 Etch matching of Y_2O_3/SiO_2 ... 73
4.2.5 Photoresist etching ... 74

5 Conclusion ... 76

6 References ... 78

7 Attachments ... 83

7.1 EVAPORATION PROPERTIES ... 83
7.2 CURVE MATCHING OF THIN FILMS ... 83
7.3 SOLUTIONS ... 88

1 Introduction

In some cases, there is a need to make lithographic patterns on optical coatings and filters. The use of this lithography is mainly for projecting images in the lighting business. There are also other uses for patterned devices with coatings for optical instruments and detectors. A convenient method to manufacture these components is by wet etching of thin films patterned by photoresist. In this report, investigations have been performed on how the different chemical solutions can etch different oxides.

1.1 Background

Drix Semiconductor is a Belgian semiconductor manufacturer who has recently started the production of an optical interference filter based on PVD. The major use for this type of optical filter is for projecting patterns in the lighting industry. In order to make this lithography a wet etching process with photoresist is involved.

Today etchings are performed by using a HF solution on SiO_2/TiO_2 multilayer stacks. This is not a good situation because of huge differences in etching rate between the oxides which results in a very bad anisotropic etch profile. It is acceptable in most cases but there is an undercutting of the etching profile which could be minimized if it was possible to find an etching agent which etches at the same rate on SiO_2 as on TiO_2.

The purpose of this thesis was to find a combination of thin films which gives a uniform etching rate in a multilayer filter, and to find a proper etchant composition. One major problem is the difficulty to etch TiO_2 and one effort was to find a substitute oxide with as high reflective index as TiO_2 has. A second issue was to study the selected oxides which are of interest in different filter designs.

There are several parameters to take into account when selecting an oxide; not only the chemical behaviour but also its optical properties are of importance.

1.2 Delimits

The morphology of the thin film was not investigated. Only estimates of the optimum coating process parameters were made in order to manufacture the coating. Some interesting oxides such as Nb_2O_5 and Ta_2O_5 were not investigated.

All etchings on the coatings were done without any photoresist or with the photoresist completely removed in order to get etching over the whole surface for easy measurements. The change of etching properties caused by patterning was not included in this investigation.

2 Theoretical background

2.1 Optical filters

In order to understand the complex questions involved in this thesis it is important to first describe the basic principles of how optical filters work.

In order make a colour filter there are two major roadmaps. The first way is to utilize the absorption of organic dyes. The other way is to take advantage of the interference of light.

2.1.1 Absorption filters

Absorption filters have the disadvantage that they can not withstand much heat. By illuminating them, the temperature will rise and this might cause problems. They are often made of organic dyes or different coloured compounds mixed in the glass which is vulnerable to high temperatures. The major advantages for absorptive filters are that they are very economic and easy to manufacture in large quantities. They are often made by coating a substrate of polymers such as polyester, polycarbonate or similar with dye. They can also be made by dissolving the dye into the substrate itself. Colour CCDs usually contain a patterned dye colour filter made of different dyes in front of the CCD detector, so called Bayer patterns [1].

2.1.2 Filters based on interference

These types of filters are sometimes called dichroic or dielectric filters. They could also be referred to as thin-film optical filters. Sometimes these can contain thin metal layers which cause absorption, but in normal cases this type of filter consists of pure dielectric compounds with none or very little absorption. The definition of dielectric materials is that they are electrical insulators and can be polarized when exposed to an electrical field. For optical interference filters, the most interesting material property is the refractive index. The most frequently used materials are metal oxides, but sulfides and sometimes nitrides can also be used. Polymers could be used in interference filters but due to their instability at high temperature, they are never used in multilayer coatings.

Three major properties can completely explain the optical behaviour of a thin film coating. These are:

- **thickness of the layer, t**

- **absorption coefficient, k**
- **refractive index, n**

The polarization of light will not be affected by the thin film if the incident angle is 90°. In case where there is no absorption a coating will then satisfy:

$$\mathbf{I=R+T} \qquad \mathbf{(2.2)}$$

Where I is the intensity of the incident beam, R is the intensity of the reflected beam and T is the intensity of the transmitted beam.

There is always dispersion in the material therefore n and k will be functions of the wavelength **λ, n(λ) k(λ),** but we neglect this in the following discussion.

In order to understand the functions of these filters, several equations can be derived from Maxwell's wave equation where the propagation and phase of a light beam change at an interface between two materials [2, 3]. It can be shown by the treatment of this wave equation that the reflectance on a single surface depends on the difference of refractive index between the two materials making the interface.

Snell's law which is derived from Maxwell:

$$\mathbf{n_1 \sin \theta_1 = n_2 \sin \theta_2} \qquad \mathbf{(2.3)}$$

gives the relationship between incident angle of the light beam and the angle after passing the surface, as shown in Figure 1. At this stage, there is still no coating at all, only the front surface of the substrate and air make an interface.

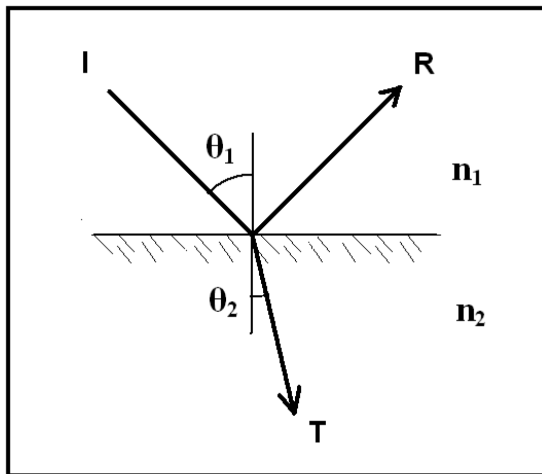

Figure 1. *Single surface reflectance following Snell's law.*

By inserting this in the Fresnel equation:

$$\mathbf{R=((\sin(\theta_1-\theta_2)/(\sin(\theta_1+\theta_2))^2} \quad \mathbf{(2.4)}$$

where R is the reflection coefficient of the incident light gives:

$$\mathbf{R=(((n_1-n_2)/((n_1+n_2))^2} \quad \mathbf{(2.5)}$$

which is valid for the case of a perpendicular angle of incidence with no polarization and no absorption. In equation (2.5) it is easy to see that the reflectance increases when the difference between n_1 and n_2 is increased (n_2-n_1). This is important in order to understand why it is often interesting to make filters using material with a difference in refractive index as high as possible. This explains why the combination of TiO_2-SiO_2 in multilayer filters is so popular where TiO_2 has an index of 2.35 and SiO_2 has an index of 1.46 in the visible spectrum.

One naked glass surface acting as a single interface is not enough to change the light spectra to make a useful filter. For example if n_2=2.35 and n_1=1.46 are inserted in equation 2.5, this will give a reflectance of 38%. In most cases, filters are needed to block light much more efficiently. In many cases blocking must be in the order of 99% or even more to achieve efficient filters. One way to solve this is by adding several interfaces. Since the reflectance is always caused by the interface of two surfaces, the only way to create several surfaces is to make a multilayer stack where every second layer is made of a high index material and each subsequent layer is made of a low index material.

Single layer coatings

In this case the important interference of light comes into place. In order to understand this one can imagine the simplest type of filters: a single coating consisting of two surfaces as shown in Figure 2. In a single layer coating there is reflection from both surfaces. They will not only reflect light, but they will also interfere with each other. By controlling the thickness of the layer, it is possible to adjust the phase difference between the two reflections so they are completely in phase and contribute to each other. This will happen when the layer has an optical thickness of exactly to ¼ of a wavelength. It is called constructive interference.

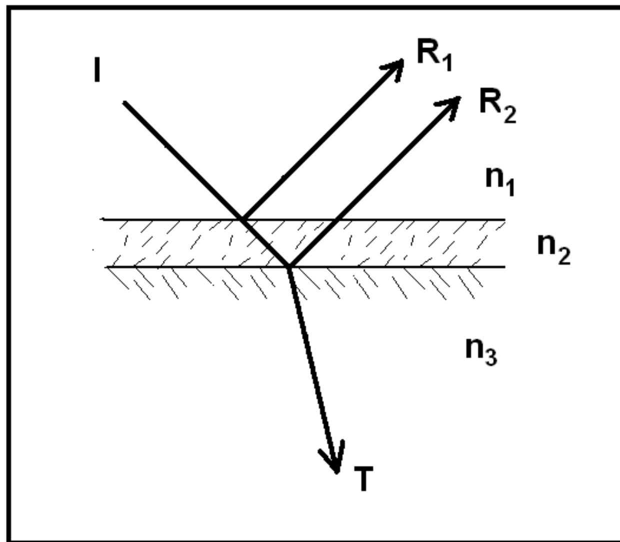

Figure 2. *Reflection of light R_1 an R_2 will interfere with each other and change the proportion of transmitted versus reflected light. If R_1 and R_2 are equal and 180° out of phase they will cancel each other out completely. This happens in a single layer anti-reflective coating where the refractive index of n_2 is equal to $\sqrt{n_3}$, if n_1=1.*

First one must consider that the speed of light is inversely proportional to the refractive index, a higher index will slow down the light:

$$\nu = c/n \quad (2.6)$$

where ν is the speed of light inside the medium. This relates directly to the thickness:

$$T_p = T_o\, n \quad (2.7)$$

It is important to distinguish between the physical thickness T_p of a thin film and the optical thickness T_o. According to equation (2.7) it is also proportional to the refractive index.

The phase of light will change 180° when reflection is caused by the surface interface changing from high index to low index. This explains why a stack of a ¼ wave thickness for each layer will interfere positive to the reflection. The path way will be ½ waves and the phase shift will cause another ½ creating a full wave shift for ¼ wave thickness.

It is rather complex and not simple to show how this is derived by Maxwell's wave equation and it is beyond the scope of this thesis. For further reading, reference [2] is recommended.

Multi layer coatings

By adding several surfaces one can multiply the power of a filter and achieve a very high reflectance. In most cases a filter will be made of 16-30 layers of alternating high index and low index material. The filter will not only cause high reflectance at the design wavelength, it will also transmit light at an offset of the design wavelength where the light reflections no longer are in phase with each other. This is of great benefit when a band pass filter is designed. Cyan, magenta and yellow filters are typical filters where some wavelengths are passing through and others are blocked. The desired spectral response is achieved by a multi layer design.

It is also possible to change the behaviour of transmittance as a function of the wavelength in almost any possible way by changing or combining the thickness and refractive index of each layer in a multilayer stack. This is a science of its own, and by combining different high and low index materials it is possible to create antireflection coatings, band pass-, notch-, high pass-, rugate- , heat- and cold- filters and much more.

2.1.3 Colour interference filters

In the following discussions the filters are assumed to be of a multilayer thin film interference type, deposited on a thick (0.1-1mm) substrate, usually made of borosilicate glass.

The most common types are cyan, magenta and yellow filters shown in Figure 3. These are subtractive colours used in all types of printing and lithography [4]. They are often made of 16-18 layers of TiO_2/SiO_2. The inverted colours (and the complementary part) are the additive colours red, green and blue. These colours are used in all types of video projectors and displays. All red, green, and blue filters are somewhat more complex and demand more layers in order to block enough of the light.

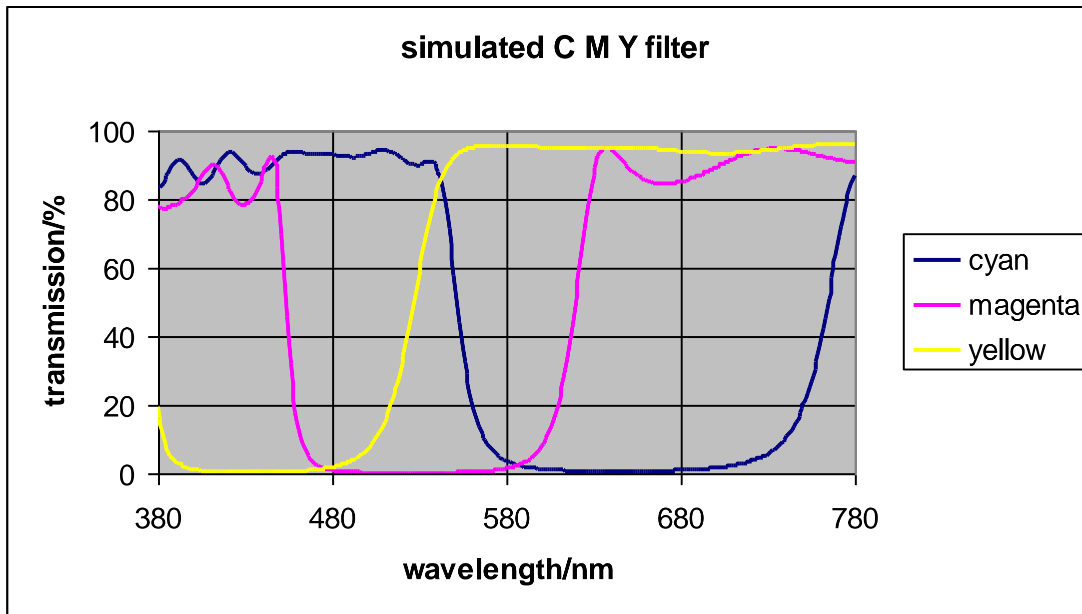

Figure 3. *Simulation of three typical filters, complementary cyan, magenta and yellow, created by a stack of 16 alternating TiO_2 and SiO_2 thin films. Each layer is ¼ of a wavelength thick [5]. This simulation was done using TFCalc software.*

2.1.4 Filter thickness

The physical thickness range for a single quarter wave layer will be in the order of 80 nm depending on the actual wavelength and index, therefore a complete filter will have a thickness of about 1 µm. A yellow filter will be slightly thinner because it is designed to reflect blue light which has a shorter wavelength compared to a cyan filter which is designed to reflect red which has a longer wavelength.

2.1.5 Computer simulations

In reality it is to difficult and time consuming to design and simulate thin film stacks manually. This is why a computer simulation is mandatory. In this thesis TFCalc from Software Spectra, Inc. was extensively used as a tool to simulate the transmission change under the influence of the etching.

A number of parameters can be set in this software such as refractive index, thickness and absorption of each layer, also as a function of wavelength (dispersion). These simulations can be matched to fit the measured thin film filter. There are other parameters as well - polarisation and incident angle - but they are not used in the calculations of these cases, since the angle incidence is perpendicular to the substrate.

2.2 Thin film processes

There is a wide variety of methods to manufacture thin films in the thickness range of 0.05-5 μm. In this thesis only physical vapour deposition (PVD) with electron beam evaporation was used (see chapter 2.2.3.3) but other methods are briefly described below.

2.2.1 Sol-gel

Sol-gel is a wet chemical method where a thin liquid gel is applied on a surface and then solidified by a thermal process [6]. This wet chemical process is not common for the production of optical filters, but there are some interests in this area [7, 8]. The most limiting issue is that each substrate has to be processed individually, which makes the production inefficient.

2.2.2 Chemical vapour deposition

Chemical vapour deposition, (CVD) is a very frequently used method for the production of coatings in the semiconductor industry [9]. Different gas compounds inserted in a reactor tank under low pressure and sometimes in presence of electric field will cause chemical reactions that will grow a desired thin film on a substrate. Semiconducting materials, oxides and nitrides can be deposited. The reaction product is deposited on a selected substrate and very pure and crystalline coatings are possible. This method is not used for production of interference filters because of limitations in the reaction products which can be made.

One very interesting thin film type is the growth of diamond like coatings which is possible at a substantial rate and thickness for protection of optics [10].

2.2.3 Physical vapour deposition

The overwhelmingly most common process in order to produce interference filters is by Physical Vapour Deposition (PVD). This is a general term which involves all types of processes in vacuum where the source material is vaporized and transported by thermal motion to a substrate where it will condense in solid phase. The process is performed under high vacuum and the mean free path for the vaporized particle is longer than the distance between the source and the substrate [11]. This means that the vaporized particle will not collide with any gas particle before it hits the substrate surface where it condensates.

The mean free path *l* can be described as:

$$\ell = \frac{k_{\mathrm{B}}T}{\sqrt{2}\pi d^2 p} \quad \textbf{(2.8)}$$

where k is Boltzmann's constant, T is the temperature, d is the molecule diameter and p is the pressure.

For room temperature the mean free path of air is 5 meters at 10^{-5} Torr. This is a quite common process pressure.

The substrate temperature has to be low enough otherwise the deposited material will re-evaporate. This is usually called the sticking coefficient [12]. Under most process conditions this is of little concern since a common process temperature of the substrate is in the 25-400 °C range and most oxides have a melting point far beyond this temperature. There are however some materials such as ZnS which have a low sticking coefficient [13]. It can bounce off the substrate surface even if the melting point is much higher than the surface temperature. It can be explained by the fact that there is a short time where the particle behaves as an ad-atom or ad-particle and has not had time to bond to the substrate. It takes a short time before the particle settles down. Therefore it can re-evaporate from the thermodynamically unfavourable state as an ad-atom. This sticking coefficient is possible to detect even for SiO_2 and TiO_2 on cold substrates, especially in the beginning of the deposition when the coating material sticks to the substrate and not to its own particles.

PVD can be divided into several sub groups and variations such as sputtering, laser ablation, thermal evaporation and electron-beam deposition and a few other more or less exotic methods. The difference between them is the way the source material is vaporized and how it condenses.

2.2.3.1 Sputtering

By ionizing an inert gas and accelerating the ions towards a solid surface or target, it can knock off particles; this is called sputtering. This is done from a solid phase directly into the gas phase like sublimation. The particles will condensate on a closely placed substrate. Energizing can be done by having a slight amount of background gas in the range of 1-10 mTorr where plasma is created by an electric field in the range of 100-400 volts. More efficient sputtering is achieved by applying a magnetic field which traps electrons in the plasma so more argon atoms are ionized and accelerated towards the target.

It is possible to insert a small amount of oxygen in the process. This leads to oxidation of the deposited thin film. Other process gases can also be added to give other compounds for example nitrides.

In DC-magnetron sputtering it is only possible to sputter metals or conductive materials such as aluminium or titanium. Added oxygen will result in metal oxide thin films.

By using a RF-magnetron it is possible to directly sputter dielectric compounds, however this process is rather difficult to master.

There are several variations to sputtering but it is difficult to control the process and achieve uniform coatings. This is why this method seldom is used for filter production. However, very dense and hard coatings are possible.

2.2.3.2 Thermal evaporation

This is the simplest type of evaporation and has been used in the industry since the '30s. The first important application was antireflective coatings where MgF_2 was extensively used since it is easy evaporated. Development of optical instruments for military application was a driving force. The evaporation is done by simply feeding electric current through a source in the shape of a boat made out of metal. Normally this source is made of tungsten, molybdenum or tantalum. There are some limitations; only a few types of dielectric materials can be evaporated, for example MgF_2, SiO, ZnS and the boats are outworn after a few evaporations. It is not possible to evaporate SiO_2 and TiO_2 because of the high melting point of these oxides. However, this method is very simple and reliable [14].

2.2.3.3 Electron beam evaporation

In most cases e-beam deposition is the preferred way to manufacture optical filters, and this thesis is aimed at thin films made by electron beam deposition [15].

An e-beam based system consists of a vacuum chamber and a source which can be heated by a powerful electron gun. Usually the acceleration voltage is in the range of 5-10 kV. By cooling the crucible with water it is possible to heat all types of material until it evaporates. Even difficult materials such as tungsten and carbon can be evaporated, although this demands temperatures in the range of 3000 °C or more. This can be done due to the fact that the e-gun has no thermal limit. The only limit is the way the source is placed and cooled.

The electron beam source is based on the same principle as the e-gun in a cathode ray tube. A glowing tungsten filament is emitting electrons which are accelerated by an electric field. The current can be up to 1 ampere. When these energized electrons impact a target they lose their kinetic energy and because of the high current density it is possible to focus large quantity of energy in a small area. By efficient water cooling of the crucible only the source material will melt and not the crucible itself. If there was no water cooling the crucible would be evaporated, contaminating the coating. By bending the electron beam in a magnet field, usually in a 270° trajectory, tungsten contamination can be avoided since tungsten particles will not be bended by the magnetic field due to their heavy mass. This makes e-beam evaporation a very clean method and high purity coatings are possible.

The source material SiO_2, TiO_2 or other compounds in Figure 4 are bombarded by electrons (j) from the e-gun (b). When it has melted and there is enough vapour pressure it will evaporate. Not shown in the image is a shutter which will allow evaporation material to reach the substrates in a controlled way. In order to monitor the thickness and the process rate, two methods are used. A quartz crystal (d) which oscillates at a resonance frequency of 6 MHz is exposed to the evaporation and material will condensate on its surface. This changes the resonance frequency slightly and allows monitoring of the process rate in the range down to ca 0.1Å/s. The crystal can only measure the physical thickness of the thin film, therefore an optical monitor is also viewing the process [16]. A beam of light (g) is reflected on a witness glass (h). Thereby the amount of reflected light can be analyzed by a monochromator and by the interference in the coating it is possible to calculate the optical thickness of the reflection. This has to be done on a separate fixed position since the substrates (f) are placed on planetary rotating devices which make it difficult to measure the optical thickness directly on the substrates.

In order to get hard dense coatings the process has to be at an elevated temperature. Infrared radiation sources (i) with a reflector are aimed at the substrates to reach temperatures over 300 ^{O}C.

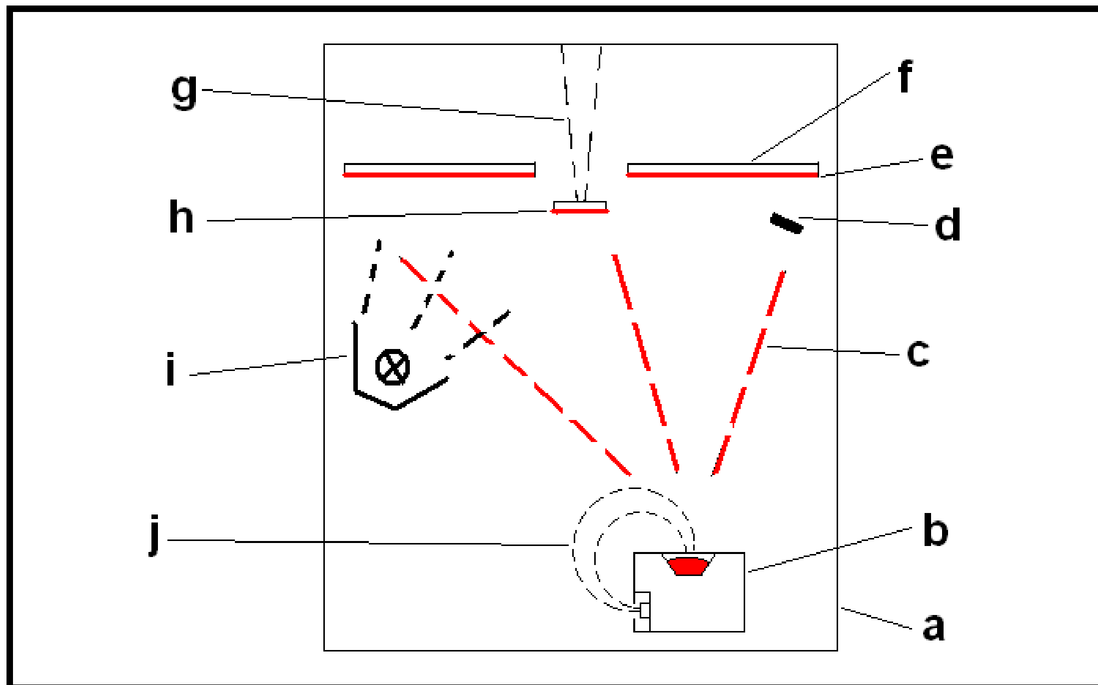

Figure 4. *PVD coating plant with e-beam. (a) vacuum chamber, (b) electron gun, (c) evaporation plume, (d) quartz crystal thickness monitor, (e) coated surface, (f) substrate (g) light path for optical monitor (h) witness glass for thickness monitoring, (i) heating radiation source, (j) electron beam path.*

2.2.4 Thin film growth and nucleation

The growth of thin film oxides by PVD depends on several parameters. The evaporation rate of the source, substrate temperature, background oxygen pressure and crystal orientation of the substrate and a few other parameters will affect the properties of the thin film.

2.2.4.1 Nucleation

The nucleation of a vaporized particle on a substrate is caused by loss of energy and bonding to the surface. When a hot particle hits the substrate surface it will not stick immediately. For a moment it will be a rather mobile particle called ad-atom or ad-particle before it condensates and chemically bonds to the surface. While it is a mobile particle it can glide around until it reaches a thermodynamic favourable position where it condensates. This is usually a nucleation site, which could be a defect or some local crystallographic orientation.

In the case of PVD at temperatures around 300 °C, there will be no mono crystal growth but more amorphous or nm-sized crystals. The growth of the film is usually columnar in structure, but depends heavily on the initial surface, nucleation and substrate temperature.

For metal oxides the coating tends to be rather porous if deposited at room temperature because the ad-particle will lose its energy quickly and freeze in its position. By raising the substrate temperature the time where the particle acts as an ad-atom will be longer due to the fact that energy is added to the surface. There will be more time for it to find thermodynamically better positions to bond to. This leads to a more compact and dense coating. MgF_2 coatings are a good example since it will be a dust layer easily wiped away by the thumb at room temperature, but by raising the substrate temperature it can be deposited as a dense and hard coating.

2.2.4.2 Epitaxial growth

In epitaxial growth a single crystal atom layer is formed one at a time. This can be done by growth on a substrate which has a matching crystal lattice constant and at very high temperatures.

2.2.4.3 Ion beam assisted deposition

It is possible to add energy to the surface by an ion source by bombarding the surface with Ar-ions under the deposition process [17]. Ion Beam Assisted deposition (IBAD) can give very dense and hard coatings even at low substrate temperatures. It is possible to produce hard coatings on plastic and heat sensitive optics.

2.2.4.4 Background oxygen

When some materials are evaporated they tend to dissociate, ZnS will dissociate completely into Zn and S (g) but recombines into ZnS on the substrate. Some oxides are problematic because they dissociate in the melt but do not recombine on the substrate. TiO_2 will decompose slowly into its most stable form, Ti_3O_5, in the melt. The released oxygen is not enough to re-oxidize TiO_2 on the surface. In order to get fully oxidized TiO_2, oxygen back pressure in the range of 10^{-4} Torr is needed as a background pressure. Oxygen will constantly impact the surface and it is possible to achieve a fully oxidized film. SiO_2 also has this tendency to lose oxygen under evaporation but is not as problematic as TiO_2.

2.2.4.5 Deposition rate

It would be desirable to have as high deposition rate as possible because of production costs. Depending on what oxide is used and the amount of oxidation needed there is a reaction limit to the process rate. For TiO_2 it is in the range of 2-5Å/sec. Otherwise it will not be fully oxidized. SiO_2 can be deposited at slightly higher rate, ca 10Å/s. Even if it would be possible to evaporate at much higher rate the coating will be less dense. It is also difficult to have good endpoint detection and control of the thickness if the rate is too high.

2.3 Lithography

In most types of pattern generation, photolithography is involved. When a newspaper is printed, or when an integrated circuit is fabricated, photolithography is a major part of the processes. The word is derived from Greek and means literary “write on stone”. In the beginning of the printing era, text and pattern were engraved on stones. A thin film of ink was covered on the top of the pattern and then pressed on paper to produce a copy. Multiple copies could then be produced. In modern printing, the engraving is not done on stone but is done by light sensitive photoresist were the pattern has been engraved by exposure of UV-light.

When a thin film surface will be pattered, there are several steps involved. The first step is to create a mask which consists of the original pattern. This mask consists of a thin layer of a patterned metal coated on a substrate of glass or plastic sheet.

The pattern of the mask is projected on the top of a photoresist coated substrate with the thin film (see Figure 5). The photoresist is sensitive to UV light. After the exposure, the exposed parts will be dissolved in a developer. The underlying parts of the thin film will, after development, be exposed to an etching agent which dissolves this thin film area and leaves an identical copy of the original mask [18].

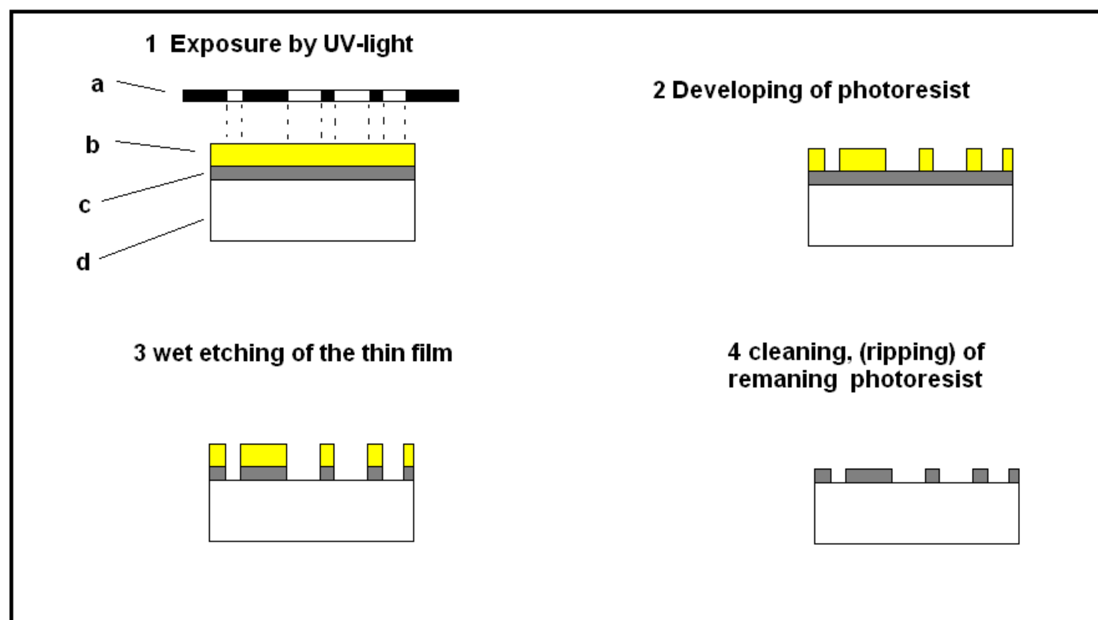

Figure 5. *Lithographic process in four steps for positive photoresist.*

2.3.1 Photoresist

There are two types of photoresist: negative and positive resist. Positive resist which is used in this thesis will give a positive image of the original pattern where negative resist will invert the image. This is due to the fact that the exposed area of positive resist will dissolve in the developer while the exposed area of negative resists hardens and will not dissolve, only the parts which are un-exposed by UV light are dissolved in the developer. The difference is due to different types of photo-induced chemical reactions involved. Most types of photoresists have a limited working range of temperature and room temperature processes are preferred.

2.3.1.1 Negative photoresist

Negative resists are often based on photo induced cross-linking of short polymer chains, this decreases the solubility in alkaline solution. This type is not as common as positive resist but in some cases it is possible to achieve higher resolution compared to positive photoresist.

2.3.1.2 Positive resist

Positive photoresists are sensitive to the wide band UV and blue light and are usually based on novolak and diazonaphthoquinones. The resists used in this thesis are based on these compounds.

2.3.1.3 Novolak resins

Novolak (N) or phenol-formaldehyde-resin can be manufactured by both a base and acid catalyzed condensation reaction with phenol and formaldehyde. Acid catalyzed polymerization promotes linear polymers with reaction on the orto-position on the phenol (see Figure 6). A slightly unbalanced molar ratio between phenol/formaldehyde which is <1 also promotes straight chains. This limits the size of the chains. [19]. Novolak is soluble in an alkaline solution but by adding diazonaphthoquinones (DQ) to the resin the solubility is inhibited.

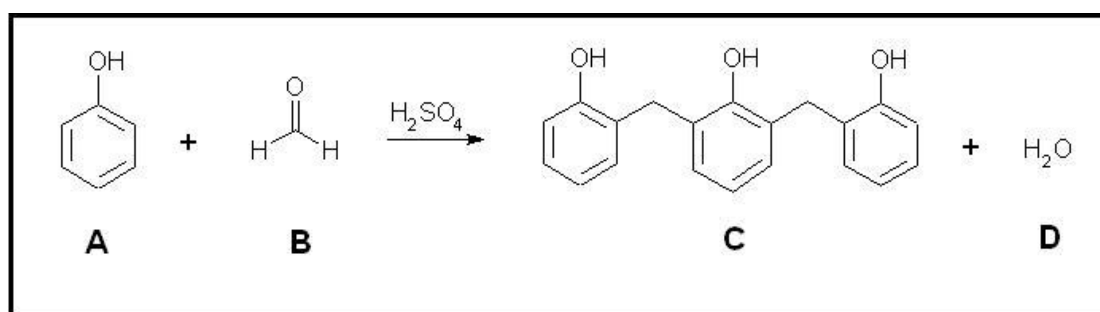

Figure 6. *A phenol and formaldehyde condensation reaction where Phenol (A) react with formaldehyde in an elimination reaction and the novolak resin (C) is formed while water condensates.*

DQ can undergo photo-induced transformation to a polar and alkaline-soluble indene acid. This transformation by exposure to UV light will amplify the solubility of the novolak resin. In the first step shown in Figure 7, the diazogroup (A) transforms to a carbene (B) where it loses its nitrogen into gas and then reacts to a keten (C) which then reacts with H_2O and transforms into an indene acid (C). The end product (C) is more easily dissolved in an alkaline solution and will boost the dissolution on novolak in the photoresist mixture [20]. The group R can differ slightly depending on manufacturer.

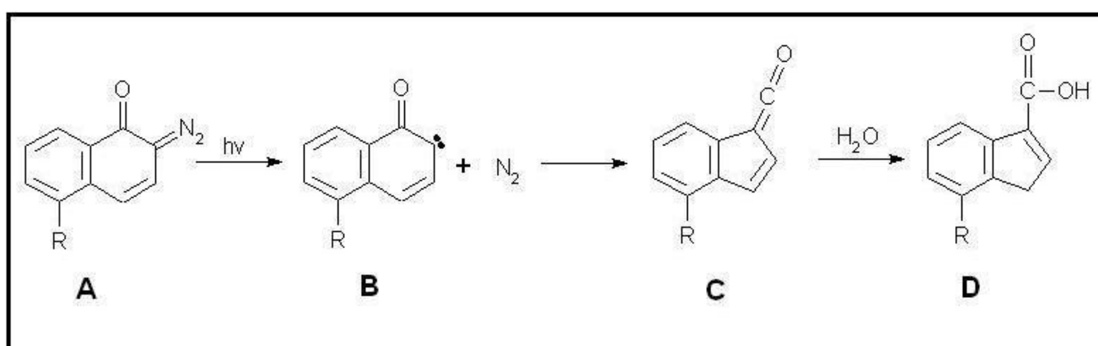

Figure 7. UV-light will induce a 3-step reaction.

The DQ/N mixture is usually dissolved in a solvent that gives good viscosity for the spinning process and to promote long shelf life so it does not react and decompose. Ketones or acid free solvents promote longer shelf life.

In this thesis only positive photoresist from Fuji OIR908-35 has been used with a thickness of 2.5 µm spin coated on the substrates. It consists of 60-80% 3-methoxypropionate as solvent, 18-32% Novolak resin, 1-6% naphthoquinone diazide ester derivative [21]. Due to proprietary reasons exact information of the content and reaction of this product is not available.

2.3.1.4 Spin coating

The photoresist is applied on the surface by spin coating. This is done by rotating the substrate at a rate of 3000-5000 rpm. A known dosage of liquid resist is poured in the centre of the substrate. By centrifugal force the liquid is dispersed very even over the whole surface. The final thickness is depending on rotation speed, viscosity and spinning time [22]. In this thesis the photoresist has a thickness of 2.5 µm. Spin coating is the only method used when the highest quality is necessary. It is possible to achieve a uniformity of 1%.

One major disadvantage with spin coating is that it is inefficient, using a very small fraction of the resist, while the remaining is wasted. Rectangular substrates can not be coated with good uniformity. For rectangular substrates other methods are preferred, such as dip-coating, meniscus and capillary coating, or extrusion coating which could be described as methods where the photoresist is dispensed by brushing. This can give very high yield [23].

2.3.1.5 Priming

The photoresist is very hydrophobic in its nature, making it suitable for hydrophobic films such as chromium or aluminium while SiO_2 and most other oxides are hydrophilic, therefore photo resists do not adhere well to such surfaces. One way of solving this problem is to use an adhesion promoter which changes the properties of the surface and give a stronger bond to the photoresist.

A frequently used promoter is hexamethyldisilazane (HMDS) [24]. On most types of dielectric filters there will be a SiO_2 layer on top. This has to be considered when designing an etchable filter. On the filters which are evaluated in this thesis there is only SiO_2 as a top layer, in order to get a consistent surface independent of the filter type.

When SiO_2 is evaporated the coating will form silanol groups –SiOH on the surface due to reaction with water and broken O-Si-O bonds after it has been exposed to air [25]. This leads to a very hydrophilic surface on the SiO_2. By treating the surface with HMDS a hydrophobic surface will be formed giving good adhesion to the photoresist (see Figure 8).

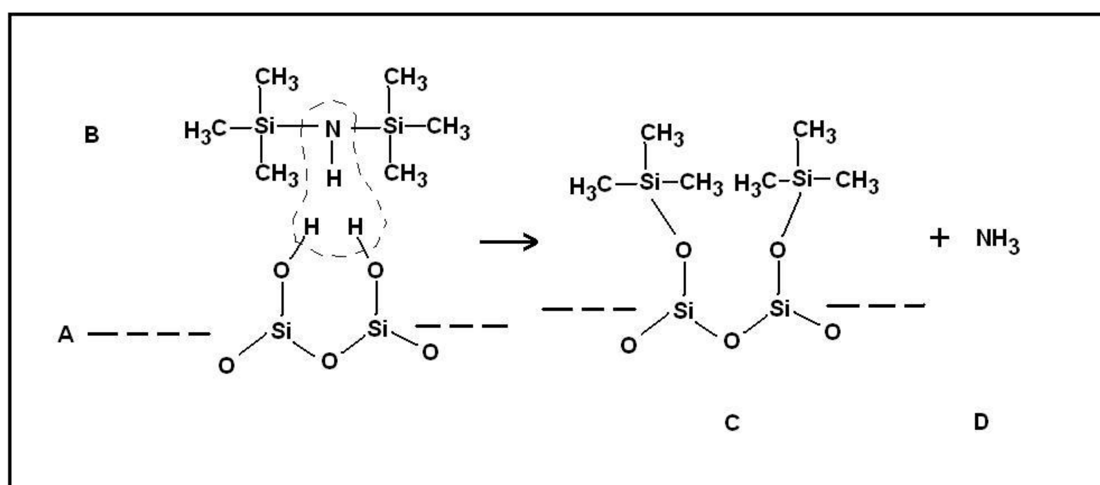

Figure 8. *Reaction of HDMS (B) with the hydroxylated SiO_2-surface (A), forming a hydrophobic –Methyl rich surface while ammonia is released.*

Another way of promoting surface adhesion of resist is to coat the top SiO_2 surface with a very thin layer of chromium in the range of 100 Å (see Figure 9). This is frequently used when gold is evaporated because of the bad adhesion properties of gold coatings. PVD-evaporated Cr has a very hydrophobic surface suited for photoresist. Cr is also bonded to SiO_2 even though the hydrophobic properties do not match. Another advantage when using Cr as primer is the fact that the etching rate is low in HF solutions. This will assist the isotropic etching and reduce undercutting of the resist. Cr itself can be etched by cerium ammonium nitrate, see chapter 2.4.

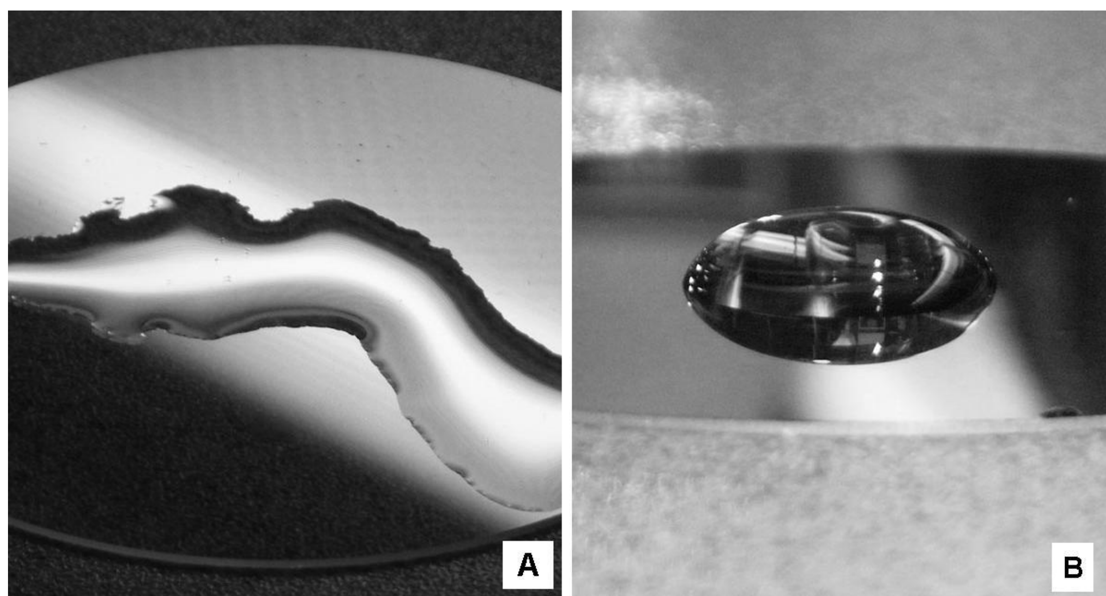

Figure 9. *Illustrative example of different surface wetting properties, (A) a drop of water on an untreated SiO_2 surface and (B) with a thin Cr coating on top.*

2.3.2 Exposure

For g-line (436 nm) photoresist shown in Figure 10, sensitive to blue and UV light, exposure can be done by many types of light sources. The most common sources are Hg-lamps with a quarts envelope so UV-light is not absorbed by the light bulb. The novolak based photoresist is sensitive in a range from 300-440nm. When the resist becomes exposed the absorbance drops due to the chemical reaction involved.

Exposure can be done by projection lithography which is common in IC-manufacturing or by contact copying where the demand for resolution is lower.

Exposure dose for novolak resists are in the range of 50-150 mJ/cm^2 depending on manufacturer and composition.

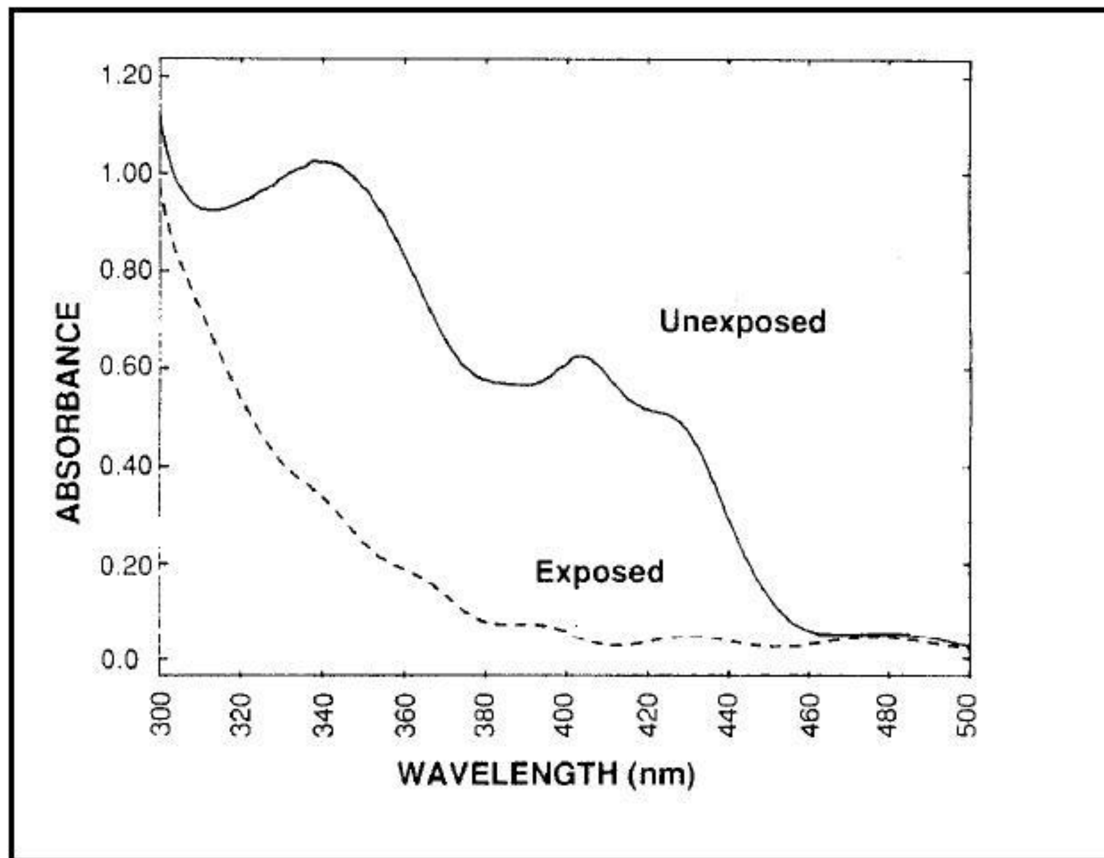

Figure 10. *Typical sensitivity curve of a novolak/Diazoquinone resin based photoresist [26].*

2.3.3 Developer

Any type of alkaline solution works well as developer for the photoresist. NaOH works fine. The concentration should be in the range of 0.262-0.280 N for novolak resists.

In cases where the substrate is very sensitive to alkali metals, NaOH or KOH is no longer suitable. Tetramethylammonium hydroxide (TMAH) which is a non metallic alkaline compound is preferred for developing sensitive coatings [27]. In this thesis a NaOH solution was used. Sometimes agents are added to improve the wettability.

2.3.4 Etching methods

In order to make the desired pattern on the thin film it has to be removed in some way. It can be done by exposing the surface to a solution, reactive plasma or by ion beams.

2.3.4.1 Wet etching

The simplest method to pattern the structure is by wet etching. When the resist is developed parts of the lithographical pattern are dissolved and the underlying coating is exposed and can be attacked by a suitable etching agent. This thesis is focused only on the wet etching process. A common etching solution is HF which works well for some oxides, such as SiO_2. Metals are often etched by other mixtures. A well known etchant for Al is a mixture of nitric-, phosphoric- and acetic acid. One major disadvantage with wet etching is the limitation at high pattern resolution. Usually the etching is isotropic by nature. If several layers with different composition are etched problems with undercutting can occur because of different etching rates between the layers. There can be undercutting of the photoresist due to bad adhesion and non uniform etching among other problems.

The diffusion of the etching compounds can cause uneven etching (see Figure 11). The cause of this non uniformity is decrease of concentration close to the surface. It is a very common problem when very fine patterns in combination with large exposed areas are etched.

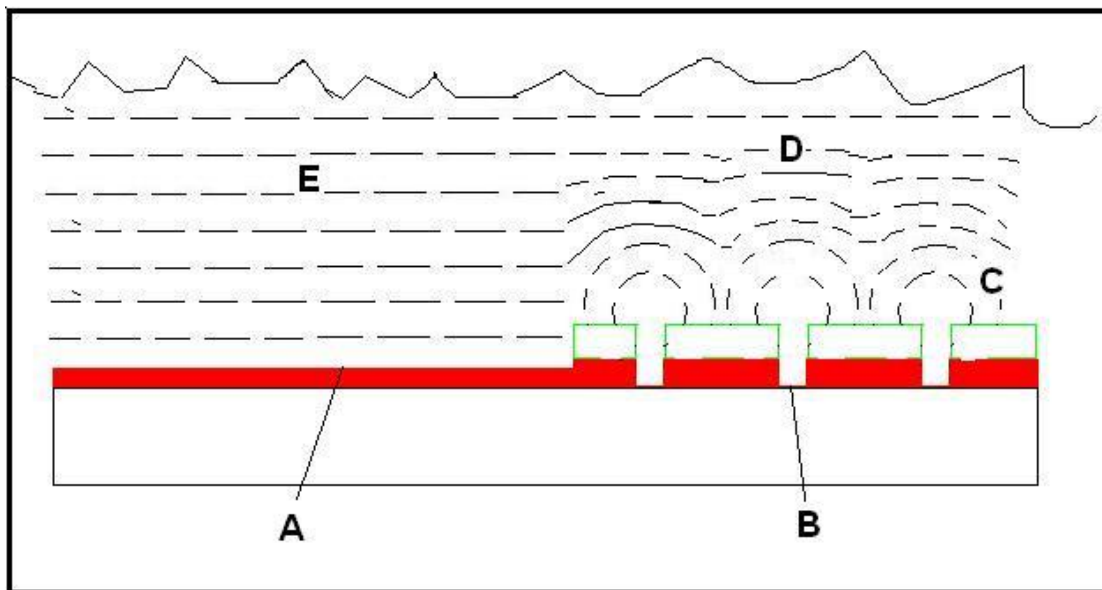

Figure 11. *Model of diffusion in a liquid. Etchant (E) is planar on a macroscopic area (A). However in point shaped substrate areas (B) the diffusion is semi spherical in proximity to the surface and planar on a distance. Since the diffusion rate is equal in both cases (E) and (D) there will be less depletion of the concentration C_o as the etchant resulting in higher etching rate. This follows Fick's law of diffusion.*

Fick's law of diffusion tells that the flux is proportional to the concentration gradient in the solution [28]:

$$-J_0(x,t) = D_0 \frac{\partial C_0(x,t)}{\partial x} \tag{2.9}$$

where J_0 is the flux, C_0 the concentration, and D_0 the diffusion constant. One way of avoiding this problem is to have very good flow of the etching liquid. If possible large exposed areas should be avoided by covering these areas with photoresist. This is possible for integrated circuits but when reproducing images this is not an option.

2.3.4.2 Plasma etching

Plasma etching is a chemical process based on a gas that is activated by an electrical field under low pressure. The reactive species selectively attack the thin film but the photoresist remain intact. CF_4 is a common etch gas for SiO_2. In a plasma reactor CF_4 is ionized and form radicals, CF3* and F*. These reacts with SiO_2 and form SiF_4. Low vacuum and low voltage are preferred. This type of etching is more isotropic compared to reactive ion etching (RIE) [29].

2.3.4.3 Ion etching

Ion etching is a pure physical process where the surface is etched by the kinetic impact of ionized and accelerated ions, preferably Ar^+, and the process demands high vacuum in order to work.

2.3.4.4 Reactive ion etching

A very popular method, which is similar to plasma etching, is reactive ion etching (RIE), which is shown in Figure 12. The same gases can be used as with plasma etching. RIE can produce highly anisotropic structures. Ions created in the plasma are accelerated towards the surface by an electric field under high vacuum and high voltage [30]. The main drawback for RIE when etching multilayer dielectric filter is the limitation of coating thickness. Heat is generated under the process which will damage the photoresist. There will also be heavy depletion of active ions (the same phenomenon as discussed in Figure 11) causing uneven etching result [31].

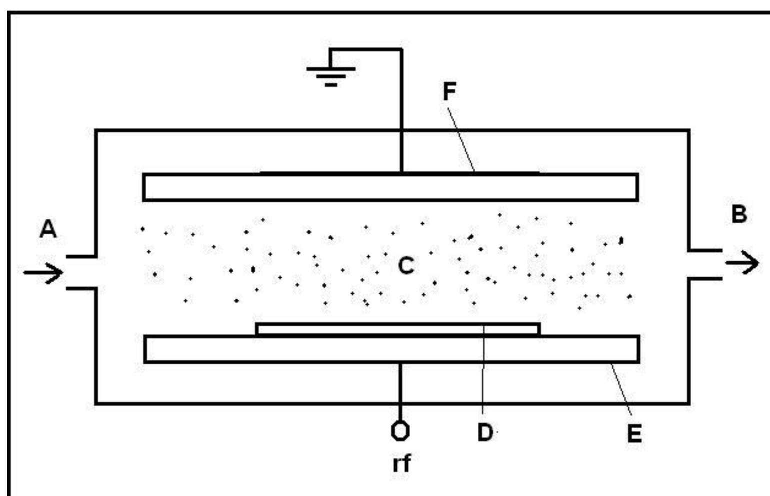

Figure 12. RIE chamber. The chamber is connected to a gas inlet (A), vacuum pump (B), plasma with reactive species (C), substrate (D), (E) conductive plate feed by radiofrequency(E), grounded electrode plate (F). Reactive ions will move towards the substrate where it can chemically react with the surface.

2.4 Wet etching chemistry

Because an optical filter consists mostly of two different oxides and the properties of these two compounds differ, the etching rate will differ. This will cause problem such as undercutting and anisotropic etching. It is desirable to find etchants that will etch with the same rate independent of the material composition on each layer. This is sometimes referred to as sandwich etching and has been studied for Si_3N_4/SiO_2 for the semiconductor industry [32, 33].

SiO_2 is very well known and there are stable isotropic wet etchants for both porous and crystalline SiO_2. The major problem for etching filters is that SiO_2 needs to be combined with a high index material, often TiO_2. TiO_2 is very difficult to etch and has a reasonable etching rate only when the coating is porous. Weaker Ti-O bonds are probably the reason for its etchability in porous state. Densification of TiO_2 will improve the bonds in the TiO_2 matrix therefore it is completely impossible to etch dense TiO_2 coatings by HF chemistry. Very little is mentioned about wet etching of TiO_2 in the literature. There are some positive results for RIE for TiO_2 [34], but RIE is quite complex and the goal here is to find wet etchants which can dissolve TiO_2.

As a general rule, alkaline oxides are dissolved by acids and acidic oxides are dissolved by bases.

Because many metals form oxides on the surface the etchant has to dissolve the oxide in order to dissolve the underlying metal. Keeping this in mind, it is possible to search for etchants that might dissolve the metal which also have to be able to etch the oxide itself. But even if the etchant is capable of etching the metal it might not always be able to break through the top oxide layer and dissolve the metal. A good example of this is etching Cr by hydrochloric acid. A thin Cr_2O_3 layer is spontaneously grown on the Cr surface and causes passivation [35], which is a very efficient barrier. It stops etching of the Cr by HCl. Cerium ammonium nitrate in perchloric acid solution is one of the few solutions capable of dissolving the Cr_2O_3 protective layer, and oxidizes Cr by the reaction:

$$3Ce(NH_4)_2(NO_3)_6 + Cr \rightarrow 3Cr(NO_3)_3 + 3\ Ce(NH_4)_2(NO_3)_5$$

where Ce is reduced from IV to III and Cr is oxidized from 0 to III. The dissolving mechanism for the passivation layer is however not well known [34, 35].

Another way of breaking the chrome oxide layer is by cathode reduction of the Cr_2O_3 passivation layer by having an electric contact of aluminium to the Cr layer. This creates a galvanic element, reducing Cr III and oxidizing Al.

2.4.1 Acid etching

It is difficult to etch most oxide thin films in any acid, some oxides are soluble in hot acids but in general the photoresist is damaged under these conditions. SiO_2 is not affected by common acids except for HF. TiO_2 can be dissolved by hot H_2SO_4. A limiting factor is the temperature sensitivity of the photoresist and etching has preferably to be performed at room temperature.

2.4.2 HF-etching

Hydrofluoric acid is a rather odd acid if compared to similar acids such as HCl and HBr. Its aggressiveness to some oxides can not be explained by its acidity because it is a rather weak acid with pKa 3.15 in diluted solutions. In HF solutions with high concentration HF_2^- will form with pKa of 1.

$$HF \leftrightarrow H^+ + F^- \qquad \text{pKa } 3.15$$

$$2HF + F^- \leftrightarrow HF_2^- \qquad \text{pKa } 1$$

The main reason for its function as an etchant is that elementary F^- has a smaller ion radius (1.4Å) compared to O^{2-} 1.6Å and the bond energy on Si-F is half compared to Si-O [38]. F^- is not involved in the reaction since NaF does not attack, only HF, HF_2^- and H^+ ions are involved.

The overall reaction is:

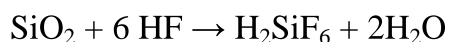

$$SiO_2 + 6\,HF \rightarrow H_2SiF_6 + 2H_2O$$

The complete mechanism is rather complicated and involves several steps. It is kinetically controlled by absorption but is not completely understood [37]. HF and HF_2^- groups are absorbed on the surface silanol groups. These are transformed into ≡Si-F and ≡Si-O-SiF_3. This turns the oxygen group more alkaline and H^+ can bind to it and the siloxane will subsequently be broken.

Buffered HF (BHF) and NH_4F results in higher pH and a more controlled etching rate. It is frequently used to etch SiO_2 since a pure HF solution gives an etching rate which is too high.

Wet etching of SiO_2 with HF is by far the most investigated mechanism. On other oxides very few studies have been performed. TiO_2 and HfO_2 among many other oxides are known to be very difficult to etch with HF.

TiO_2 can be etched by HF under certain circumstances but only low quality porous coatings which probably involve weak Ti-O bonds. Sol-Gel coating of TiO_2 has been shown to be etchable but the refractive index in these coatings is 2.1 indicating a very porous layer. The etching rate for these Sol-gels is in the range of 1Å/s [40].

2.4.3 Alkaline etching

The only possibility to etch thin films in an alkaline solution is by using photo masks by nitrides since novolak resin based photoresist rapidly dissolves in these solutions. There is one patent describing a photoresist for alkaline etchants containing two different polymers based on styrene and acrylonitrile for one and epoxy for the other [41].

TiO_2 is soluble in strong alkaline solution [42].

2.4.4 Catalytic etching of TiO_2

A common well known recipe for etching TiO_2 is 1 part HN_4OH, 2 parts H_2O_2 and 1 part water [43]. Very little is described in the literature about the peroxide etching mechanism. Corrosion of Ti in alkaline peroxide has been studied for the pulp industry which has led to some understanding of the reactions involved [44, 45].

H_2O_2 in basic solution react to form OOH^-:

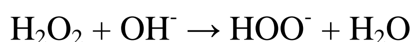

$$H_2O_2 + OH^- \rightarrow HOO^- + H_2O$$

It is proposed that hydrated Ti-oxide is attacked by HOO^-

$$TiO_2\,x(H_2O) + OOH^- \rightarrow (Ti[OH]_2O_2)_{ads} + (x-1)H_2O + OH^-$$

At sufficiently high pH and high peroxide concentrations the Ti-complex will dissolve with the evolution of oxygen:

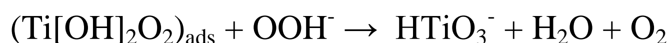

$$(Ti[OH]_2O_2)_{ads} + OOH^- \rightarrow HTiO_3^- + H_2O + O_2$$

2.4.5 Redox etching

Some oxides can be reduced or oxidized into a more solvable state. Thin films of CeO_2 can be etched by reduction. CeO_2 is quite difficult to dissolve by wet chemistry and it is very resistant to most etchants. Ce^{3+} however is easily soluble by many acidic solutions. Reduction can be done on the Ce^{4+} by the use of Prussian blue $K_4[Fe(CN)_6]H_2O$ in HCl thereafter Ce^{3+} can be dissolved. The etching rate is rather low, 100 Å/min [46]. There are very few oxides this strategy can be applied to, for example TiO_2 has no oxide state which is more easily soluble. In most cases the oxidation state of the oxide is not changed under the etching process.

2.4.6 Photochemical etching

In some cases it is possible to induce etching by irradiating the thin film by light. Very little is mentioned in the literature about photo induced etching of oxides such as SiO_2, TiO_2 and other oxides. However there has been some interest in photochemical etching of III-V compounds by irradiation with an eximer laser (193 nm) in different gases, for example HCl gas [47]. Nb_2O_5 thin films have also been successfully photochemically etched in HF solutions [48]. One great advantage of this method is that is would be possible to etch anisotropic structures if the surface is illuminated by a highly collimated light source. It is very difficult to find anything at all in the literature but this could be a promising research area for the future.

2.4.7 Electrochemical etching

By applying a potential to the surface of the substrate it would be possible to overcome the activation energy so that a weak etchant could attack and dissolve the surface. One case example is the breaking of the oxide layer on Cr by cathodic reduction. One big obstacle with this method is that most oxides are electric insulators and therefore can not be put at a desirable potential. Electrons can be injected in quartz under vacuum and can be made conductive temporarily but this method has limited use [49].

2.5 Etching anisotropy

The direction in which the etching is propagating will affect the etching result. This is shown in Figure 13. In pure isotropic etching the etching rate will be the same in all geometrical directions. If the etching is anisotropic then the etching rate is directionally dependent and will result in deeper etch trenches in the thin film. Under wet etching conditions in amorphous thin films the result is isotropic. In some cases anisotropic etching can appear under wet etching in crystalline compounds. Depending on crystal orientations different etching rates will occur. It is common to take advantage of this etch behaviour in MEMS technology (Micro Electro Mechanical Systems). Etching of single crystal silicon by KOH is a common way to produce anisotropic etching [50].

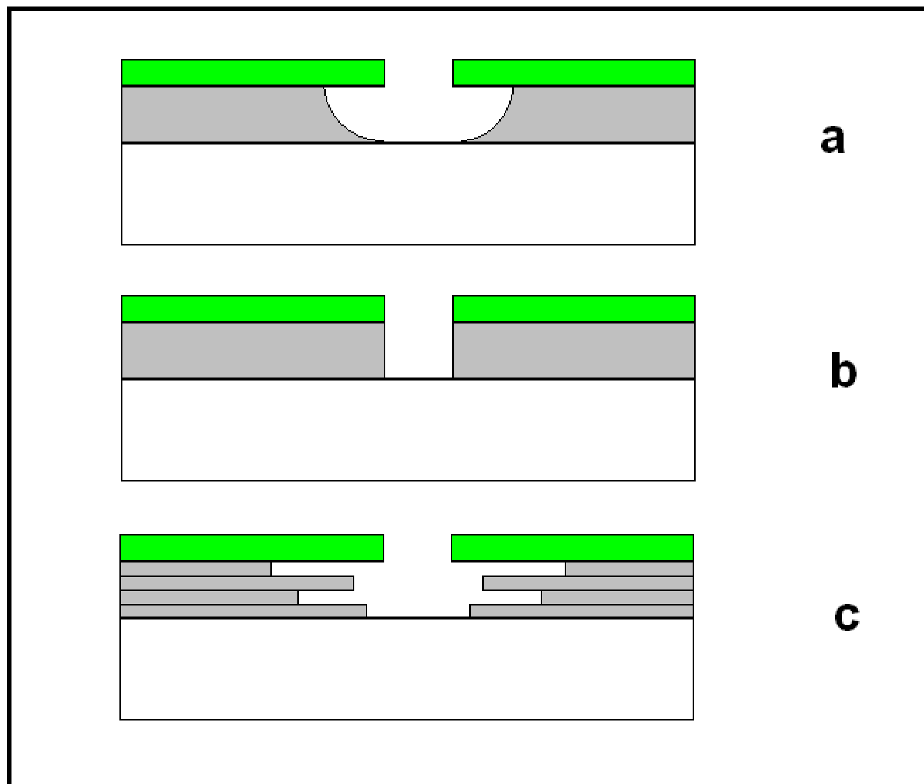

Figure 13. *The green layers represent photoresist, grey different oxides and white represent substrates. Example (a) shows a perfect isotropic etching, typical for wet etching. Case (b) is a perfect anisotropic etching result, desirable because this will make a copy identical to the resist mask. Example (c) illustrates what happens with a multilayer where different oxides have different etching rates.*

Photo induced wet etching would generate a more desirable anisotropic etch. Also RIE results in anisotropic etching due to direction of the electric field while plasma etching gives more isotropic etching.

2.6 Pourbaix diagrams, pH and redox environment

A useful tool to show and understand corrosion is the graphical representation of the Nernst equation in the form of a Pourbaix diagram [51]. By showing a graph with the potential E as a function of pH when the substances are in thermodynamic equilibrium it is possible to see the solubility.

2.6.1 Nernst relation

This fundamental relation is the base for all electrochemistry. It can be shown that:

$$E = E^{\circ}_{reaction} + RT/(nF) \cdot \ln K \qquad \textbf{(2.10)}$$

$$K = [C]^c\,[D]^d/[A]^a\,[B]^b \qquad \textbf{(2.11)}$$

Is valid for a reaction of type: $aA + bB \leftrightarrow cC + dD + ne$

This would give a three dimensional relationship with E= f(pH; [X]) where X is a selected species of interest.

The Pourbaix diagram is calculated from a fixed concentration of the species of interest. This simplifies the diagram into two dimensional coordinates.

If a reaction containing two soluble species M, N on each side of the reaction then the function (or line) is set on the point where [M]/[N]=1. In the case where there is solid interaction (where the activity is set to 1) then the function is displaying the pH and E value for a saturated solution.

A horizontal line will indicate there is no pH dependence and no $[H^+]$ or $[OH^-]$ is involved in the reaction. The solubility is only depending on the potential.

A vertical line will indicate that there is no oxidation or reduction in the reaction. The oxidation state is not changed but it is pH dependent.

A diagonal line shows that there are both pH and redox reactions present.

One way of changing the horizontal value would be to simply change the pH in the solution by adding a suitable acid or base. It is not as easy to see how to move in vertical position and change the electrochemical potential in the solution. One way of doing so could be to apply an electric potential to the surface. It could also be changed by adding some oxidizing or reducing species into the solution. By bubbling oxygen into the solution the position moves upwards and by bubbling hydrogen it moves downwards in the diagram.

There is a limit due to the electrochemical properties of water which is showed by two dotted lines. This is from the reaction:

$$2H_2O \leftrightarrow O_2 + 4H^+ + 2e^-$$

and the bottom line:

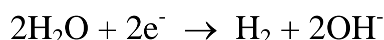

$$2H_2O + 2e^- \rightarrow H_2 + 2OH^-$$

represents hydrogen evolution. Outside this area no species can exist in water solution since water itself will decompose. However close to the line there is a slight elasticity due to the kinetics so for a short while it is possible to go outside the line.

It is also very important to keep in mind what is actually going on in the reactions, what compound should be used representing different areas in the diagram. For example when an oxide such as TiO_2 is inserted in water there might be a monolayer of H_2O reacting with the surface. Even if TiO_2 is the subject of interest the diagram can represent TiO_2 by another species such as TiO_2•(H_2O). What species should be put in the diagram is not trivial and can sometimes be very confusing if the reactions are not known.

2.6.2 Case example manganese system

To illustrate the use of Pourbaix diagrams, manganese is shown in Figure 14. The two diagonal dotted lines represent the water stability area where species are stable. It can be seen that MnO_4^- ions are unstable because their predominance area is at very high potentials. However it is still possible to have water solutions of MnO_2^- because the kinetics is rather slow and a solution can exist for a while before it decomposes in the reductive environments. Mn immediately oxidizes when the metal is put in solution because Mn is also outside the water stability area. Two different concentrations are viewed in Figure 14, A and B. The vertical line between Mn^{2+} and $Mn(OH)_2$ is slightly shifted when the concentration is changed. This illustrates the change in solubility of the specific compound by changing the pH in the solution.

MnO_2 is stable inside the water stability area but the area is quite wide even at very high Mn concentrations. This gives a hint that MnO_2 maybe could be quite easy solvable by reduction in low pH solution into Mn^{2+}, but not easily oxidized in water solution since this would oxidise water first.

Why not use MnO_2 as a high index material in etchable dielectric filters then? The refractive index is reasonably high 2.4 [52], so it should be possible to replace TiO_2 as a high index material. Unfortunately there is heavy absorption in the thin film preventing its use in dielectric filters [53]. There would probably be difficulties with environmental stability and absorption of moisture in MnO_2 thin films.

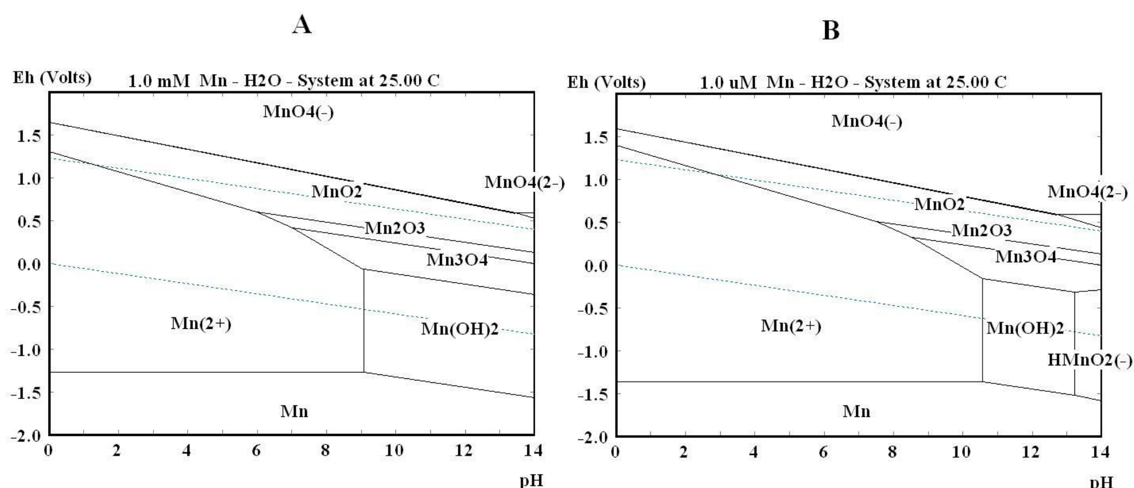

Figure 14. *Pourbaix diagrams for the manganese system under different concentrations, (A) 1 mM and (B) 1 µM.*

It is important to know that Pourbaix diagrams only show the properties in thermodynamic equilibrium. The kinetics of the reactions are not considered here. This means that there may be reaction steps which have activation energies that prohibit the dissolution. But it is a good guideline to show if the reaction would at least be possible to dissolve an oxide or not. Pourbaix diagrams are better suited in corrosion science where the reaction rate is much lower.

2.6.3 Pourbaix simulations

Calculating Pourbaix diagrams is very time consuming so therefore computer software is mandatory. The software is based on data from experimental thermodynamic and electrochemical properties. By using the Nernst equation Pourbaix diagrams can be calculated for selected species. In this thesis HSC Chemistry version 6.12 from Outotec Research Oy has been used. The case example in Figure 14 is calculated from this software.

2.7 Etching rate determination

In most cases an etching rate in the range of 2-10 kÅ/min is desirable. There are several strategies how to measure the etching rate on a thin film. Only a few methods are described here. One way is to measure the thickness prior and after a known etching period. From these start and end values the etching rate can be calculated. Another approach is to measure the etching rate in-situ by optical transmission spectroscopy. Both methods have its pros and cons. Attention must be taken in order not to confuse between the optical and physical thickness of a thin film since the difference is the refractive index shown by the equation (2.7). If nothing else is stated the etching rate is expressed as physical thickness, Tp.

In this thesis only Optical transmission spectroscopy was used for etching rate determination, but Stylus profilometry (Chapter 2.7.3) and ellipsometry (Chapter 2.10.1) was used for determining the optical properties of the thin film on coating on silicon wafer.

2.7.1.1 SiO_2 index problem

There are problems in determining etching rate by optical means for coatings with a refractive index in proximity of the substrate index. The resulting interference pattern will be weak and the etching rate will be difficult to detect. For good optical etching rate determination SiO_2 can not be measured if it is coated directly on a borosilicate glass substrate. By having a very thin end point layer of aluminium the interference pattern can be amplified which enables easier measurements.

2.7.2 Tolansky method

This method is based on Fizeau interferometry [54]. This is a physical thickness method. The measurement is done by etching a small strip or trench on the thin film thereafter the trench is coated with a thin reflective aluminium or silver layer. A semitransparent flat surface is placed on the etched trench at a slight tilt angle. This will create interference fringes when illuminated by a monochromatic light source. By measuring the displacement of the interference fringes on a microscope it is possible to calculate the depth of the etched trench to a high degree of accuracy. The method is simple, reliable and any type of thin film can be measured. The disadvantage is that the method is very time-consuming since each etched strip must be post coated with reflective metal before measurements can be done.

2.7.3 Stylus profilometry

This is also a physical method and the basic principle is very simple but sensitive to disturbances and errors. I consists of a very fine diamond needle which is moved across a trench or a etch step [55]. The movement of this needle is recorded by sensitive electromagnetic coils or by optical sensors via reflection of a laser beam. It is a quick method.

2.7.4 Optical in-situ etching rate measurement

By using an optical fibre light will pass through the coating under attack by an etchant. An interference pattern is recorded by an optical spectrometer and the resulting interference pattern can be analyzed [56]. If the fibre is in proximity to the etched surface a small area of the thin film will be viewed and variations in the etching rate can be minimized (see Figure 15).

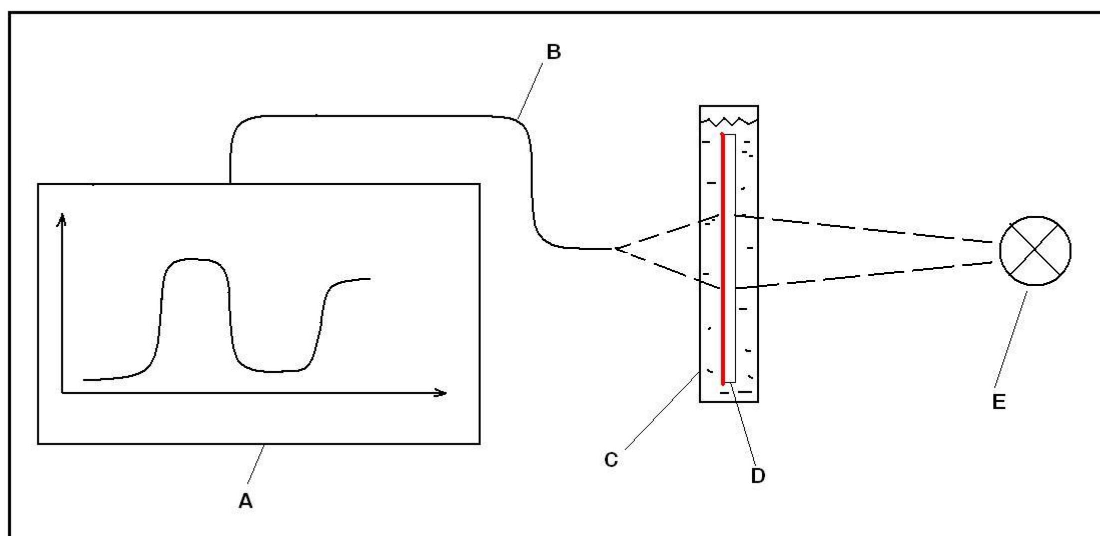

Figure 15. The optical in-situ etching rate measurement. Spectrophotometer (A), optical fibre (B), etch cell (C), sample (D), light source (E).

2.7.4.1 The etch cell

When measuring the etching rate in a solution the cuvette must be able to hold the substrate in position and in the same time be able to transmit light to the fibre detector. Some plastics are better suited than others in order to contain the etchant. Glass can not be used because of the HF content in some etchants. Polyethen, polyprophene and similar polymers can withstand most etchants and solvents. Unfortunately they do not function well as optical windows because of their milky appearance. PMMA is a quite good choice since it withstands most acids and HF except concentrated sulphuric acid. The plastics can also be glued with epoxy resin which has reasonable good tolerance against most acids, at least if the exposure of etchant is limited in time. Acetone must be avoided because it quickly dissolves PMMA.

2.8 Thermal shift

All thin films grown by PVD have a structure more or less far from its crystalline structure. The thin film can be from a completely amorphous structure to a polycrystalline columnar structure. The growth is strongly dependent on parameters such as substrate temperature, pressure, and evaporation rate. There are always more or less empty spaces in the thin film structure compared to its crystal form. Low substrate temperature favours an amorphous structure while high temperature favours a crystal structure.

One advantage by having a porous amorphous structure in a thin film is the favourable etchability. The disadvantage is spectral instability with shifting temperatures. In most cases the goal is to achieve a stable filter that still is etchable. Thermal post treatment will improve the stability but in general make the filter unetchable [57]. Combining easy etchable coatings with thermal stability is one of the major concerns in this thesis.

The cause of the shift is due to voids that absorb moisture. When the temperature is changed, water is liberated and the refractive index is lowered. The spectra will subsequently shift to shorter wavelengths equation (2.6). This is a semi reversible process, when moisture re-absorbs due to lowering of temperature the spectra shift back to it original characteristics.

An instrument was built in order to investigate the thermal behaviour of the thin films. By heating the substrate to a high temperature, in this case 300-320 °C, for a couple of minutes and record the optical spectra prior and after the heating, a certain wavelength shift could be measured. This is a good tool for measuring the stability of the thin film.

2.9 Thin film stress

Due to the PVD process there can be both compressive and tensile stress in the film. This can cause problems in some cases because if the stress in the film is too high the film will crack or peel of. There are more or less complex ways to measure the stress but a very easy method is to coat a thin disc of glass and then measure the bending of the surface [58]. The stress σ on a circular substrate can be derived from:

$$\sigma = \frac{\sigma}{r^2} \frac{E_s}{3(1-\nu)} \frac{d_s^2}{d_f} \qquad \textbf{(2.12)}$$

where E_s is the Youngs modulus and ν is the Poissons ratio of the glass substrate and d_s is the substrate thickness, r is the deflection of the disc caused by stress.

By just watching the reflection on a thin film coated disc from a point source it is easy to get a rough estimate of the stress due to the fact that the glass is bending like a convex or concave mirror. In this thesis only a rough estimate of stress was done.

2.10 Optical characterisation of the thin films

As mentioned in chapter 2.1.2 three important parameters must be determined in order to know the properties of a thin film, the refractive index (n), extinction coefficients (k) and the physical thickness (t).

It is a detective work to find these parameters and several methods can be used in conjunction. In this thesis the extinction coefficient was assumed to be close to zero, this means that the absorption must be low.

2.10.1 Ellipsometry

Ellipsometry is a method very well suited to evaluate the optical properties on a thin film [59]. A collimated laser beam is reflected on a well characterized surface, usually polished Si, coated with the thin film of interest. By measuring the reflectance ratio for both p- and s-polarized light at several incident angles it is possible to determine n, t and k. It is easier to do the calculations if k is assumed to be zero.

In theory it is possible to measure thin films on glass but in general a coating on Si is preferred. One problem in measuring coatings on a thin glass is that there is back reflection disturbing the measurement.

In this thesis an SE-400 by Sentech instruments was used, and all measurements were done on thin films deposited on both polished Si-wafers and glass in the same run.

2.10.2 Optical spectroscopy

To find t, n and k, it is also possible to measure spectra and match it with simulated curves. When a good match is found it could indicate for n, k and t. There are some problems because dispersion is causing uncertainties and it is sometimes difficult to find best match because there are three unknown parameters. It is somewhat simpler if k can be excluded.

In the case for SiO_2 it is necessary to find the thickness using this method because an underlying aluminium end point layer will make ellipsometric measurements impossible on glass.

2.11 The selection of dielectrics

For several reasons Y_2O_3, TiO_2, SiO_2, HfO_2, ZrO_2, MgO, MgF_2 and Al_2O_3 were selected for evaluation (see Figure 16).

There are several properties that must be fulfilled in order to find suitable dielectrics which can be used to design a good etchable multilayer filter. All filter stacks are built by alternating high and low refractive index material. The low index material is of little problem in etching aspects. SiO_2 is well suited for this task since it is easy etched in HF-solutions. It has a very low refractive index and it is possible to deposit a very dense layer with good etchability. It has low absorption. The only disadvantage is that it is rather difficult to evaporate with an e-gun because of a tunnelling effect (see 2.11.7) in the melt due to the fact that the material sublimates when being evaporated.

The major problem is the high index material in the filter stack. It usually consists of TiO_2 but TiO_2 is very difficult to etch when it is made dense and thermally stable.

It is critical to find a high index material which still it etchable in manageable ways. The material must not absorb light in the visible range and it should be chemically reasonably stable and not be dissolved by moisture or oxidized or reduced by time. The material should be not to expensive, not radioactive, and not toxic. It is possible to use oxides, sulfides, nitrides and fluorides but oxides are preferred in optical coatings. Nitrides are in some cases excellent, for example Si_3N_4, and the index is relatively high. But it is difficult to etch and can not be grown in a PVD-system [60]. The only sulfide used previously as high index film (2.35) is ZnS but it is contaminating the system easily and is rarely used today [61]. Fluorides are sometimes used as low index material. MgF_2 is very popular but not as high index material.

The choice is left to oxides because it is easy to add oxygen in the chamber and improve the thin film under the coating process. Most oxides are relatively stable and easy to handle. The question persists if they are etchable.

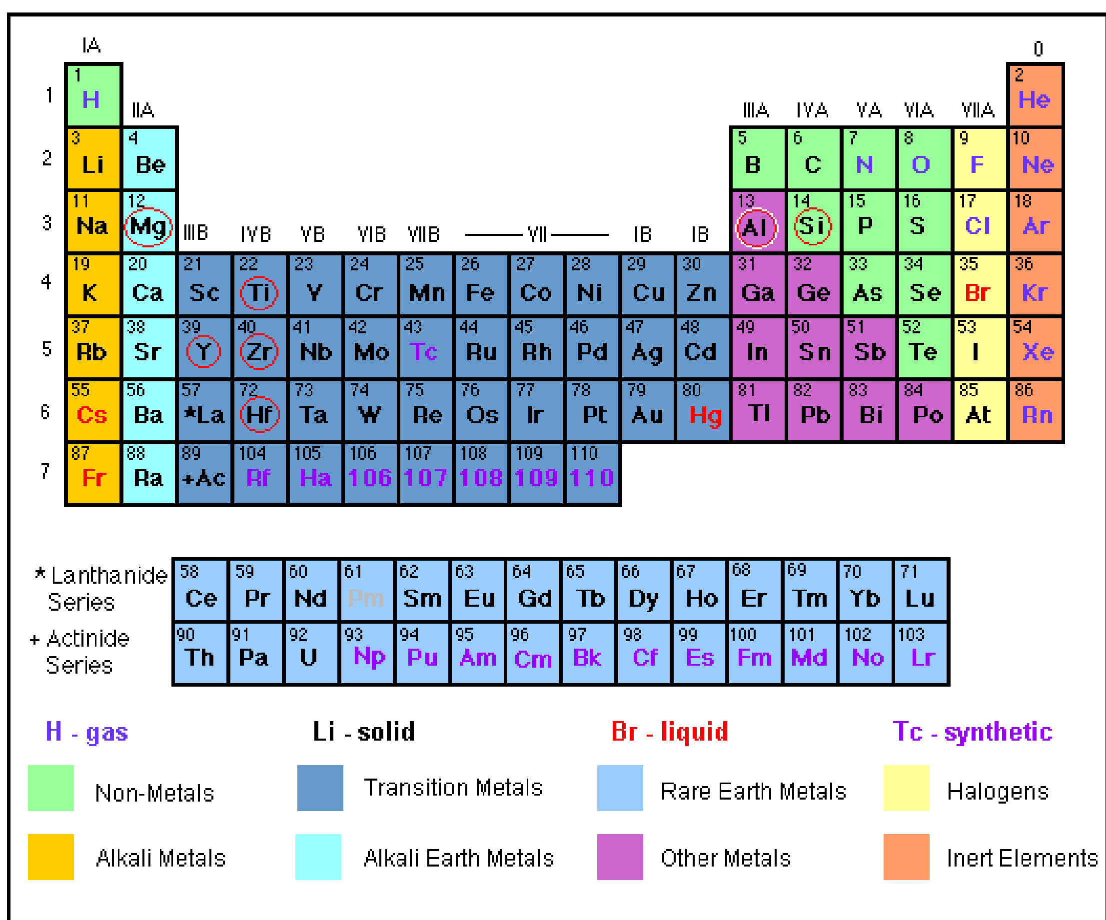

Figure 16. *The selected elements for this thesis marked with circles.*

There are many possible choices when examining the periodic table, but most useful high index oxides are in the transition groups. It was impossible to select everything so a best guess was made for the selection of oxides. The oxide in IIB and IVB were chosen because they are lying close to Ti, have good optical properties and a reasonably high index. It was thought these might be able to be a replacement for Ti. Mg was also selected but its oxide has slightly too low refractive index but can be useful in special filter designs demanding intermediate index material. The oxide of Al has also slightly too low index to replace TiO_2 but was also interesting to evaluate due to the same reason as for MgO. MgF_2 was also selected even though it is used as low index material. Since SiO_2 is used in the filter stack it was also selected. There were several other interesting oxides that could be evaluated but due to limited time it was not possible to test them. For example the oxides of Nb and Ta are interesting since they also have reasonably high index Ta_2O_5 shows very low absorption in the UV and is suitable for making UV filters [62].

2.11.1 MgO

MgO has some use as intermediate index material in optical coatings, for example in anti reflection coatings. The index is ca 1.70 at 50 °C substrate temperature and 1.75 at 300 °C, at a wavelength of 550 nm [63]. It has to be evaporated in an e-gun where it sublimates [64]. It has good transmittance in the visible region from 190 nm to 6 μm therefore it is an attractive UV material. It forms hard and dense layers [65]. At higher substrate temperature it becomes more crystalline. MgO can be evaporated without background oxygen pressure but an added O_2 pressure of $1x10^{-4}$ torr will result in lower absorption in the UV.

One problem with MgO coatings is that it reacts slowly with CO_2 in the air and produces a hazy surface, therefore using MgO as the front surface of multilayer coatings has to be avoided.

MgO is a weak alkaline oxide and it dissolves in acids (see Figure 17). Powder MgO reacts with water and forms $Mg(OH)_2$ but its solubility in water is low. It is also soluble in ammonia [66]. Mg exists in oxidation state 0 or II only.

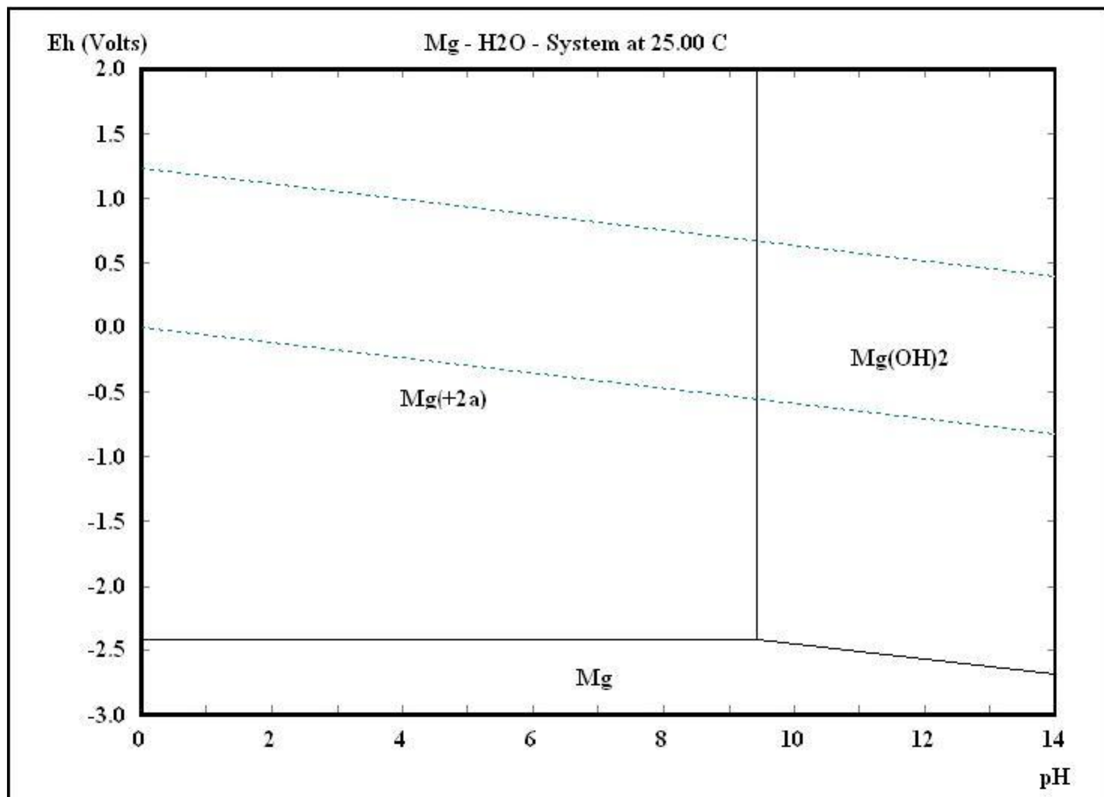

Figure 17. *Pourbaix diagram simulated at 10mM for Mg. As seen there is a large pH interval where it is soluble in H_2O. At pH>9.5 there is passivation.*

2.11.2 Al_2O_3

Al_2O_3 has a refractive index of 1.62 at 600 nm when deposited at 300 °C [67]. It has very little absorption in the range from 200 nm to 7 um. It dissociates very little under evaporation but some oxygen back pressure in the chamber can be beneficial. It must be evaporated from an e-gun. It can produce very dense hard layer with almost 100% packing density [68]. The thin film has very good adhesion to silver but if it is used as protective coating SiO_2 or some other moisture barrier must be on top because Al_2O_3 act as a very bad moisture barrier [69]. Al_2O_3 is an amphoteric oxide and it is possible to dissolve it in both acid and basic solutions (see Figure 18).

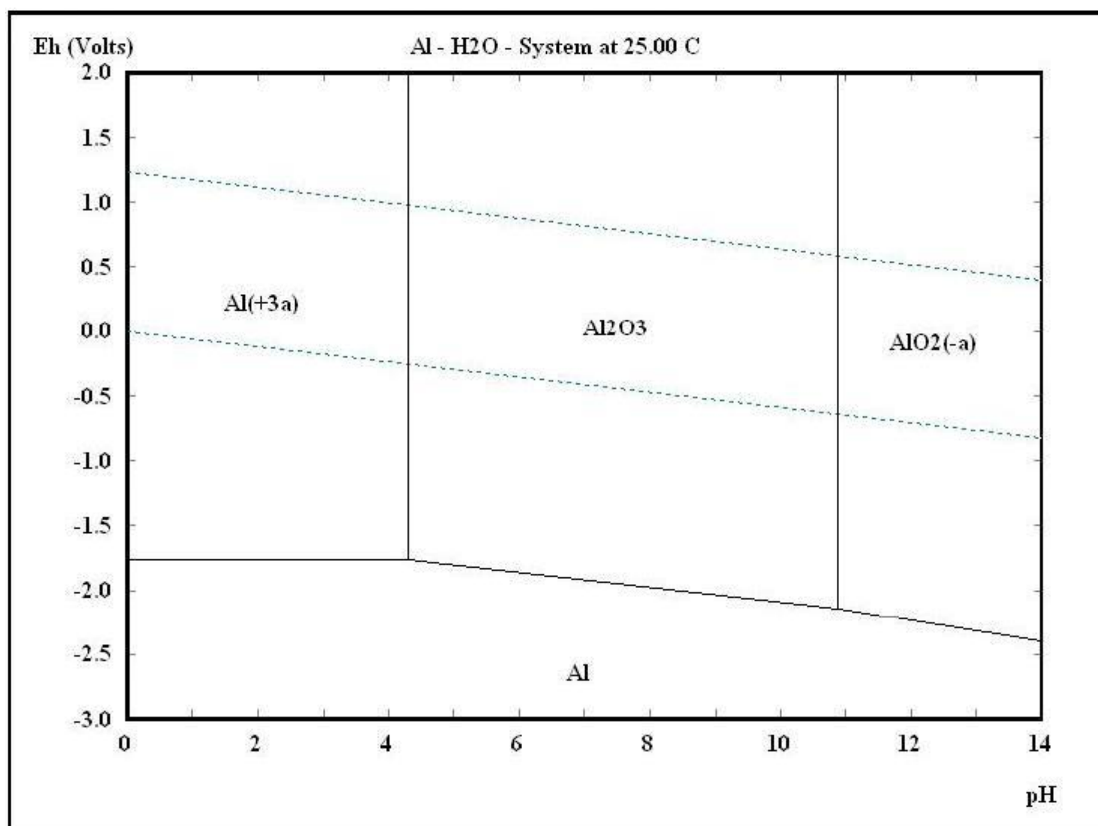

Figure 18. *Pourbaix diagram of Al at 1 mM. As seen Al_2O_3 is stable between pH 4-11.*

In reality amorphous Al_2O_3 does only dissolve in HF and phosphoric acid but not in H_2SO_4. Also it does not dissolve in 30% NaOH. Crystalline Sapphire annealed at >1000 °C is not soluble in HF [70]. The only important oxidation state is III. Oxidation state II has been observed in high altitude grenade explosion residue by aluminium containing explosives [71].

2.11.3 TiO_2

Ti, Zr and Hf belong to the same group and have a successively larger mass. With Ti as the lightest atom, they all share similar chemical properties. TiO_2 is a very popular high index material and is frequently used in almost all kind of optical filters. The refractive index is 2.2-2.42 depending on process conditions [72]. It is transparent in the visible, but shows slight absorption in Near UV and IR especially if Ti is not fully oxidized to IV and is therefore most suitable in visible applications. It is easily evaporated from an e-gun but dissociate heavily to the most stable form which is Ti_3O_5 [73]. The TiO_2 melts completely in an e-gun crucible and it is common to use an insulating liner of molybdenum to contain the melt. In order to re-oxidize the evaporated oxide into its oxidation state IV an oxygen background pressure is introduced in the process.

TiO_2 is an amphoteric oxide which means it is soluble in acids and bases (see Figure 19) [74]. It can occur naturally in three different crystal forms: rutile, brookite and anatase [75]. There are several oxidation states for Ti: 4, 3 and 2 but the most common is IV and only oxidation state IV gives colourless compounds. Oxidation state I has been observed as TiH in hollow cathode lamps [76]. It is easy dissolved in boiling Sulphuric acid [77] and by catalytic etching with H_2O_2 as mentioned in chapter 2.4.4.

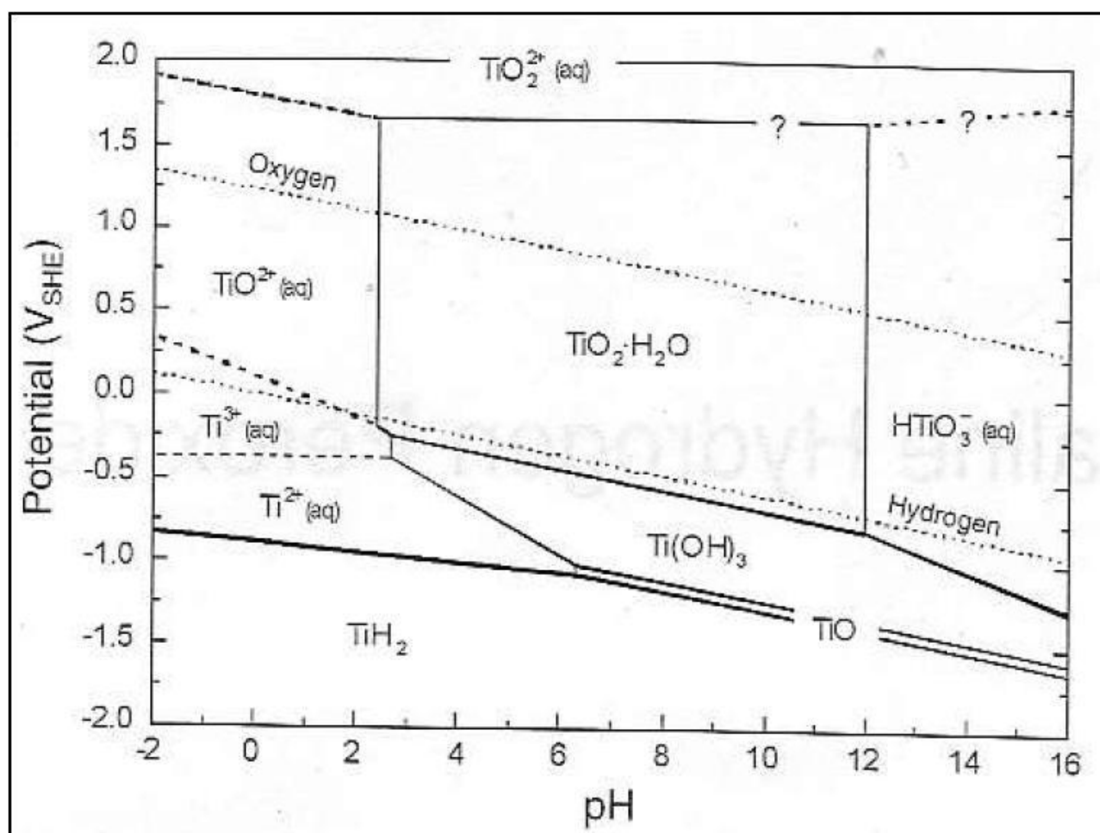

Figure 19. *Pourbaix diagram of Ti at 1 uM [42].*

In reality a thin film TiO_2 is very difficult to wet etch if it is deposited on substrates at >300 °C. In that case the most frequently used methods are various kinds of plasma etching techniques where etching rate up to 2000 Å/min is possible [78].

2.11.4 ZrO_2

ZrO_2 has a refractive index of ca 1.95 and a low absorption from 250 nm-10 µm. It slightly dissociates under e-beam evaporation, so background O_2 pressure is important in order to grow non absorbing coatings. It is preferably evaporated by an e-beam source from a graphite liner where it melts [79].

Hf is always present in findings of Zr. Zr metal have a thin ZrO_2 passivation layer which is even more efficient than TiO_2. This is why Zr is very popular in alloys in demanding applications such as in nuclear reactors where it withstands corrosion very well. The oxide is amphoteric (see Figure 20).

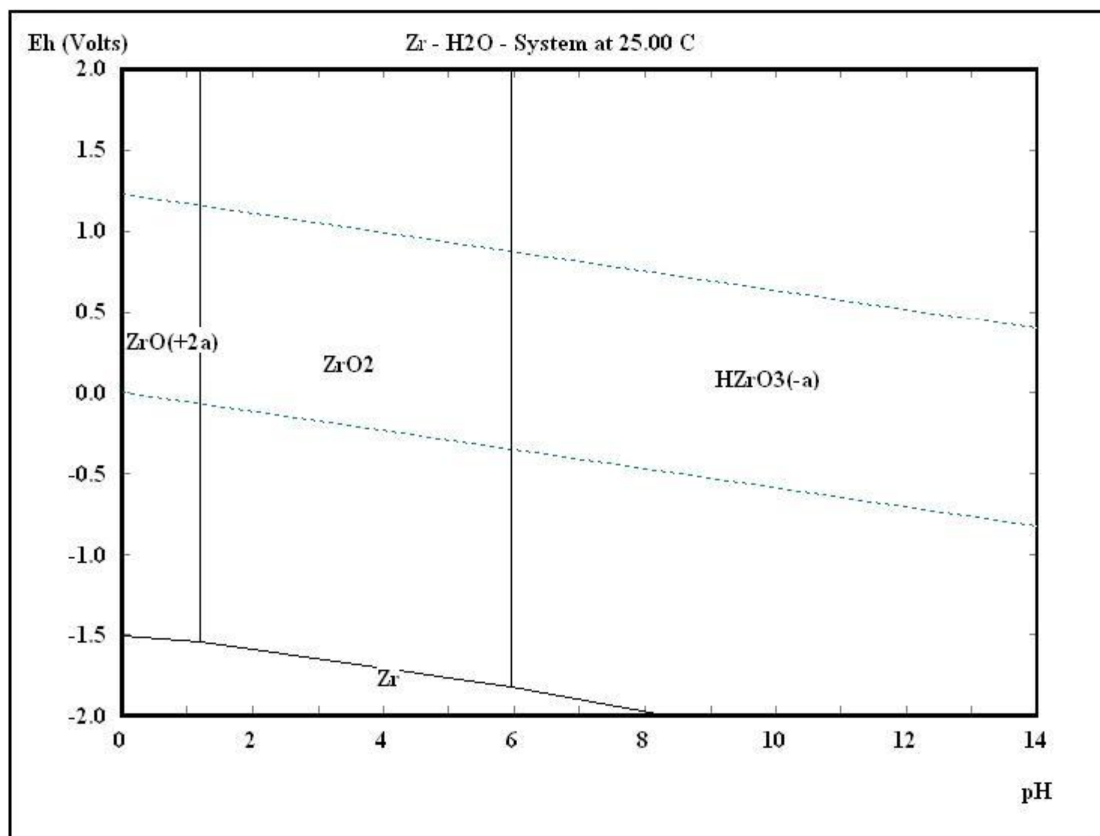

Figure 20. *Zr Pourbaix diagram at 1µM.*

ZrO_2 thin films tend to be inhomogeneous but can be stabilized by adding some other oxide. It can be made more stable with small amounts of Y_2O_3 in the coating, yttiria-stabilized zirconia (YSZ). This compound is of interest in corrosion resistant coatings [80]. IV is the common oxidation state but III and II exist also. Some successful etchings have been achieved by MOCVD techniques [78]. The etching mechanism is explained by HF attack on the surface Zr-OH bonds leaving a Zr-F bond and H_2O. The etching rate is rather low, at best 450 Å/min on MOCVD deposited ZrO_2 [81]. Zr metal is resistant in boiling H_2SO_4 at less than 70% concentration and in HF [82]. Boiling 20% HCl can attack Zr metal. It should be noted that thin Zr films behaves differently compared to bulk Zr.

2.11.5 HfO_2

Hf was discovered as late as in 1922. HfO_2 is interesting as a high index material for UV filter applications since the absorption is low down to ca 220 nm. The refractive index is ca 1.9 at 500 nm. The refractive index is 2.15 at 250 nm and 250 °C substrate temperature. The coating is fairly hard. The most dominant oxidation state is IV. HfO_2 is amphoteric but more alkaline compared to TiO_2 (see Figure 21).

HfO_2 must be melted carefully in a liner to avoid tunnelling, see 2.11.7 and will slightly dissociate, so therefore a slight background O_2 pressure is needed to get fully oxidized and absorption free HfO_2 coatings. At low substrate temperatures the coating is porous and it is recommended to evaporate under elevated temperature conditions in order to get high packing density [83].

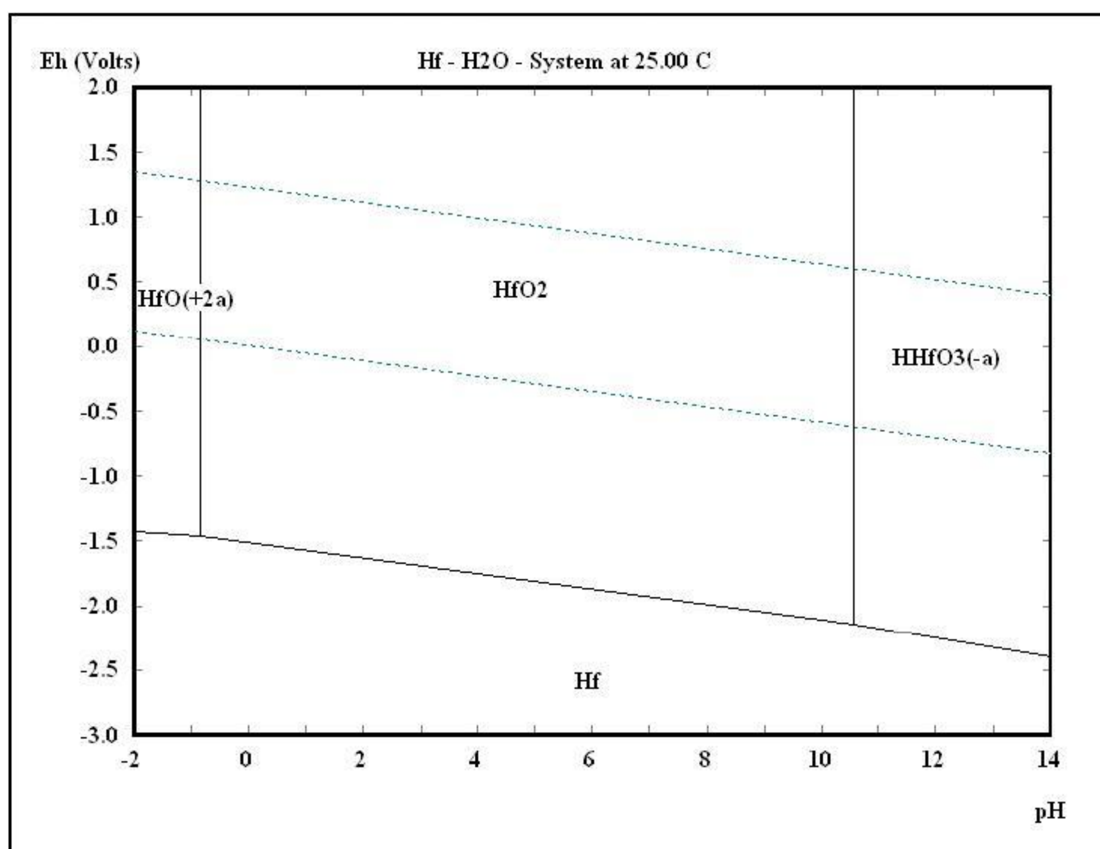

Figure 21. *Pourbaix diagram of Hf at 1 uM.*

Very little is mentioned about solubility in the literature but it is probably slightly tougher against attack compared to Ti. Since Ti can be dissolved in boiling H_2SO_4 it is likely Hf should be that also. There have been some studies by wet etching of HfO_2 since it is an interesting replacement for SiO_2 as gate material in semiconductors. Some success has been achieved in etching MOCVD deposited HfO_2 films were etching rates up to 178 Å/min has been recorded in HF solutions [81]. It should be noted that the material can behave completely different under other deposition conditions.

2.11.6 Y_2O_3

Y_2O_3 is an intermediate index material with refractive index of 1.8 at 550 nm and it is useful from 300 nm-14 µm. It has to be evaporated from a graphite liner where is sublimes, and it behaves like most other oxides by dissociating slightly when evaporated [84].

The oxidation state is exclusively III [85]. Y_2O_3 is an amphoteric oxide slightly more alkaline and should be soluble in acids [86].

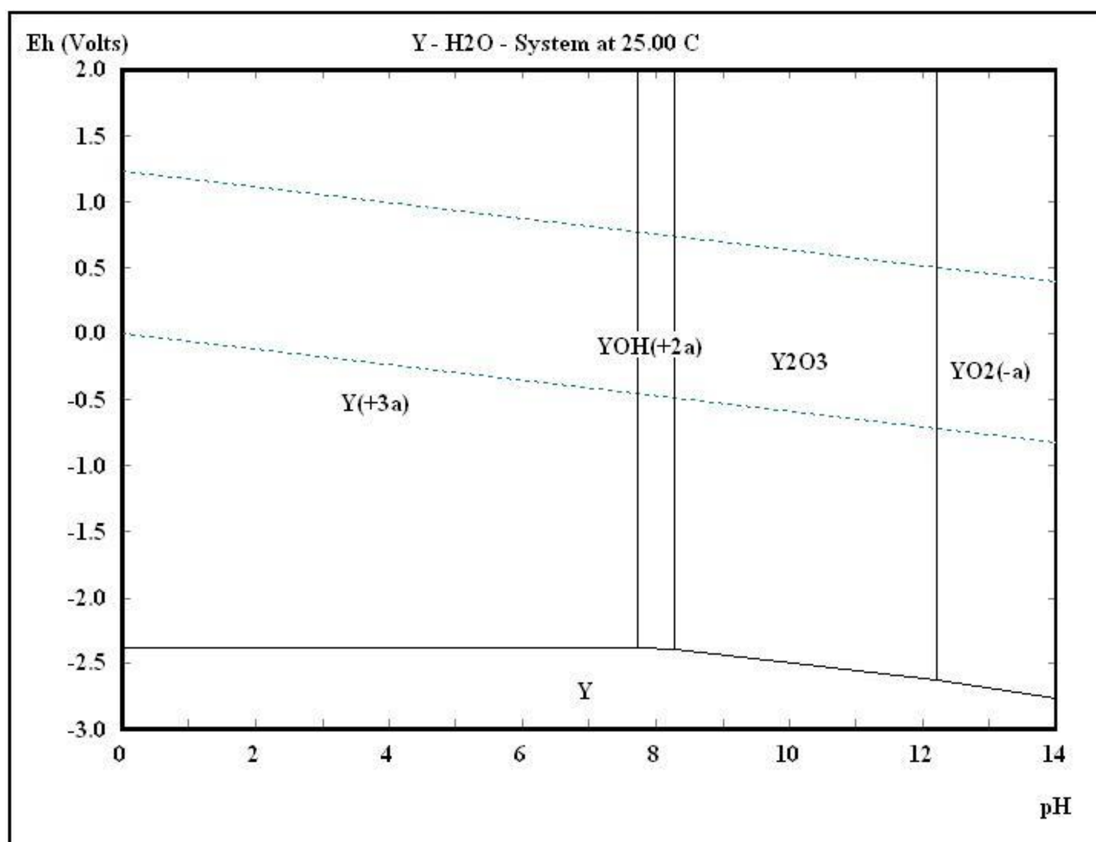

__Figure 22.__ Pourbaix diagram of Y at 100 mM.

As shown in Figure 22 the concentration is very high with a wide pH range of soluble ions. This could be an indication that it actually is slightly easier to dissolve the oxide in acid compared to TiO_2. The Pourbaix diagrams for Ti, Zr and Hf are simulated at much lower concentrations, 1 µM still with very limited pH range.

Very little is mentioned in the literature of the etchability of Y_2O_3 for thin films.

2.11.7 SiO_2

SiO_2 is extensively used as a low index material in many applications. Its refractive index is 1.46 at 550 nm and can be made transparent from 200 nm - 3 um as a thin film. It is completely amorphous and must be evaporated by an e-gun. I will slightly dissociate but it is not always necessary to add oxygen in the coating process. It will sublimate and the source is subjected to problematic tunnelling when evaporated, this means the e-beam digs a hole in the SiO_2 and makes evaporation uneven [87, 88, 89].

SiO_2 is an acidic oxide indicating it is soluble in alkaline solution, (see Figure 23A). It can be dissolved by boiling NaOH giving a Na_2SiO_3 solution. It is soluble both in HF and in alkaline solutions [90]. The HF chemistry is very well known due to the massive use in the semiconductor industry as mentioned in chapter 2.4.2. Oxidation state 4 is the most stable but oxidation state II also exist as SiO. This has also been used as coating material since SiO is easier to evaporate form a thermal source. The disadvantage is a slight absorption in blue. Etching rate can be as high as 1500 nm/min in 10:1 solution of HF for CVD type SiO_2. The solubility of Si increases dramatically when fluoride compounds are added at low pH (see Figure 23B). Fused quartz has an etching rate of 26 nm/min [91].

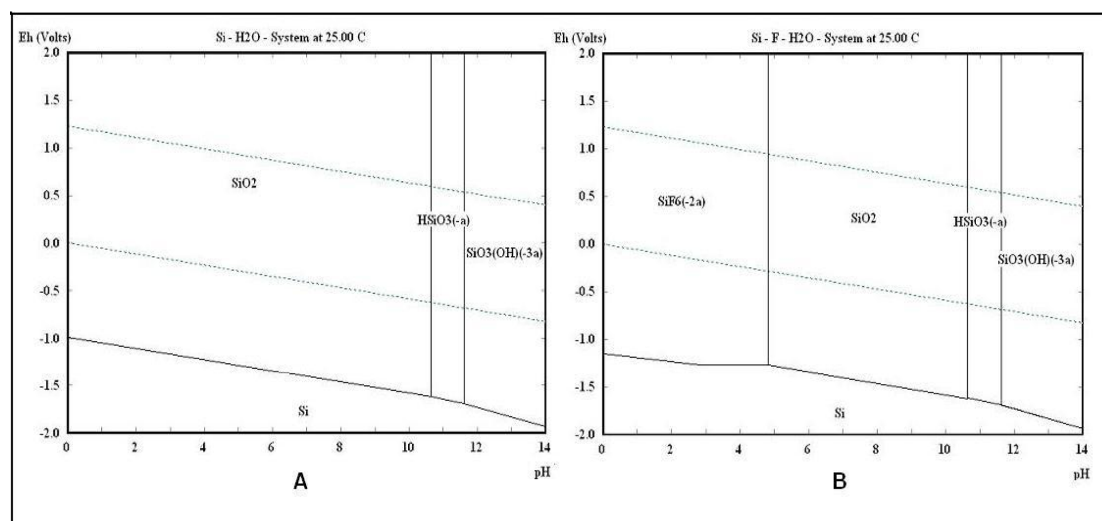

Figure 23. *Solubility of Si at 1mM (A) and solubility when [F]=100mM is present (B). Note the soluble SiF62- in the region pH 0-5.*

SiO_2 is even slightly soluble in cold water, 11 ppm at 25 °C, however this is a very slow process, mostly of interest in a geological perspective [92].

Etching of silicon can be used by a mixture of nitric acid and HF. The nitric acid oxidizes Si into SiO_2 which is soluble in HF. A pure HF-solution does not etch Si, therefore this is a very good selective etch in cases were it is of interest to etch SiO_2 coatings on a silicon wafer and the underlying Si substrate should not be damaged.

2.11.8 MgF_2

MgF_2 is one of the lowest index materials making it very popular in anti reflective coatings. It has a refractive index of about 1.39 when deposit at 300 °C. This results in rather hard and dense coatings. Deposition at room temperature results in very porous and useless films easily wiped off with a finger. It has very good UV-transmission down to 120 nm and is transparent up to 7 um. Evaporation is easily done in a thermally heated tungsten boat, but can be evaporated by e-beam [93]. One major disadvantage for MgF_2 films is the high tensile stress making it difficult to produce multilayer coatings.

It is not possible to simulate MgF_2 and create Pourbaix diagrams due to lack of solubility data. The solubility for $MgCl_2$ is 72.7 g/100 ml compared to zero for MgF_2. This huge difference between the chloride and fluoride is probably due to the difference in ion size and stronger Mg-F bonding. It is also soluble in HNO_3 and slightly in acids [94].

3 Experiment

3.1 Production of the thin films

All thin films were produced by PVD with in a BAK 550 box coater with a planetary system. Evaporation of the materials was done by an electron beam gun. The samples were manufactured in fall 2008 in Lint, Belgium (see Figure 24). The thin films were deposited on polished Si wafers and 1 mm thick borofloat glass from Schott. For the stress measurements, 0.1 mm thick borofloat glass was used as substrates. In each batch, all three substrates were coated simultaneously. The layers were made relatively thick, 2000-5000 Å, in order to make the etching observations easier and to be able to find the refractive index and thickness T_P.

***Figure 24**. A retrofitted Balzers BAK 550 box coater with completely new interior and computer controller. All coatings used in this thesis were produced by this machine.*

10 different samples were fabricated in the first series.

Identity	T1	S1	S2	Z1	Z2	Y1	H1	A1	M1	MF1
compounds	TiO_2	SiO_2/Al	SiO_2/Al	ZrO_2	ZrO_2	Y_2O_3	HfO_2	Al_2O_3	MgO	MgF_2

***Table 1.** Compounds grown in the first test series.*

All 10 thin films were grown at a substrate temperature of 325 °C. The evaporation properties differed slightly among them, but the best known evaporation parameters were used shown Table A1. The thin films S1 and S2 were grown with an 80 Å thick aluminium interface layer as an endpoint layer for easier etch rate determination.

Five additional complete magenta filters were also fabricated, M200-M325 processed at substrate temperatures between 200–325 °C. These filters were fabricated at relatively high O_2 pressure. Another magenta filter called N250 was also added in the study. This was processed at lower oxygen pressure at 250 °C. from a standard production batch in the late 2009. The N250 filter was used in the later stage of the study to evaluate etching performance.

3.2 Physical characterization of the thin films

The 10 different single layer thin films in the first series produced at the late 2008 were characterized by ellipsometry and by transmission spectral curve fitting, respectively. The refractive index n, physical thickness T_P, thermal behaviour and stress were thus evaluated.

3.2.1 Ellipsometric measurements

The ellipsometric measurements were done on a SE-400 Sentech instruments equipped with a HeNe-laser which generates light at a wavelength of 632 nm. For each measurement, three different incident angles were selected for the laser thereafter computer software calculated the most probable reflective index and thickness. It was very important to keep the surface as flat as possible and the alignment of the substrate was critical. Measurements were done only on the thin films deposited on Si-wafers. Coating S1 and S2 could not be measured because both contained aluminium layers underneath.

3.2.2 Transmission spectra

By the measurements from a spectrophotometer in the range of 200-900 nm, it was possible to make curve fitting for each coating in order to match a simulated curve from the TFCalc software. The curve fitting models were optimized around 500 nm and the surrounding wavelengths were not fitted equally well due to the dispersions of the thin films. The information was still enough to find the thickness T_P. This method resulted in more reliable values compared to the ellipsometric measurements. It was also possible to extract dispersion data but these calculations were not done.

3.2.3 Surface profilometry

The physical thickness was measured by a Tencor Alphastep 200 stylus profilometer. In order to measure the T_P, some minor areas of the Si wafers was covered by pieces of thin aluminium foil during deposition. Thereafter the aluminium pieces were removed, creating sharp edges on the thin films. The stylus could then travel over these edges to find the T_P.

Because this instrument was not well-calibrated, this part of the measurements was not carried out for all the thin films. Only three measurements were done on Y1 and one measurement on Z2.

3.2.4 Thin film stress

Borofloat glasses with a thickness of 0.11 mm and 48 mm in diameter were coated with the selected compounds from Table 1. By observing the resulting curvature, it was possible to measure the internal stress of the films. A very simple setup was used where the test pieces were placed in front of a pinhole with a cross mark. By observations through the pinhole at different distances to the substrate, it was easy to find the radius of curvature of the substrate.

The surface stress caused a curvature of the substrate and created a focal point. This focal point could easily be found by the pinhole. By turning the substrate, so a concave surface always was directed towards the pinhole, both compressive and tensile stress could then be measured.

3.2.5 Thermal shift

In order to measure the thermal shift, two spectra were taken from each coating. The first spectrum was taken at room temperature. After that the sample was heated to 300-320 °C, the second spectrum was then taken 10 minutes after this condition has reached. The spectral shift caused by the heating was recorded. This gave a rough indication about the thermal stability of the filter. In the case of a multilayer filter, the shift was measured at a point in the spectrum where the transmission was at 50 % at the right cut-off. In the case of a single layer filter, the shift was measured from a local minima and a local maxima point.

3.2.5.1 Thermal shift of single layers

This test was done in order to see if there were any differences in thermal shift between T1 and S1. The same type of spectra as shown in attachment Figure A9 and A10 were recorded at room temperature. Thereafter the samples were heated to 320 °C for 10 minutes. The peak waves λ_P shifted after the heating procedure and was recorded, giving the thermal shift values. The observed shift from each measured peak from 419-810 nm was normalized to 600 nm for easy comparisons.

3.2.5.2 Post thermal annealing

The Drix M200-M325 and N250 magenta samples were thermally treated in order to see if post annealing could improve the long term thermal stability. Even if the material was un-etchable after post annealing, this test could reveal the possibility of future improvements for etchable thin films. The tests were performed by measuring the thermal shift before and after a heat treatment in an oven for a specific period of time. The change of thermal shift was then recorded.

First test

One M325 sample was first measured at the starting period and then placed in an oven set at 500 °C. Before each shift measurement, the sample was allowed to cool down to room temperature. The thermal shift was measured at 320 °C after 10 minutes of heating. The resulting values were not normalized since the shift was close to 600 nm. 6 measurements were taken under a period of 144 hours. The time for the samples to cool down before each measurement was not specified in this test and could vary.

Second test

In order to get a more consistent reading, samples from M250 and M325 were baked at 420 and 500 °C for up to 148 hours. All samples were cooled down and soaked in de-ionized water at 20 °C for a couple of minutes and then blown dry with pressurized air prior each measurement. The data were taken on both 50% transmission flanks on the spectra around 460 and 630 nm. Values were normalized at 600 nm.

Third test

Even more care was taken in this test compared to the first and second test. It was performed around 12 November 2009 and it was done with one from the latest magenta production, N250, containing lower oxygen pressure in the coating process.

The post annealing was done at 350 °C for 36 hours. Prior to each shift test, the material was settled to room temperature then soaked in water for at least 10 minute then blown dried in pressurized air and let standing in air for 3 hours before each measurements. A spectrum was recorded and the sample was heated to 300 °C for 10 minutes before each reading. The shift was normalized at 600 nm.

3.3 The in-situ etching instrument

A simple but reliable etch cell was constructed of PMMA. The complete instrument can be viewed in Figure 25. The inside width of the etching cell was 10 mm and the sample was placed in the centre by a holder in the lid. It was then possible to quickly insert the sample in the cell filled with etching liquid. A fibre spectrometer of the type Ocean optics USB2000 was used with a multimode fibre with a numerical aperture of 0.22. The distance from the tip of the fibre to the thin film surface was 20 mm which gave an active measurement diameter of 9.7 mm on the sample. It was difficult to have any smaller area due to the construction but it was believed that the etching uniformity was at an acceptable range.

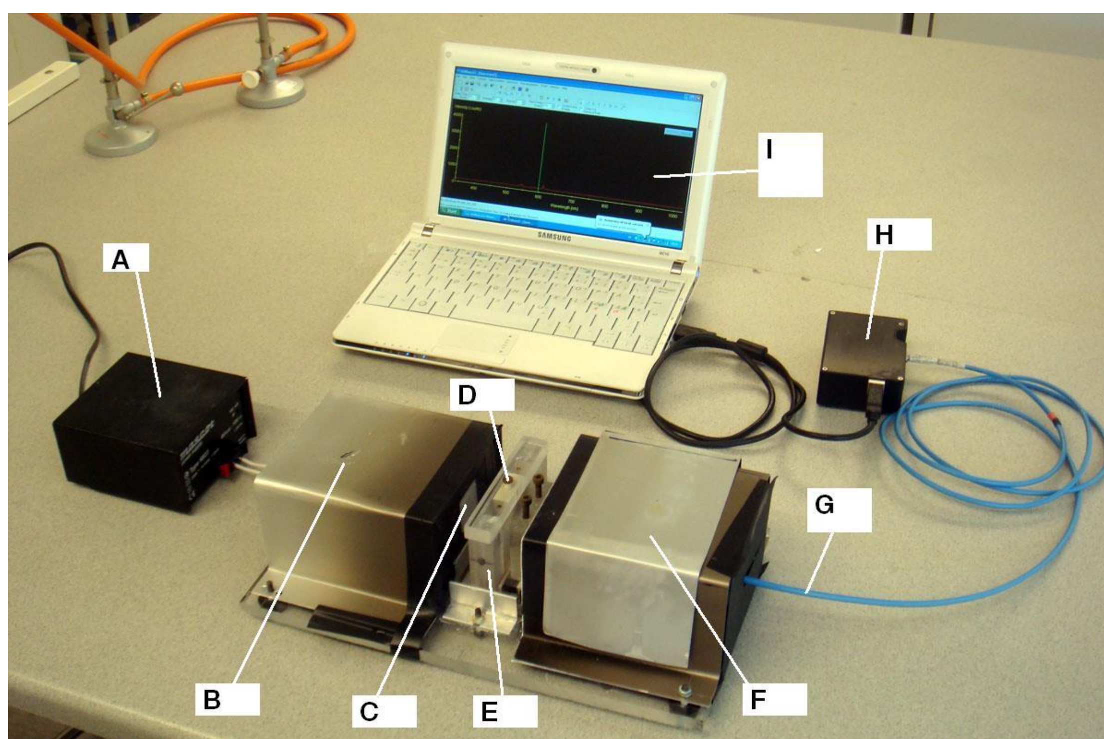

Figure 25. *The etching cell. A 12 V power supply (A) is connected to a halogen lamp (B), this illuminates a diffuser (C) in order to get uniform light, slightly seen as a square, In the middle the etching cell (E) with lid (D). The optical fibre (G) is pushed as close as possible to the etching cell window and is connected to a fibre spectrometer (H) and a computer with software for sampling of spectra (I). A removable cover (F) protects the measurement form stray light.*

The inner dimension of the etch cell was 41x10x56 mm giving a volume of 22.9 cm^3. The total thickness of the cell was 16 mm.

3.4 Etching tests

3.4.1 Etching tests of multilayer coatings

The M225-M325 and the N250 magenta filters were evaluated in terms of etchability in 3% HF.

3.4.1.1 HF etching of magenta filters

An etching test with 3% HF was used to evaluate the five different magenta samples, M225 to M325. The etching time of a complete filter was determined by visual observations. The etching behaviour was also observed.

3.4.1.2 In-situ etching measurement vs simulation

A series of spectra were recorded at a sampling frequency of 0.5Hz from 400-900 nm under a complete etching sequence of the magenta filter N250 in 3% HF solution. The idea behind this experiment was to evaluate whether it was possible to simulate matching spectra for a complete etching sequence or not. The simulation model was done by TFcalc by calculating 19 different thin films with one top layer removed for each simulation. This would then correspond to an assumption that the real etching would remove one layer at a time.

3.4.2 Etching test of single layer oxides

The single layer coatings, both on borofloat and Si wafers from the first test series (see Table 1), were cut in small pieces about 2x2cm in side. These pieces were tested in a wide variety of etchants.

3.4.2.1 TiO_2, HfO_2 and ZrO_2

All three oxides from group IVB was evaluated in such a way that it was possible to make comparisons among them.

First test

T1, H1 and Z2 coated on borofloat glass were exposed for 10 minutes to 77 % H_2SO_4 at a temperature of 170 °C in a reflux boiler. Visual inspections were made in order to analyze the etching result. Glass substrate could be used since this did not dissolve in the etchant.

Second test

The three samples of T1, H1 and Z2 were exposed for 30 min in 77% H_2SO_4 at a temperature of 96 °C. Spectra were taken both before and after etching and the wavelength shift was noted in order to calculate the amount of material etched away. The etchant was heated in a boiling water bath.

HF etching

1) 3% HF solution was used on Z2 and H1 coated on Si-wafers and visual observations were made. An etching test with 5% HF solution was performed on T1 coated on Si-wafer for comparison.

2) Concentrated HF (47%) was tested on Z2, T1 and H1 on silicon substrate and visual observations were made.

Catalytic etching of TiO_2

T1 (TiO_2) on glass was tested by catalytic etching in 9 different solutions containing 10 ml 34% H_2O_2 and 0, 0.1, 0.2, 0.5, 1, 2, 4, 5, and 10 ml conc. HN_3 in each solution. Water was added to give 20 ml total volume in each solution. The pH was measured with a calibrated standard pH-glass electrode. Etching time was 6 minutes for all samples. Since the solution rapidly decomposed, it was impossible to etch through the whole coating. Spectra were taken before and after each etching test and the etching rate was calculated from the measured spectral shift caused by the changed thickness of the thin film.

Catalytic etching of ZrO_2 and HfO_2

One sample from T1, Z2 and H1 coated on Si-wafers were etched for 2 hours in a solution consisted of 34 % H_2O_2, conc. NH_3 and H_2O in a ratio of 2:1:1. Visual observations of the etching were made.

3.4.2.2 SiO_2

First Test

Because SiO_2 have an index close to the borofloat substrate index, a very thin layer of Al ca 80 Å thick with a transmittance in the range of 20-70% was present between the substrate and the SiO_2 coating. This improved the spectral reading. One S2 sample was etched in 3% HF for 5 seconds. The coating was quickly dipped in the solution thereafter quickly rinsed with water. One spectrum was taken before the etching and one after. Spectra were taken when the coating was dry. The reason for this procedure was that water with a refractive index of 1.33 makes the interference weaker on the thin film. The measurements in air improved the measurements.

Second Test

One sample of S2 was etched by 3 % HF solution for 19 s. The etching was recorded in-situ and the sampling frequency was 1 Hz for the spectra. Nine of the most interesting curves were selected for the analysis.

Third Test

A sample of the S2 coating on borofloat glass was etched in 0.5% HF solution. The etching time was measured by visual observations.

Fourth test

This test was done to show the difference in morphology between the aluminium layers from the S2 coating and a sputtered standard aluminium coating. A 5000 Å thick coating from Drix was etched in a 2 % HF solution. The etching rate was calculated from visual observation.

Fifth test

A sample of the S2 coating on borofloat glass was baked at 500 °C for one day in an oven. Visual observation was made.

3.4.2.3 MgO

First test

A M1 sample was etched in 6.0 M H_2SO_4 solution and the etching time was measured. One sample was post baked in an oven for 24h at 500 °C and the etch time was measured. Both tests were performed on borofloat glass.

Second test

M1 coated on borofloat glass was used as a case example for the evaluation of the in-situ etching instrument. A sample of MgO was etched in a 3.0 M H_2SO_4 solution and several spectra was recorded with a sampling frequency of 0.5 Hz. Five different transmission curves were selected. By comparing the measured curves with the simulated curves from the TFCalc software, the thickness could be calculated and the etch rate could be determined at 4, 8, 12, and 16 seconds.

3.4.2.4 Y_2O_3

First test

Several different acids were tested on Y1 coatings on Si wafers. One sample was tested in 20 % HF solution. Y1 was also etched under hydrochloric acid (HCl) of two different concentrations, 4 and 0.3 M, respectively, in order to see if the etching rate had a linear relationship with the concentrations. 6.0 M H_2SO_4, 3% HF and 6.0 M NaOH solutions were also tested. In all these tests, the etching rate was recorded by visual observations.

Second test

It was discovered that the presence of HF in the etchant inhibits the reaction on Y_2O_3. Therefore, a test was performed in order to see how the etching rate was inhibited by HF. Three different concentrations of HF at 0, 0.24 and 0.48 % with 2.0 M HCl was used in a etching test on Y1 coated on Si-wafer. Visual observations of the etching time were made.

Third test

The idea behind this test was to see if the HF would form some compound with the Y_2O_3 surface preventing further etching in acid.

One sample of Y1 coating on Si wafer was treated with concentrated HF for 60 seconds. The sample was rinsed with water then etched in 2.0 M H_2SO_4. The etching time was recorded. One sample was etched directly in 2.0 M H_2SO_4 and the etching times were compared.

3.4.2.5 MgF_2

Samples of MF1 coated on Si wafers were etched with 6.0 M H_2SO_4 for 20 minutes, concentrated HF and 6.88 M NaOH for 5 minutes, all done at room temperature.

3.4.2.6 Al_2O_3

Samples of A1 were exposed to concentrated H_2SO_4 at room temperature and to 57 % H_2SO_4 at 85 °C for 13 minutes. A1 was etched with concentrated HF and BHF where etch time was observed.

A peroxide etching test was made on one A1 sample with an etchant consisted of 34 % H_2O_2, concentrated NH_3 and H_2O in a ratio of 2:1:2.

A sample of A1 was etched with 5.88 M NaOH and observations were made.

A1 was coated on Si wafers in all these tests.

3.5 Etch matching of Y_2O_3/SiO_2

The discovery that HF inhibits the etching process of Y_2O_3 in an acidic solution gave the idea to find a matching pair of oxides with equal etching rates. Since the etching rate of Y_2O_3 reduces when increasing the HF concentration (See section 4.2.3.4 Second test) and the etching rate of SiO_2 increases linearly with the HF concentration (see section 4.2.3.2, third test), there should exist a concentration point where they both intersect. The idea behind this experiment was to find this concentration point.

Six different solutions of different concentrations of HF at 0, 48, 96, 140, 190 and 240 mM were prepared and the concentrations of H_2SO_4 were 6.0 M. Six samples from S1 and six samples from Y1 coated on Si wafers were immersed into solutions of the individual concentrations and the etching time were recorded by visual observation. Two graphs were calculated from the knowledge of their thicknesses.

3.6 Etching rate of photoresist

Two tests were performed on the photoresist, i.e. Fuji OIR908-35 2.5um spin coating. In general, positive photoresist withstand acids reasonably well, but it starts to dissolve in an alkaline solution.

First test

The goal of this experiment was to determine the alkaline pH limits in which photoresist starts to dissolve into the solution. In order to have a safe limit, the etching rate of the photoresist should not be faster than the etching rate of the underlying thin film. There should be enough safety margin in order to achieve good etch performance without undercutting. If the limit is set to 10 minutes exposure in the etchant, the acceptable etching rate of the photoresist would be 40 Å/sec before the etchant will reach the underlying coating which it is protecting. This value should only be considered as a guideline and a safety margin should be chosen.

The samples were immersed in three solutions containing 96.5, 150 and 251 mM of NaOH under constant stirring. The setup was shielded from all UV light in order to avoid exposure of the photoresist. The time for complete dissolution of the photoresist was recorded.

Second test

One sample of photoresist was immersed in a concentrated NH_3 solution and the behaviour of the photoresist was observed.

4 Results and discussion

4.1 Characterisation of the thin films

4.1.1 Ellipsometric measurements

Ellpsometric measurements were more difficult to master when the thin films were too thick. Z1 was probably incorrect for this reason (see Table 2).

Coating		index, n	Tp/Å	Remark
A1	Al2O3	1.642	5081	Very stable
H1	Hf2O3	1.965	2760	
Y1	Y2O3	1.77	4260	Very stable
Z1	ZrO2	1.979	10345	Uncertain
Z2	ZrO2	1.87	2420	Stable
MF1	MgF2	1.376	4364	Stable
MGO	MgO	1.714	4190	
T1	TiO2	2.26	4644	

Table 2. *Ellipsometric results with physical thickness T_P in Å.*

As mentioned in chapter 2.10.1 the thin films were assumed to have none absorbance and was only measured on Si-wafers.

4.1.2 Transmission spectral fitting

There was a sharp dip around 300-350 nm in the measured spectra (see attached Figures A1-A10). This did not make any difference in the curve fitting model since the fitting was done only at 500 nm.

Coating	Compound	Index, n	T_P /Å
A1	Al2O3	1.64	5022
H1	Hf2O3	2.01	2748
Y1	Y2O3	1.79	4350
Z1	ZrO2	1.86	5524
Z2	ZrO2	1.97	2398
MF1	MgF2	1.38	4529
M1	MgO	1.71	4488
T1	TiO2	2.35	4487
S1	SiO2	1.46	7363
S2	SiO2	1.46	7020

Table 3. *In these measurements the SiO_2 thicknesses (S1 and S2) could be easily measured even though a thin aluminium layer was present.*

As seen in Table 3, most T_P values are well-fitted within the ellipsometric measurement except Z1. It is believed the Z1 value is more reliable in the present fitting, see chapter 2.10.2.

4.1.3 Surface profilometry

The thickness of Y1 was measured three times with the resulting values of 4000, 4000 and 3900 Å.. Z1 was measured a single time with a thickness of 2200 Å. See chapter 2.7.3 for the theory behind this method.

These values are considered as an aid to support the correct values for the spectral fitting. The values are in reasonable good proximity to the values estimated by the optical fitting method.

4.1.4 Thin film stress

The radius is positive if the substrate is concave and the thin film is faced towards the observer. A positive value leads to tensile stress, and a negative value compressive stress. The smaller the radius, the higher the stress level it will be.

Material		radius/cm
MgF2	MF1	50
MgO	M1	-30
HfO2	H1	280
TiO2	T1	300
SiO2 (1)	S1	200
SiO2 (2)	S2	200
Al2O3	A1	170
Y2O3	Y1	220
ZrO2 (1)	Z1	300
ZrO2 (2)	Z2	300

***Table 4**. Results from the thin film stress measurements.*

Most coatings showed weak tensile stress, see Table 4, but the radius was so large that was difficult to measure. The stress was believed to be in a range where multilayer coatings are possible to be made. There were no calculations done for the stress but equation 2.12 in chapter 2.9 can be used to find the values. MgF_2 showed very strong tensile stress and should be avoided in multilayer coatings. MgO should also be avoided in multilayer coatings since it showed very strong compressive stress.

4.1.5 Thermal shift

Since there was only one measurement from each of the samples in the post thermal annealing test (4.1.5.2) the results in this part were not statistically sounded. Therefore, the post annealing test, gave somewhat an unclear result, still showed an indication of thermal stability of the tested thin film materials. However, the measurements on several points in a single acquisition in the thermal shift for a single layer coating (4.1.5.1) gave a better statistical proof on each specimen.

4.1.5.1 Thermal shift single layer

The shift seemed to be the same over the whole visible spectra for both S1 and T1, but the shift in S1 coating were almost double in comparison to T1.

S1 shift			T1 shift		
λ_P /nm	Shift/nm	n-shift/nm	λ_P /nm	Shift/nm	n-shift/nm
419	15	21.5	438	6	8.2
464	16	20.7	474	6	7.6
509	17	20.0	525	9	10.3
595	18	18.2	589	12	12.2
655	24	22.0	679	14	12.4
810	15	(11.1)*			
Average		20.5			10.1

Table 5. *Thermal shift for SiO_2 (S1) and TiO_2 (T1). * The shift at 810 nm could be contributed to measurement error. The n-shift was the normalized value at 600nm. λ_P was the measured peek of the waves.*

The reason why the wavelengths reduced when heated could be explained by the evaporation of the absorbed water from the porous coatings and caused a lower refractive index. This could be an indication of the packing density of the coating. It seems that the TiO_2 had a slightly better packing density compared to the SiO_2.

4.1.5.2 Post thermal annealing

It proved to be very difficult to measure the post thermal annealing changes because small errors in handling of the samples could affect the measuring result. The first test was done on a very rudimentary basis, the second was a failure. But the results did show some interesting observations. The third and the last test were done with great care and with a much better precision.

First test

As seen in Figure 26, there is a clear trend in these measurements towards lower shift. It should be pointed out that there is no statistics involved, but there is a reason to believe that the trend is shifting to a low level with a longer baking time.

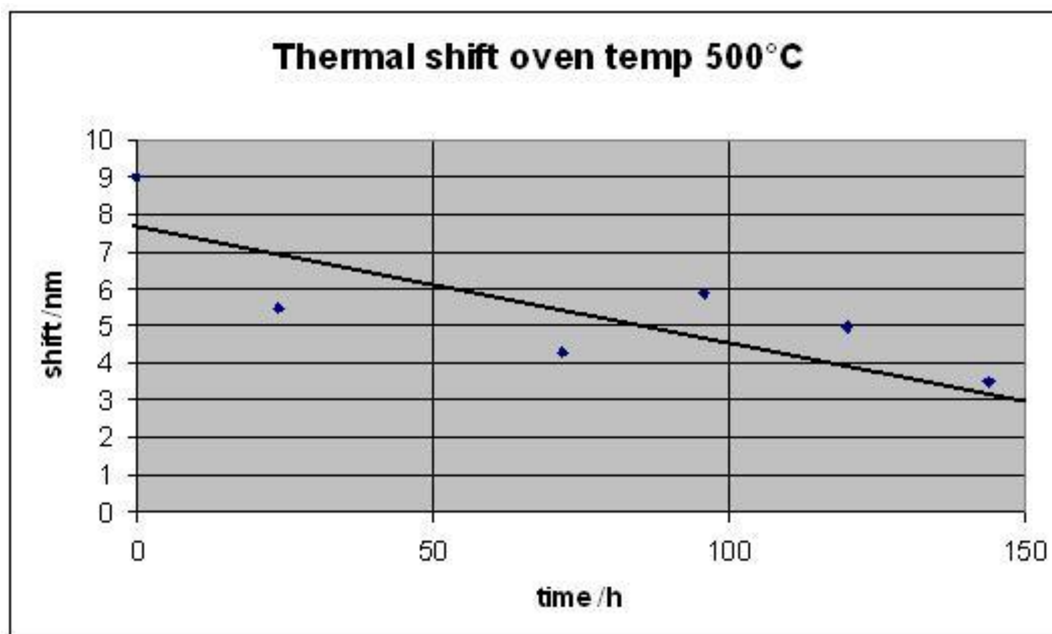

Figure 26. *The graph shows a trend down with less thermal shift.*

In a 24 hour annealing test, it showed that the shift was completely reversible if it was measured again directly after being cooled down because the spectra got back to its original position. The long term post annealing seem to be irreversible probably due to change of the morphology in the coatings, see chapter 2.8.

Second test

There was no clear trend in this test and it was difficult to interpret the result from these measurements even though efforts have been made in order to improve the way the samples were handled. However, observations showed that the sample developed cracks on the thin film surface after 48 hours at 500 °C. Very fine microscopic fractures, around 0.5-1mm long in size, were found all over the surface. This finding is important since it indicates possible limitations at too high temperatures.

Third test

This was a more successful post annealing test.

A very clear trend can be viewed in Figure 27 where the N250 coating showed improved thermal shift stability even after an hour post annealing period. The dramatically improvement in shift stability was due to changes in the thin film growth process or due to better handling of the sample, but the change is too large to be explained only by random statistics.

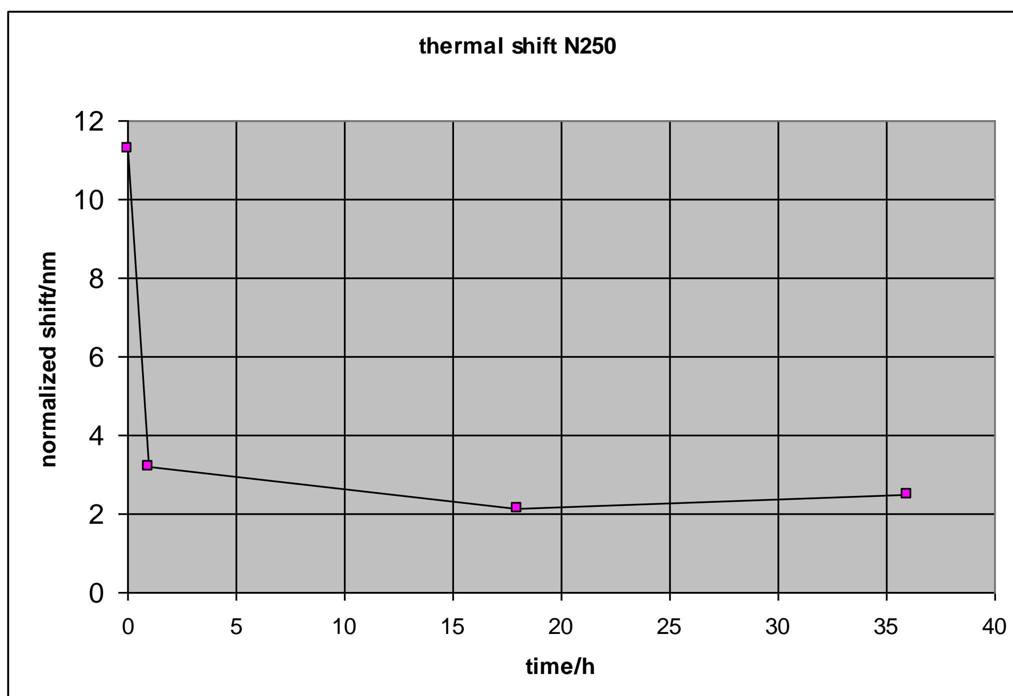

Figure 27. *Post annealing test for magenta filter N250.*

4.2 Etch tests

4.2.1 HF etching of M225-M325 magenta filters

In all cases from sample M225 to M325 the SiO_2 layers etched away quickly and left behind a residue of TiO_2, which was more or less slowly etched away depended on the substrate temperature in the coating process. This correlates well with the TiO_2 Pourbaix diagram in Figure 19 and the more easily soluble SiO_2 Pourbaix diagram in Figure 23.

coating	T_S °C	T_1/s	T_2/s	λ_S /nm
M200	200	8	30	9.2
M250	250	10	30	9.04
M275	275	10	110	7.5
M300	300	16	Non etchable	8.8
M325	325	22	Non etchable	7.3

***Table 6**. The wavelength shift λ_S is normalized at 600 nm and T_S is the substrate temperature in the coating process.*

The data in Table 6 is showing the etching times T_1 and T_2. The time T_1 corresponds to the point when there was only a grey soft residue left. The time T_2 indicates the complete removal of all coating with no residue left. T_1 could be interpreted as SiO_2 etching time even though etchant are penetrating through the layers and therefore will not give corresponding etching rate for single layer SiO_2. However, there is a clear trend in longer etching time for both T_1 and T_2 until sample M275 where the coating become very difficult to etch due to a huge etching rate difference between TiO_2 and SiO_2 that caused lots of grey residues. There would be no residue at all if the etching rate for SiO_2 is equal to the etching rate for TiO_2. But, this was never the case in any of the samples.

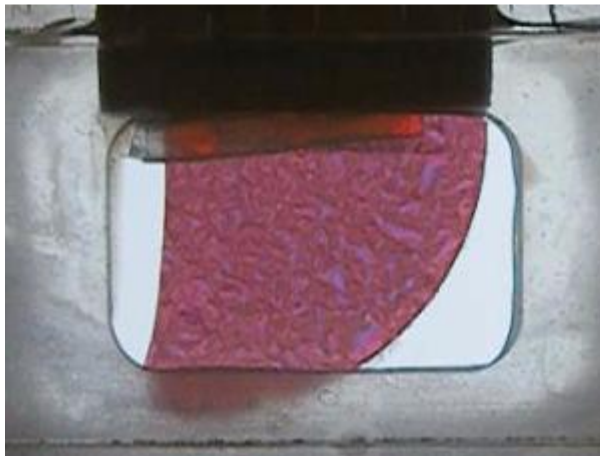

***Figure 28.** Magenta material M275. This photo was taken under the etching process where the thin film had begun to peel off. There is still some colour present in the filter indicating interference from SiO_2/TiO_2.*

The thermal shift λ_S in Table 6 was also measured. There is a trend indicating a slight improvement of thermal shift stability but there is a demand for achieving much lower shifts close to zero in order to have a stable filter. This was not the case even for the M325 material indicating post annealing is necessary. These measurements clearly highlight the etching problems for the filters.

It was not possible to measure the in-situ etch spectra on these filter since the etching behaviour was so bad.

4.2.2 In-situ etching measurements of the N250 magenta filter

The two resulting graphs, one from the simulation (Figure 30) and one from the in-situ etching test (Figure 29) are compared with each other.

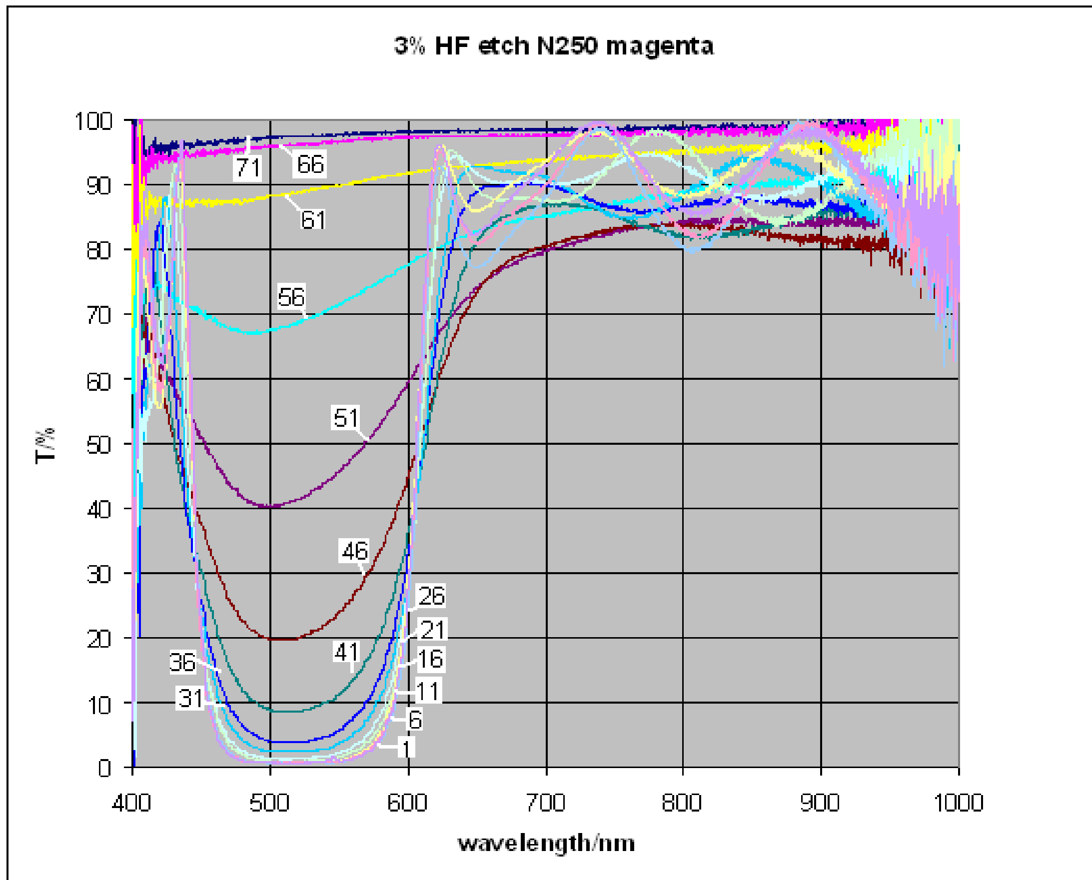

Figure 29. *This graph represents transmission through the layers for sample N250 Magenta filter. The number for each graph should be multiplied by 2 to get the time. Total etching time was 142 sec.*

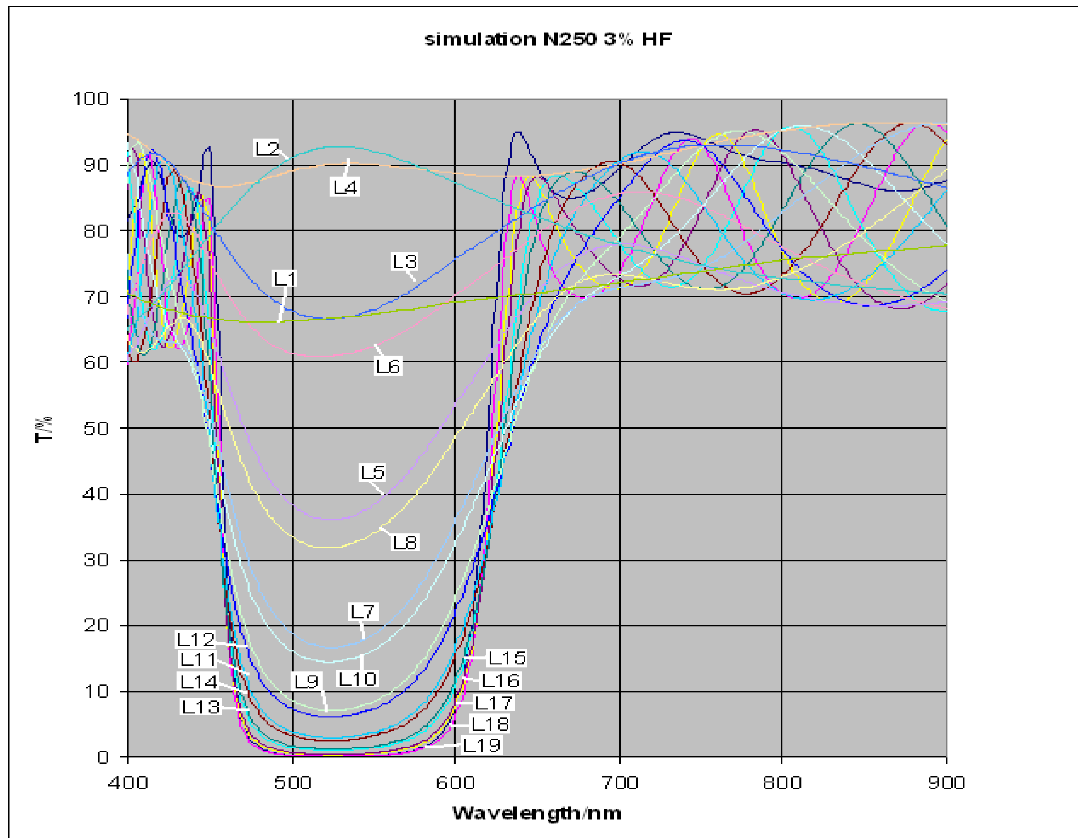

Figure 30. *Simulated spectra for an etching through 16 layers L1-L19, the number of curves is 19 because there were some double layer present.*

As seen in Figures 29 and 30, there is an efficient blocking of light from 470–610 nm. In both simulation and measured filter, the effect of blocking slowly reduced until the etching was complete. The simulation shows reasonably good agreement with the etching test. The wavelength range from 650-900 nm and 400-450 nm was under the whole etching phase through the layers reasonably transparent, >70% T. This also agrees with the simulations. However, the fine interference patterns in these parts are not similar. This is probably due to the fact that the etching was not removing layer by layer, but going through several layers in parallel. This made it very difficult to find equal graphs in the etch test as in simulation because of this non-linear etching behaviour. This is the reason why the numbers of curves are not the same, 19 for the simulation and 17 for the measured spectra. Even if 19 curves would have been selected they would not match better.

Figures 29 and 30 should only be viewed in a broader perspective not the fine interference pattern in the high transmission parts. Under these circumstances they both behave in a similar way.

4.2.3 Single oxides etching results

4.2.3.1 TiO_2, HfO_2 and ZrO_2

The multilayer filters M225-M250 growth at a substrate temperature of ≤ 250 °C was possible to etch. However the single layer thin film of T1 was only available grown at 325 °C. This T1 thin film was almost impossible to etch at room temperature. The only etchant which is possible to use at room temperature is peroxide and the reaction rate is actually slow.

First test

It completely dissolved the coating for T1 (TiO_2) and Z2 (ZrO_2) but left a very thin residue for HfO_2 on the surface. It is clear that HfO_2 is the toughest material among them withstanding aggressive acid attacks. See Pourbaix diagram Figure 21 in chapter 2.11.5.

Second test

Table 7 shows the calculated etching rates for the three oxides in H_2SO_4. There was is clear trend in increasing the difficulties to etch at higher atomic numbers. The value for H1 is very uncertain since the shift is in the range of 1-2 nm.

Material		Etching rate/Å/s
T1	TiO2	0.244
Z1	ZrO2	0.048
H1	HfO2	0.005

Table 7. *Group IVB oxides etching rate in hot* H_2SO_4.

It is not possible to use such etching conditions together with photoresist since it would decompose rapidly, but the etching test showed the extraordinary corrosion resistant properties of each of the tested materials.

HF etching

1) T1 in a 5% HF solution for 7 minutes showed zero etching rate. The Z2 coating flaked heavily after 20 seconds and dissolved after ca 30 minutes. H1 flaked heavily after 3 minutes and the residue was unaffected. Indicating no etching process was present.

2) In concentrated HF, the Z2 flaked heavily after 10 sec and was completely dissolved after 20 sec. HF is attacking ZrO_2 as mentioned in chapter 2.11.4 but the process is slow. H1 showed heavily flaking after 2-4 minutes, thereafter visible powders formed which dissolved after 1 hour. For the T1, uniform etching was in the first 9 minutes and flaking started afterwards. After 2 hours, only small residue left on the surface.

Several tests were made with many different mixtures of HF and other acid mixtures, but in all cases, etching was very bad and leaving flakes and unsolved residues at the end. The etching rate was low for concentrated HF and was not possible to use. ZrO_2 seems to be more easily dissolved in HF comparing to TiO_2, and HfO_2 is the most resistant of all. ZrO_2 always resulted in the worst of "flaking" This bad etching made it impossible to do any in-situ measurements in any cases.

Catalytic etching of TiO_2

The resulting etching rate as a function on pH can be viewed in Figure 31. This follows the prediction made in chapter 2.4.4 where high pH is mentioned for the reaction to occur. There is a very clear trend that the etching rate drops to zero at pH 7.7. The etching rate seems to be flattened above pH 10. This was probably due to the decomposition of H_2O_2 which begun to evolve oxygen at this rate which was indicated by vivid bubbling in the solution. The etching rate is however far too low to be used in practice even at the highest rate at pH 10.

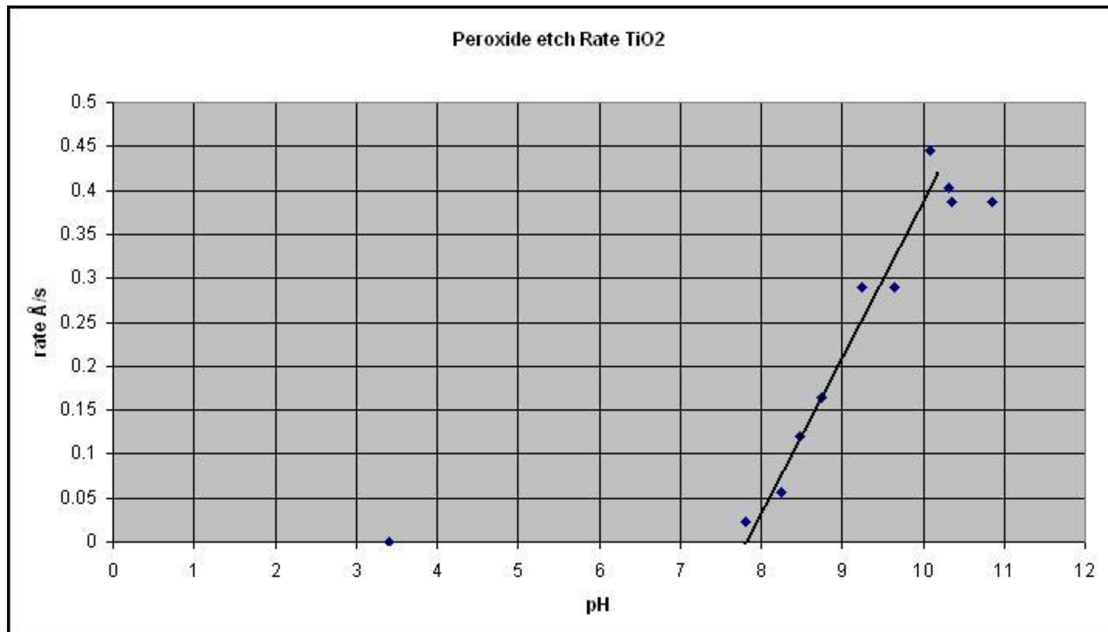

Figure 31. *The etching rate as a function of pH, drops to zero at pH 7.7.*

Catalytic etching of ZrO_2 and HfO_2

There was no visible etching on the Z2 and H1 sample after exposure for 2 hours in the peroxide solution. The T1 sample showed a visual etching rate indicated by a colour shift on the coating. No etching rate was determined for T1. However, when the inspection was made after 24 hour, all coatings were gone for the T1 coating.

4.2.3.2 SiO_2

First test

As shown in Figure 32, the spectrum of the un-etched S2 sample has clearly a visible interference with the complete layer of SiO_2-Al layer. After 5 seconds etching, a very smooth curve is indicated and only a small portion of interfence reside is left as the absorption part. This shows that only the aluminium layer was remaining. It was assumed that all SiO_2 was removed by etching. The thickness of S2 found by curve matching was 7020Å and this gave an etching rate of 1.4k Å/s in a 3% HF solution.

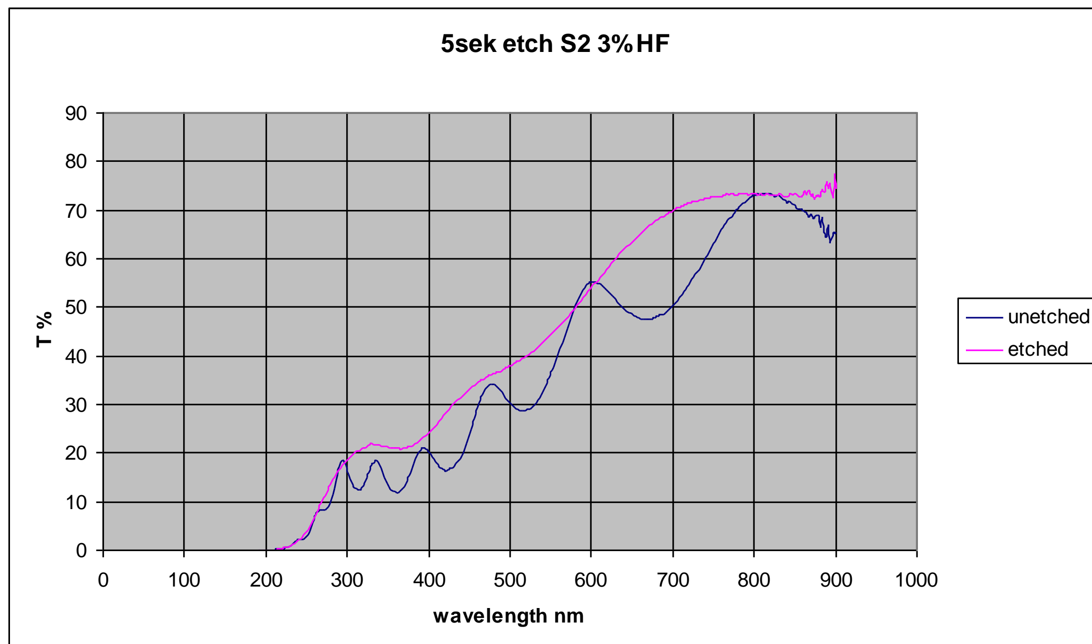

Figure 32. *Transmission spectra prior and after 5 s etching for S2 (SiO_2).*

Second test

When the in-situ etch measurements was performed, the problem was that there were very weak interference present. It was, however, possible to barely see when the underneath Al layer started to etch. As can be seen in Figure 33, the curve at 0 sec shows weak interference and the curve at 4 sec shows no remaining interference, but the curve is on the same position as the 0 s curve. This indicates that all the SiO_2 is etched away after 4 sec. This would give an etching rate of 1700 Å/s. This is in good agreement with the first test but higher than the values mentioned in chapter 2.11.7 indicating porous coatings. The curves from 6 to 19 s show the transmission of the 80 Å Al layer that is slowly etched away. This took about 15 sec. The etching of this Al layer had a rate of only 5 Å/s.

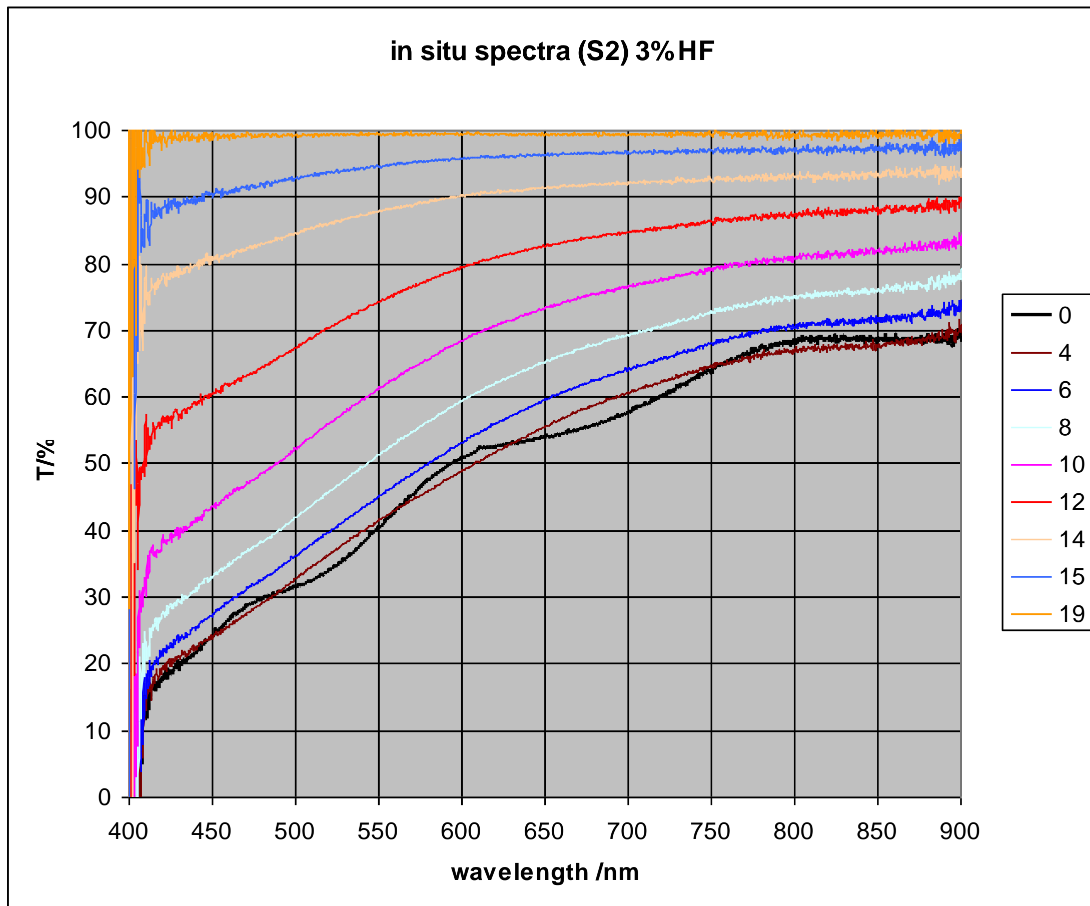

Figure 33. *Measurement from in-situ etching of S2. Each line represents time from 0-19 seconds. At 0 s, weak interferences are present but at 4 sec the line is completely smooth and indicates that only aluminium remains. From 6-19 seconds, the etching is progressed by raising the transmission until it becomes 100% T. The etching of Al is very slow even though it is only an 80 nm thick layer.*

Third test

The etching time for the removal of the SiO_2 layer on the S2 sample was 40 s and 130 s for the complete removal of both the SiO_2 and Al coatings. This means the etching rate was 175 Å/s for SiO_2 or about 1/10 of the rate compared to the first and second test. The HF concentration was 1/6 so it indicates the etching rate is reasonably linear with the HF concentration.

Fourth test

The 2 % HF solution etched the sputtered aluminium layer with an etching rate of 50 Å/sec compared to 5 Å/sec for the thin Al layer under in the S2 coating from the second test. Even though the HF concentration was slightly lower in this test it clearly indicates a completely different morphology compared to the S2 coating because of the large difference in etching rate.

Fifth test

It was observed that the aluminium layer became completely transparent and probably completely oxidized into Al_2O_3 after the sample had been baked for one day.

4.2.3.3 MgO

First test

MgO was found to be very easy to etch in H_2SO_4 the etching time was 20 s for complete removal of the thin film, resulting in an etching rate of 210 Å/s. The good etchability correlates well with the solubility in acids shown in the Pourbaix diagram Figure 17 in chapter 2.11.1. Baking of the thin film for 24 h in 500 °C gave an etching rate of 83 Å/s, still fast. It seems that the coating changed its morphology after baking.

Second test

The result of this test is shown in Table 8. The etching rates calculated for each times (4,8,12 and 16 s) was the averaging from zero in all cases. .Figure 34 shows the five selected transmission spectra from where the minima were picked out in order to calculate the etching rate. The result is the average rate and not the rate at the moment of interest. This is not important since it still gaves a clear view of the possibility to use the instrument for time resolved etching experiments. The etching rate seems to be slower in the beginning and then accelerates. This could be due to heating of the thin film and changes of the etchant composition close to the surface. It could be explained by Fick's law of diffusion, see chapter 2.3.4.1.

Time/s	λ minima/ nm	Simulated T_P /Å	etched mat/Å	Etching rate/Å/s
0	605	4420	0	
4	590	4310	110	27.5
8	565	4130	180	45
12	535	3920	210	52.5
16	490	3582	338	84.5

Tablet 8. *Etching rates in-situ etching of MgO in 3.0 M H_2SO_4.*

The reaction probably produced species which affected the chemistry and caused these etching rate changes. The etching rate from the first test was slightly higher, taking into account the different acid concentration. It is believed to be the same while considering it was a different experimental setup.

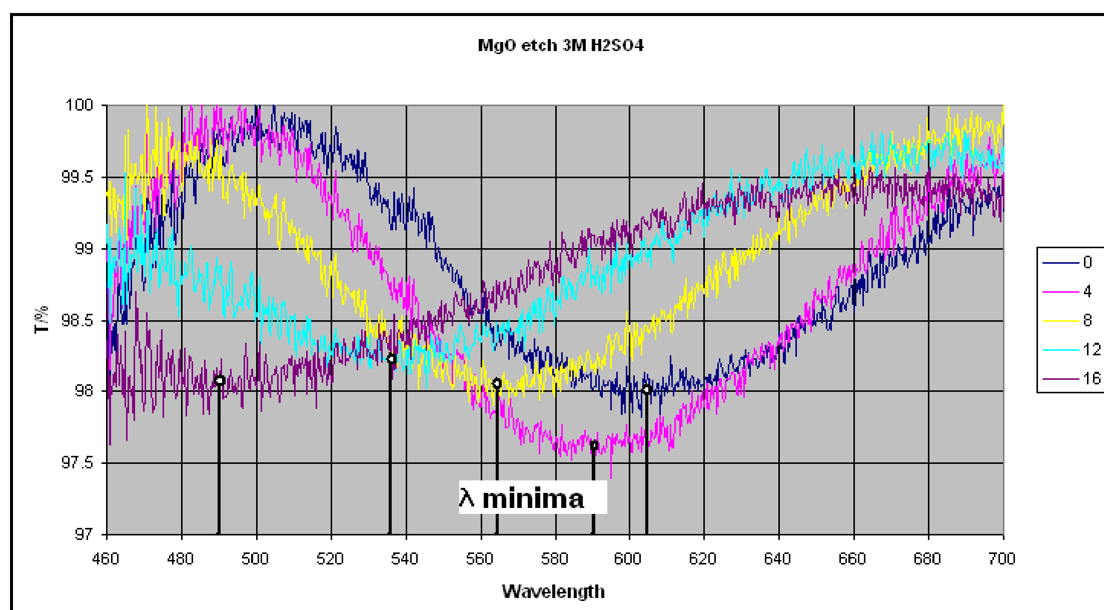

Figur 34. *In-situ etching of MgO in 3M H_2SO_4. The graphs show the etching time from 0-16 sec for 5 different recordings of the spectra under the process.*

4.2.3.4 Y_2O_3

First test

The sample etched in 20 % HF solution dissolved after 18 hours. The samples etched in 4.0 M HCl dissolved in 10 s giving an etch rate of 435 Å/s, and in the 0.3 M HCl solution, sample dissolved in 198 s resulting in an etching rate of 22Å/s. It seems to be reasonably for a linear relationship.

6.0 M H_2SO_4 gave an etch time of 16 sec, which is equal to a rate of 270 Å/s; 3% HF did not affect the Y1 coating at all. 6.0 M NaOH solutions did not etch the surface.

It should be noted that Y_2O_3 seemed easier to be solved in acids compared in alkaline solutions. It followed the rules of solubility for the oxides as mentioned in section 2.11.6. The etching proceeded very nice and evenly in all the acids with no flaking and peeling.

Second test

As seen in Table 9 the etching rate have a strong dependency of the HF concentrations in an acidic solution. A high concentration of HF slows down the etching rate dramatically. This discovery was used when etch matching was done with SiO_2 (see 4.2.4).

Conc HF / %	[HCl] / M	Etching rate/ Å/s
0	2	72.5
0.24	2	17.4
0.48	2	4.8

Table 9. *Etching rate for Y_2O_3 in presence of HF.*

Third test

The Y1 sample treated in HF solution had an etch time of 24 s and the sample which were not treated with HF had an etch time of 16 s. The differences are not obvious, but it could have affected the surface to make it withstanding the etchant better.

4.2.3.5 MgF_2

In the etch tests on MF1 with H_2SO_4, HF or NaOH, no detectable reaction could be observed. MgF_2 seemed to be difficult to etch.

4.2.3.6 Al_2O_3

A1 was difficult to etch with concentrated H_2SO_4. No visible change after etching was observed neither in the 85 °C 57 % H_2SO_4 nor the concentrated cold one.

Etching process completed within 20 sec in concentrated HF. BHF took more than 10 minutes and left a dirty residue.

The peroxide etch did not affect the surface at all.

The NaOH solution slowly etched the Al_2O_3 surface. There was no prominent surface change after 4 minute etching, but the coating was etched completely after 60 minutes.

It seems that HF solution is the fastest etchant for Al_2O_3 coatings.

4.2.4 Etch matching of Y_2O_3/SiO_2

The graphs in Figure 35 show the measured etching rates for both SiO_2 and Y_2O_3 in HF solution. At 0.11 M, the both graphs intersect at an etching rate of 20 Å/s. The rate at this point is slightly too low to be used in practice but this experiment was done only to show that matching pairs could be a manageable pathway for some oxides. See etching anisotropy in chapter 2.5.

The measured etching rate for the SiO_2 coating included the etching time of the underlying 80Å Al layer. It is not known what etching rate the Al layer had, but it was assumed that its etching rate is insignificant compared to that of SiO_2 at such a high concentration of H_2SO_4. Only the SiO_2 coating contained an Al layer. The real value of the etching rate with Al excluded should increase the slope on the SiO_2 graph in Figure 35 and would move the intersection point at slightly lower HF concentration. Even if the error was large, still, there would be an intersect somewhere between 0-0.11 M.

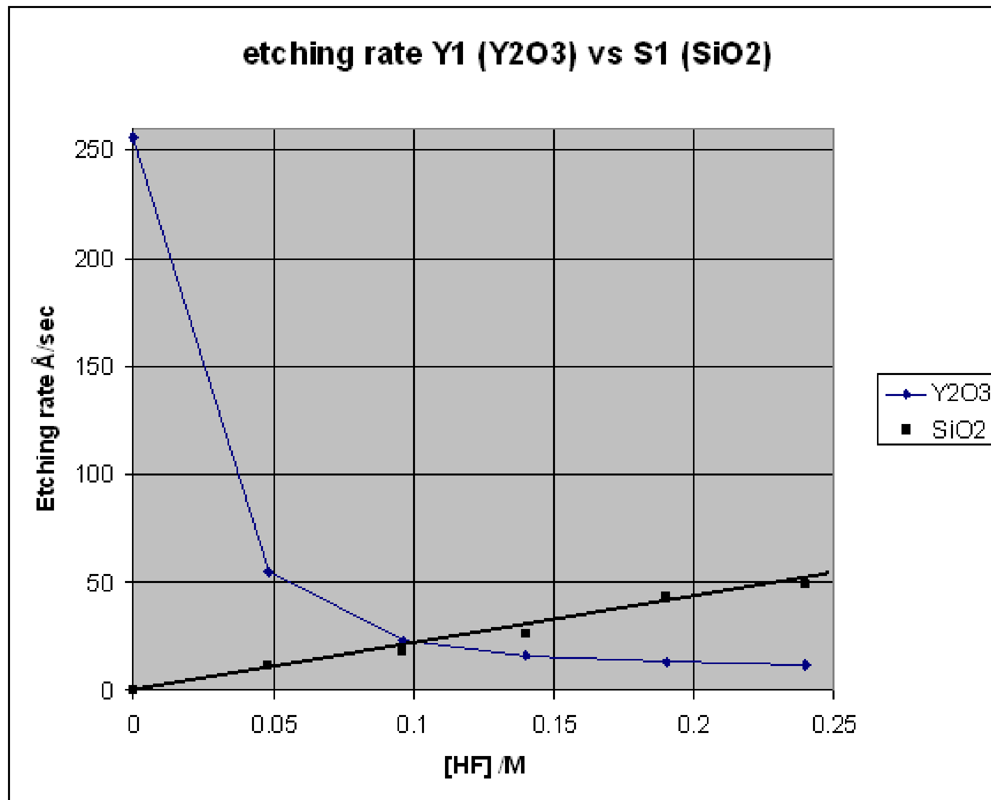

Figure 35. *Etching rate for SiO_2 and Y_2O_3 at different HF concentration and 6.0 M H_2SO_4. Samples from S1 and Y1 were used in this test.*

4.2.5 Photoresist etching

First test

The pH in the three NaOH solutions was calculated using Debye–Hückel model with a program called Chembuddy. The result is shown in Figure 36. Even though measurements were done only from three different concentrations, there seems to be a reasonably good linear relationship. The etching rate is slowed towards zero at pH 12.9. It should be possible to use the photoresist at pH 13 where the etching rate is 25 Å/s, see chapter 2.3.1.3 for the novolak photoresist chemistry. A common standard developer is 5.6 g/l NaOH solution. This would give a pH of 12.97 and an etching rate of about 25 Å/s which correlates very well to the measured value in Figure 36.

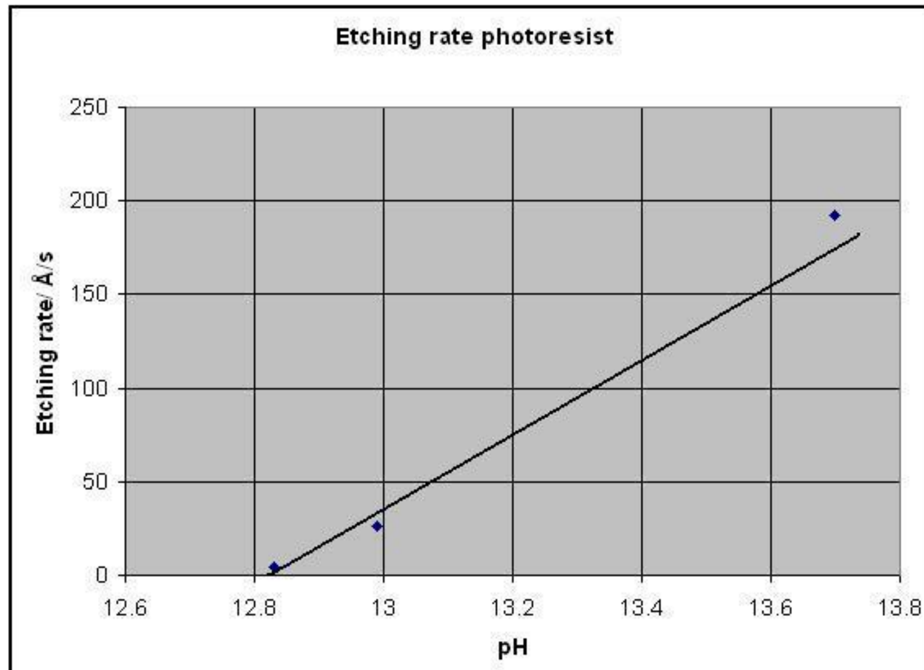

Figure 36. *This graph shows the etching rate of photoresist as a function of pH.*

Second test

The pH in the concentrated NH_3 solution was measured to 12.93. The photoresist coated on the sample did not dissolve, but slowly decomposed into a fragile solid compound after a couple of hours. This indicates that it should be possible to be etched in a slightly alkaline solution like ammonia. According to Figure 36, it is also within that pH limits.

5 Conclusion

There is a broad variety of experimental data from this investigation of the etchability of the oxides and it is not easy to present a unified result. One important conclusion is that, it is difficulties to etch TiO_2 at room temperature with any etchant. ZrO_2 has a low but measurable etching rate in HF solution, but not useful in practice because the coating is heavily damaged by HF etchants.

All the oxides of compounds from Group IVB have high refractive indexes and have high corrosion resistance. Hf is one of the most resistant oxides withstanding extremely corrosive environments.

MgO, Y_2O_3 and Al_2O_3 are reasonably easy to etch. However, the indexes for these oxides are too low to be used as a high index pair in most of the multilayer filter designs.

One interesting discovery is the inhibition of reaction on Y_2O_3 in acidic environment by the presence of HF. This is not yet studied in details, but the HF-inhibition of Y_2O_3 was successfully used to show the principle of etching rate matching for pairs of oxides.

Most of these results and graphs of etching rates are not statistically proofed and should therefore be treated in that way later on. But, it could become the guideline to show in which direction the composition should go for and as a guideline for further investigation. Most of these measurements are good enough.

One problem with the PVD grown thin films mentioned in this thesis is that small changes in the coating process can have a significant influence to the physical and chemical properties of the thin films. This is clearly shown in the etching behaviour of the M275 and M300 samples, where a 25 °C difference in the process temperature can drastically reduce the etchability of these filters

The evaluation of the in-situ etching rate instrument was successful and this thesis proved the method would be a very useful instrument. It was even possible to measure the changes of etching rates under a dynamic etch process as done for the MgO thin films.

It proves to be more difficult to monitor etching in a complete multilayer filter. But, this could be contributed by the extremely unsymmetrical etching rates for TiO_2 and SiO_2 in the samples. It will probably be easier to measure multilayer thin films which are composed of reasonably equally thin films in respect of etching rates.

The measurement of the etching rates of the photoresist was also successful. A good relationship was found to the pH that gave good knowledge of the pH limits to the photoresist. It was found possible to use photoresist in slightly alkaline solutions.

The measurements of the thermal shift stability of the filters are non-conclusive at present moment. But for sample (N250) it gave great improvements. This is an important tool for the future in order to develop a better etchable and thermal stable filter.

6 References

[1] B. E. Bayer, Color imaging array, US Pat. No. 3971065, 1976.

[2] Hecht, Optics, 3rd Ed., 1984, p377-432.

[3] A Macleod, Thin-film optical filters, 3rd Ed., 2003, p12-83.

[4] S. Gustavson, Dot gain in colour halftones, Linköping University, Diss. No. 492, September 1997.

[5] F. Flory, Thin films for optical systems, 1995, p17-19.

[6] A. Elshabini-Raid, Thin film technology handbook, 1998, p1:37-1:38.

[7] D. P. Partlow, Thirty-seven layer optical filter from polymerized sol-gel solution, Applied Optics, 1 april 1990, p1527-1529.

[8] D. S. Hinczewski, Optical filters from SiO_2 and TiO_2 multi-layers using sol-gel spin coating method, Solar Energy Materials & Solar Cells, 87, 2005, p181-196.

[9] P. van Zant, Microchip fabrication, 4th Ed., 2000, p363-366.

[10] M.C. Costello, Diamond protective coatings for optical components, Diamond and Related Materials, Vol. 3, June 1994, p1137-1141.

[11] D. M. Hoffman, Handbook of vacuum science, 1998, p17-21.

[12] Mattox, Handbook of physical vapor deposition (PVD) processing, 1998, p116.

[13] E. Ritter, Dielectric film materials for optical applications, Physics of thin films, 8, 1975, p1-49.

[14] R. R Willey, Practical design and production of optical thin films, 2nd Ed., 2002, p167-170.

[15] Mattox, Handbook of physical vapor deposition (PVD) processing, 1998, p273-275.

[16] A. Macleod, Thin-film optical filters, 3rd Ed., 2003, p500-509.

[17] S. Mohan, A review of ion beam assisted deposition of optical thin films, Vacuum, vol. 46, No. 7, 1995, p645-659.

[18] P. van Zant, Microchip fabrication, 4th Ed., 2000, p193-199.

[19] G. Angel, Handbok i kemisk teknologi, vol. III, 1948, p481-484.

[20] W. M. Moreau, Semiconductor lithography, 1988, p29-35.

[21] Fujifilm, Material safety data sheet, Product No. 800357, Product name OIR 980-35.

[22] P. van Zant, Microchip fabrication, 4th Ed., 2000, p217-221.

[23] G. A. Luurtsema, Spin coating for rectangular substrates, Thesis in Master of Science, Berkley, 1997, p12-16.

[24] W. M. Moreau, Semiconductor lithography, 1988, p289-291.

[25] W. M. Moreau, Semiconductor lithography, 1988, p647.

[26] Shipley, Microposit S1800 series photoresists, product sheet.

[27] P. van Zant, Microchip fabrication. 4th Ed., 2000, p246.

[28] A. J. Bard, Electrochemical methods, 2nd Ed., 2001, p148-149 and p169.

[29] W. M. Moreau, Semiconductor lithography, 1988, p690-698.

[30] G. Fortufio, Study of reactive ion etching of Si and SiO_2 for CF_XCl_{4-X} Gases, Plasma chemistry and plasma processing, vol. 8, No. 1, 1988, p19-34.

[31] M. Rymenans, Discussions, Belgium.

[32] W. M Moreau, Semiconductor lithography, 1988, p672.

[33] Maeda, Method of etching films of silicon nitride and silicon dioxide, US Pat. No. 3979241, 1976.

[34] A. Matsutani, Microfabrication of dielectric multilayer reflector by reactive ion etching and characterization of induced wafer damage, Jap. J. of Appl. Phys., Vol 30, 1991, p482-429.

[35] G. Hägg, Allmän och oorganisk kemi, 6th Ed, 1973, p659.

[36] Chromium etching, Product information, Michrochemicals GmbH, 2009, p12-15.

[37] T. Chen, Anion effects on the electrochemical regeneration of Ce(IV) in nitric acid used for etching chromium, Journal of Hazardous Materials, 152, 2008, p922–928.

[38] W. M. Moreau, Semiconductor lithography, 1988, p647-649.

[39] G. A. C. M. Spierings, Wet chemical etching of silicates in hydrofluoric acid based solutions, J. of Mat. Sci. 28, 1993, p6261-6273.

[40] T.N.M. BERNARDS, Characterisation of Sol-Gel TiO_2 Films by Etching, Journal of Sol-Gel Sci. and Tech. 10, 1997, p193-202.

[41] Z. F. Zhong, Alkaline resistant negative photoresist for silicon wet etch without silicon nitride. US pat. No. US2008/0261145 A1.

[42] CRC handbook of Chemistry and physics, 67th Ed., pB-140.

[43] Peter Leisner, Discussions, Jönköping, Sweden.

[44] J. Been, Titanium corrosion in alkaline hydrogen peroxide, Corrosion, Vol. 56, No. 8, 2000, p809-818.

[45] E. Ruiz, Titanium corrosion in alkaline hydrogen peroxide bleaching environments, 2nd Mercosur congress on chemical engineering.

[46] A. Kossoy, Chemical reduction and wet etching of CeO_2 thin films, Journal of the electrochemical society, 152 (2), 2005, pC65-C66.

[47] J. Meiler, Laser-induced photochemical etching of InP by HBr and HCI, Applied Surface Science, 43, 1989, p416-423.

[48] Douglas, Anisotropic niobium pentoxide etch, US Pat. No. 5201989, 1993.

[49] E. Rodrigue, Electrochemical etching of quartz, IEEE Ultrasonics Symposium, 2007, p2586-2589.

[50] K. Williams, Etch rates for micromachining processing, J. of Microelectromecanical systems, Vol. 5, No. 4, 1996, p256-269.

[51] A. Bard, Encyclopaedia of Electrochemistry: Corrosion and oxide films, Vol. 4, p16-22.

[52] Sample dispersion & refractive index guide, Malvern Instruments Ltd, MAN0079, Version 3, 1997.

[53] A. Mallick, Preparation and properties of manganese dioxide thin films for applications in selective surfaces, SPIE, Vol. 1727, 1992, p380-391.

[54] Maissel, Handbook of thin film technology, 1970, p11-8 to 11-10.

[55] P. van Zant, Microchip fabrication. 4th Ed., 2000, p439-440.

[56] W. M. Moreau, Semiconductor lithography, 1988, p686.

[57] Chao-Tsang, Optical and Mechanical Property changes in Thin-Film Filters with Post Deposition Thermal Treatment, Jap. J. of Appl. Phys., Vol. 45, No 3A, 2006, p1783-1787.

[58] Maissel, Handbook of thin film technology, 1970, p12-22 to 12-24.

[59] A. Elshabini-Riad, Thin film technology handbook, 1998, p8-34.

[60] K. B. Sundaram, Wet etching studies of silicon nitride thin films deposited by electron cyclotron resonance (ECR) plasma enhanced chemical vapor deposition, Microelectronic Engineering, 70, 2003, p109-114.

[61] R. R. Willey, Practical design and production of optical thin films, 2nd Ed., 2002, p227.

[62] G. Abromavicius, Improvement of optical properties and radiation resistance of optical coatings based on Nb_2O_3 and Ta_2O_5, Proc. of SPIE, Vol 6596, 65961O, 2007.

[63] A. P. Bradford, Optical properties of evaporated magnesium oxide films in the 0.22-8-u wavelength region, Applied Optics, Vol. 11, No 10, 1972, p2242-2244.

[64] R. R. Willey, Practical design and production of optical thin films, 2nd Ed., 2002, p274.

[65] H. K. Pulker, Characterization of optical thin films, Applied Optics, Vol 18, No. 12, 1979, p1969-1977.

[66] G. Hägg, Allmän och oorganisk kemi, 6th Ed., 1973, p624.

[67] A. Macleod, Thin-film optical filters, 3rd Ed., 2003, p622.

[68] R. R Willey, Practical design and production of optical thin films, 2nd Ed., 2002, p286

[69] G. Hass, Reflectance and durability of Ag mirrors coated with thin layers of Al_2O_3 plus reactively deposited silicon dioxide, Applied Optics, Vol. 14, No. 11, 1975, p2639-2644.

[70] J. Vossen, Thin film processes, 1978, p435.

[71] E. R. Johnson, Further spectral observations of grenade glow clouds in the lower thermosphere, Aust. J. Phys., 20, 1967, p577-582.

[72] H. Selhofer, Properties of titanium dioxide films prepared by reactive electron-beam evaporation from various starting materials, Applied Optics, Vol. 41, No 4, 2002, p756-762.

[73] R. R. Willey, Practical design and production of optical thin films, 2nd Ed., 2002, p264-271.

[74] G. Hägg, Allmän och oorganisk kemi, 6th Ed., 1973, p648.

[75] D. W.A. Sharp, Miall´s dictionary of chemistry, 5th Ed., 1981, p464.

[76] N. Andersson, Emmision spectra of TiH and TiD near 938nm, Journal of chemical physics, Vol. 118, No. 8, 2003, p3543-3548.

[77] M. Ahmed, Syntheses and crystal structure of titanium oxide sulfates, Acta Chemica Scandinavia, 50, 1996, p275-283.

[78] S. Norasetthekul, Dry etch chemistries for TiO_2 thin film, Applied surface science, 185, 2001, p27-33.

[79] Cerac incorporated, Zirconium oxide, ZrO_2, for optical coatings, 2007.

[80] Q. Xiao, Y_2O_3 stabilized ZrO_2 thin films deposited by electron-beam evaporation, Vacuum, 83, 2009, p366-371.

[81] V. Lowalekar, Etching of zirconium oxide, hafnium oxide and hafnium silicates in diluted acid solutions, J. Mater. Res. Vol. 19, No. 4, 2004, p1149-1155.

[82] R. Winston, Corrosion and corrosion science, p436.

[83] Cerac incorporated, hafnium oxide, HfO_2, for optical coatings, 2007.

[84] R. R. Willey, Practical design and production of optical thin films, 2nd Ed. 2002, p282-283.

[85] D.W.A. Sharp, Miall´s dictionary of chemistry, 5th Ed, 1981, p499.

[86] CRC handbook of Chemistry and physics, 67th Ed, pB-143.

[87] R. R. Willey, Practical design and production of optical thin films, 2nd Ed. 2002, p258-263.

[88] Cerac incorporated, silicon dioxide, SiO_2, for optical coatings, 2007.

[89] R. Chow, Silicon dioxide and hafnium dioxide evaporation characteristics from a high-frequency sweep e-beam system, Applied optics, Vol. 35, No. 25, 1996, p5095-5101.

[90] G. Hägg, Allmän och oorganisk kemi, 6th Ed, 1973, p572-581.

[91] K. Williams, Etch rates for micromachining processing-part II, J. of Microelectromecanical systems, Vol. 12, No. 6, 2003, p761-778.

[92] Rimstidt, Quartz solubility at low temperatures, Geochimica et cosmochimica Acta, Vol. 61, No. 13, 1997, p2553-2558.

[93] R. R. Willey, Practical design and production of optical thin films, 2nd Ed., 2002, p271-273.

[94] CRC handbook of Chemistry and physics, 67th Ed., pB-105.

7 Attachments

7.1 Evaporation properties

date (2008)		P_{O2} /mbar	T_S /°C	S_{EVAP} Å/s	Liner	Monitor λ/nm	T_W /QWOT	Notes
29-okt	T1	3*10-4	325	1.5-2	Mo	550	9	
30-okt	S1	3*10-4	325	4.00	Non	550	9	Al-layer 1Å/s
30-okt	S2	3*10-4	325	4.00	Non	550	9	Al-layer 5-6Å/s
06-nov	Z1	3*10-4	325	2.00	graphite	550	9	heavy caving burned in liner
07-nov	Y1	1x10-4	325	2.00	Non	550	7	nice bahaviour
10-nov	H1	1x10-4	325	4.00	Non	550	5	slight spitting
10-nov	A1	1.5*10-4	325	3.00	Non	550	8	Stable
12-nov	M1	1*10-4	325	3.00	Non	550	7	very stable
12-nov	MF1	0	325	4.0-6	Ta	550	5	Thermal
12-nov	Z2	2*10-4	325	1.0-2	graphite	550	4	cave in, slight burn in liner

Table A1. *Evaporation properties for the first series of thin films;* P_{O2} *was the oxygen back pressure,* T_S *substrate temperature,* T_W *QWOT quarter wave optical thickness of the witness plate,* S_{EVAP} *evaporation rate.*

7.2 Curve matching of thin films

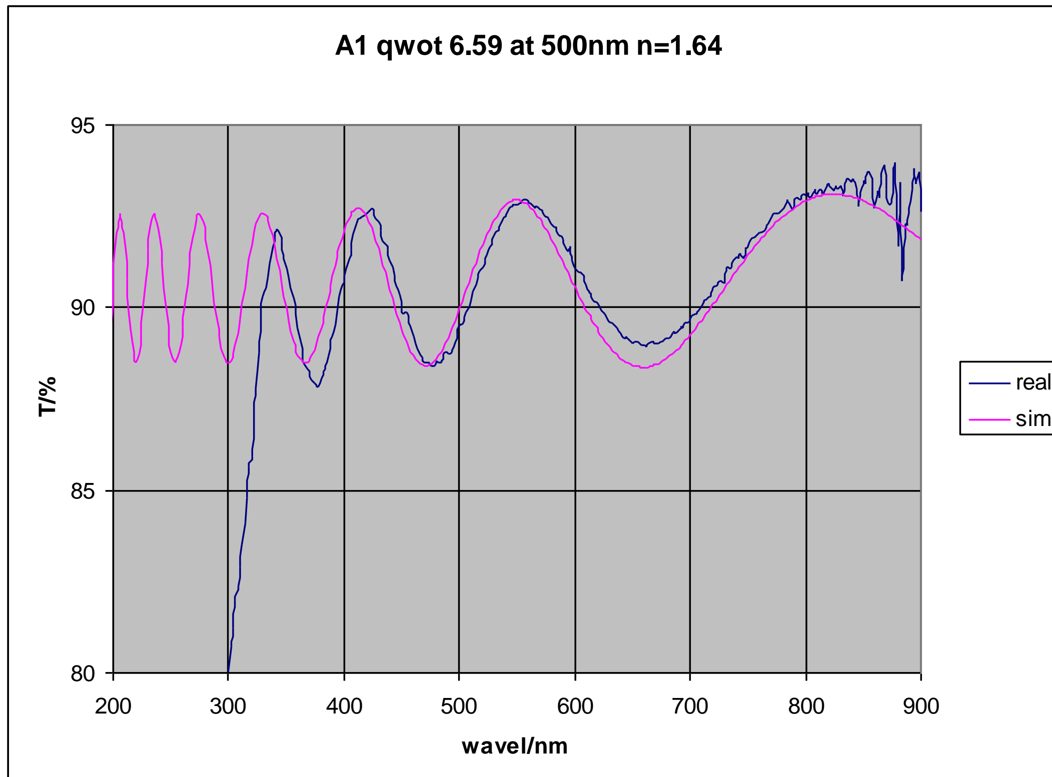

Figure A1. *A1 best fit.*

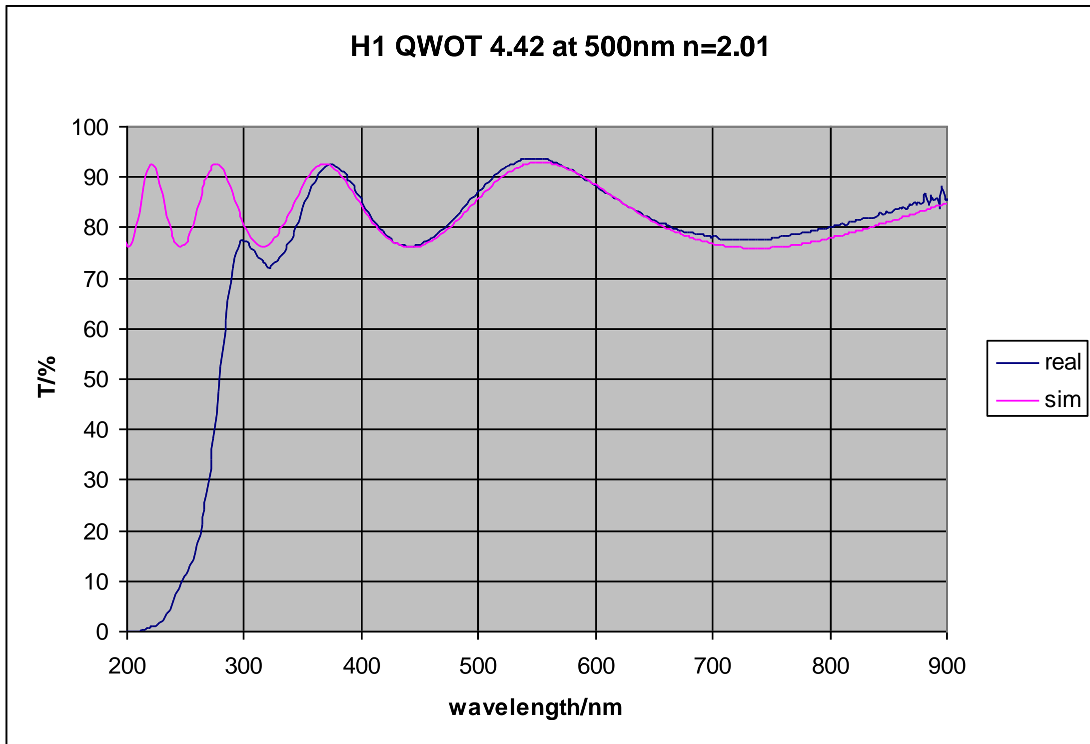

Figure A2. *H1 best fit.*

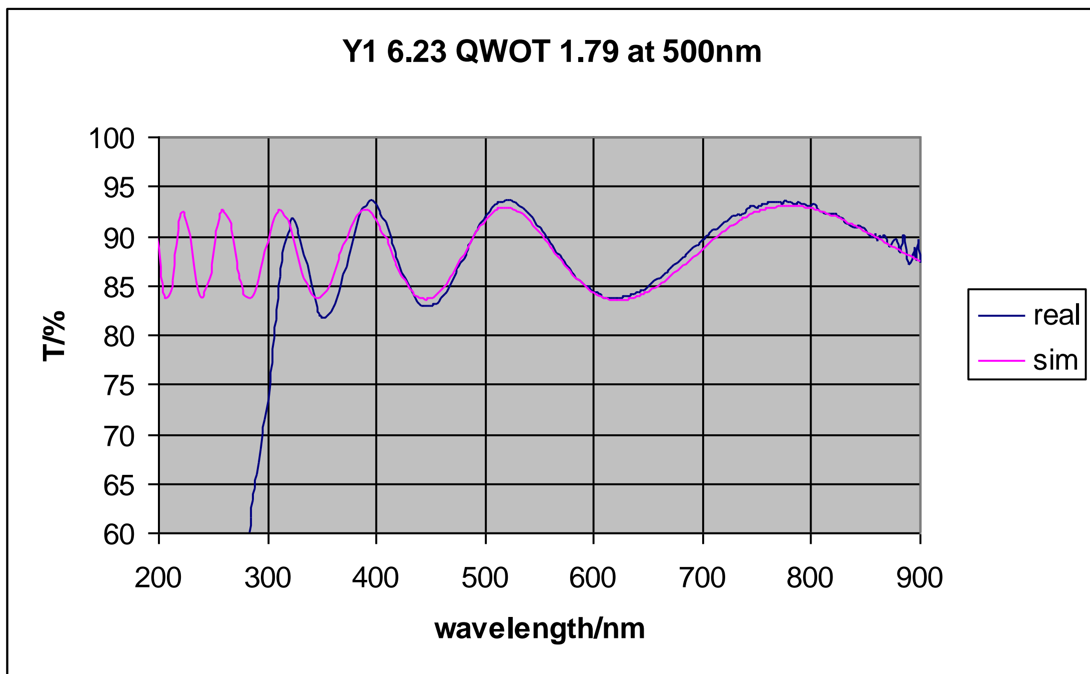

Figure A3. *Y1 best fit.*

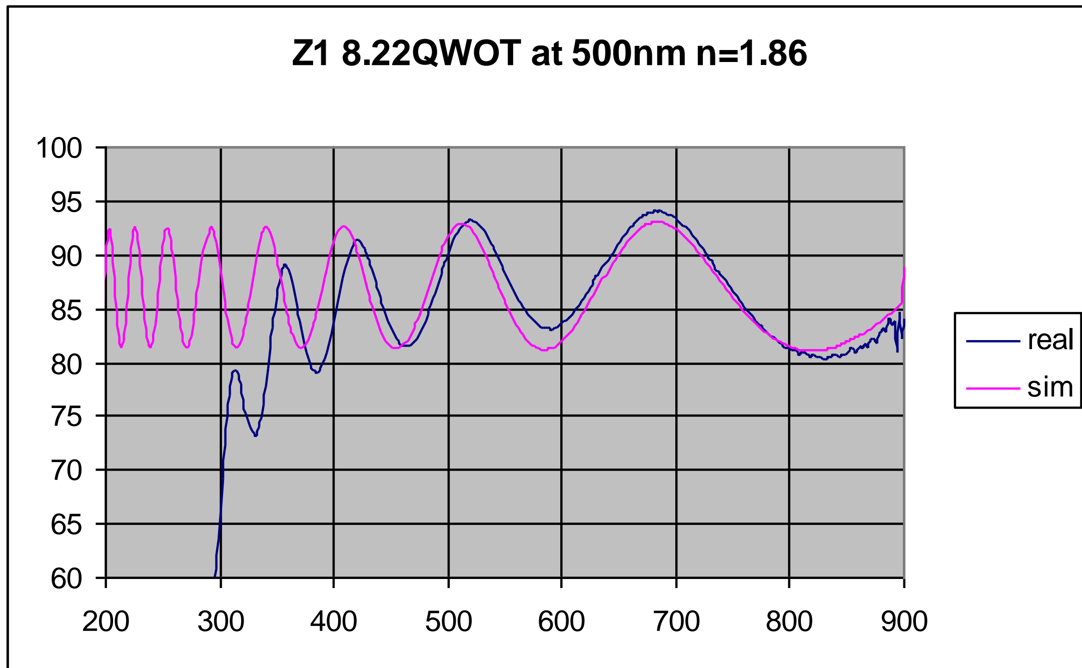

Figure A4. *Z1 best fit.*

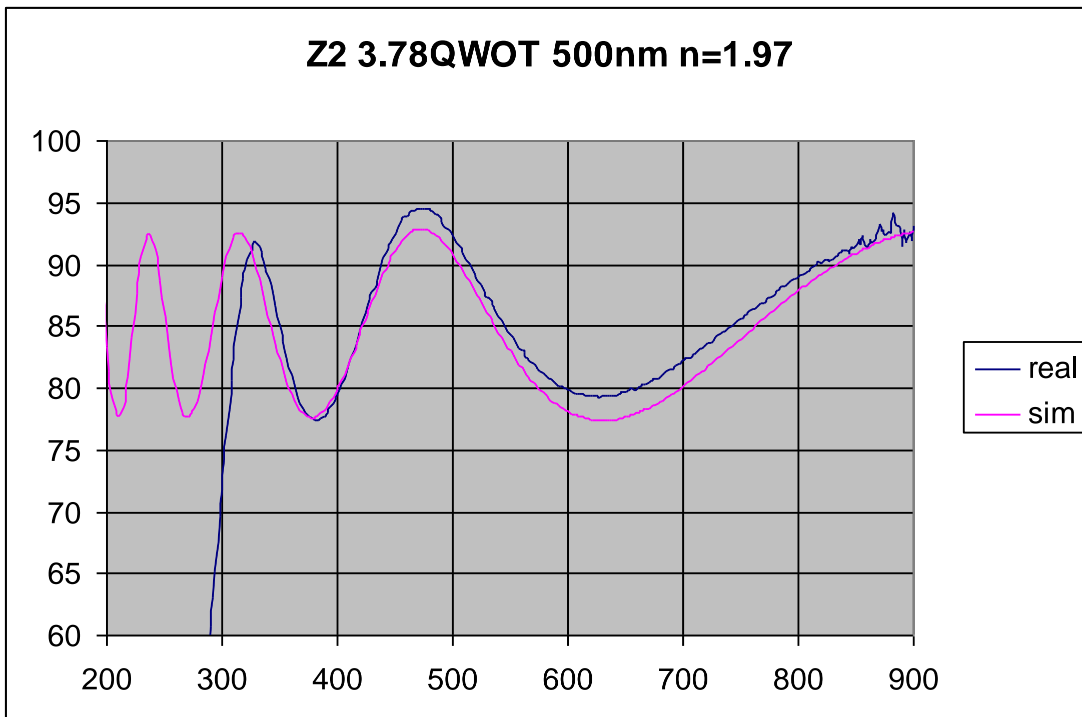

Figure A5. *Z2 best fit.*

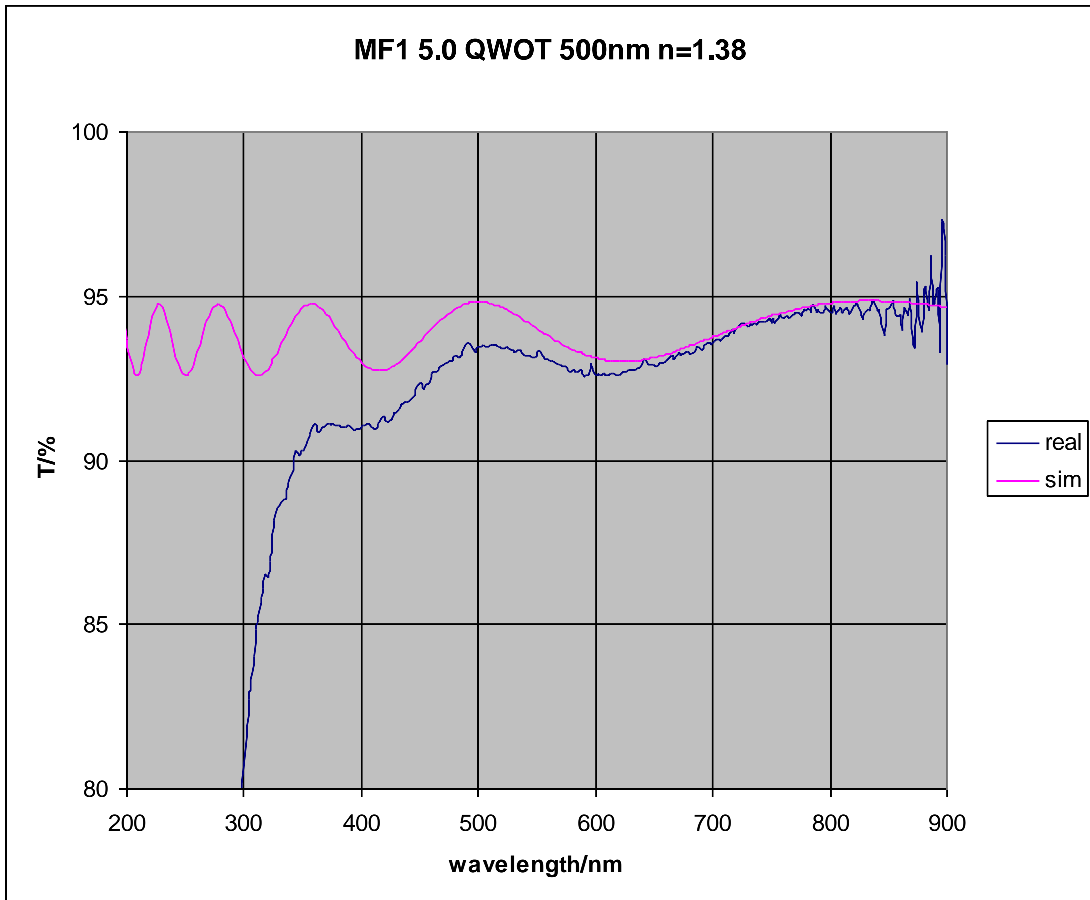

Figure A6. *MF1 best fit.*

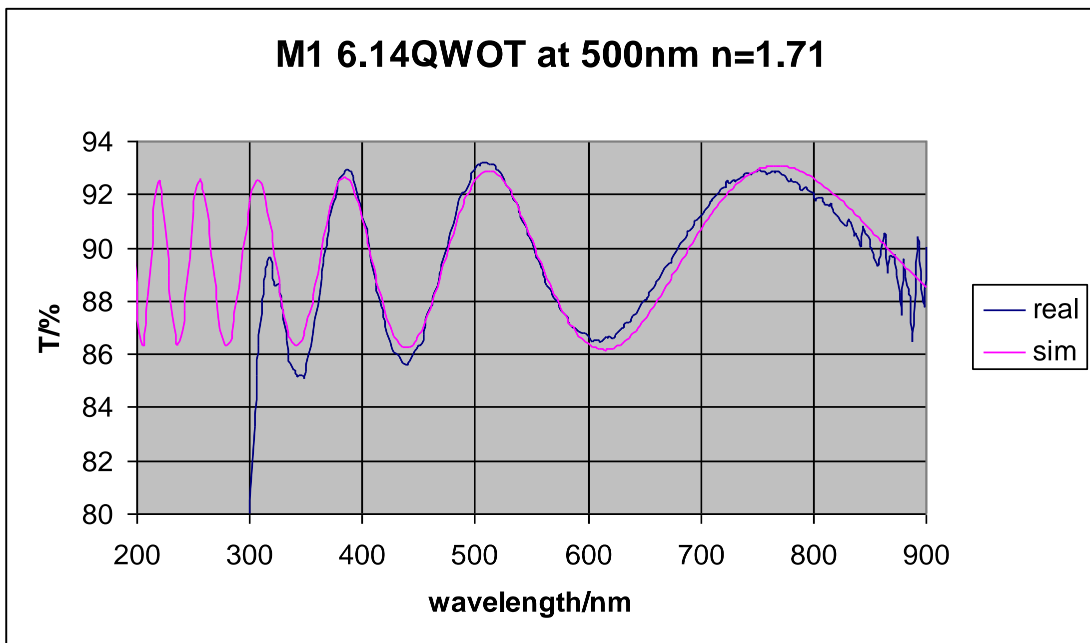

Figure A7. *M1 best fit.*

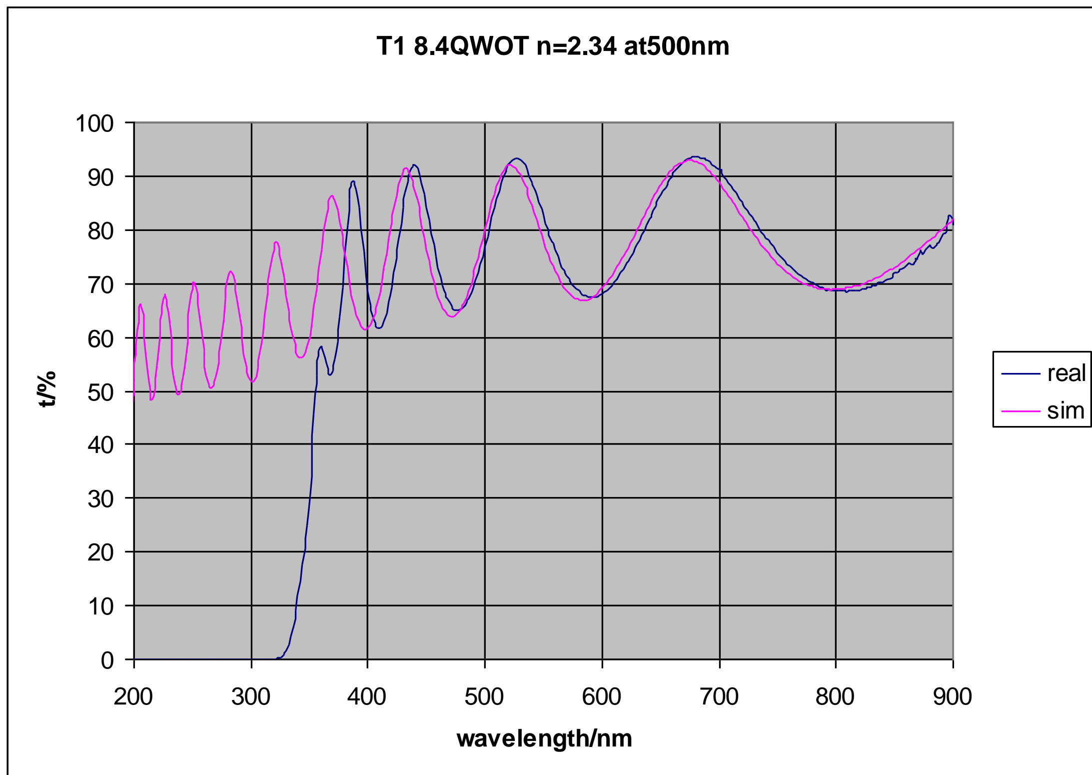

Figure A8. *T1 best fit.*

Figure A9. *S1 best fit.*

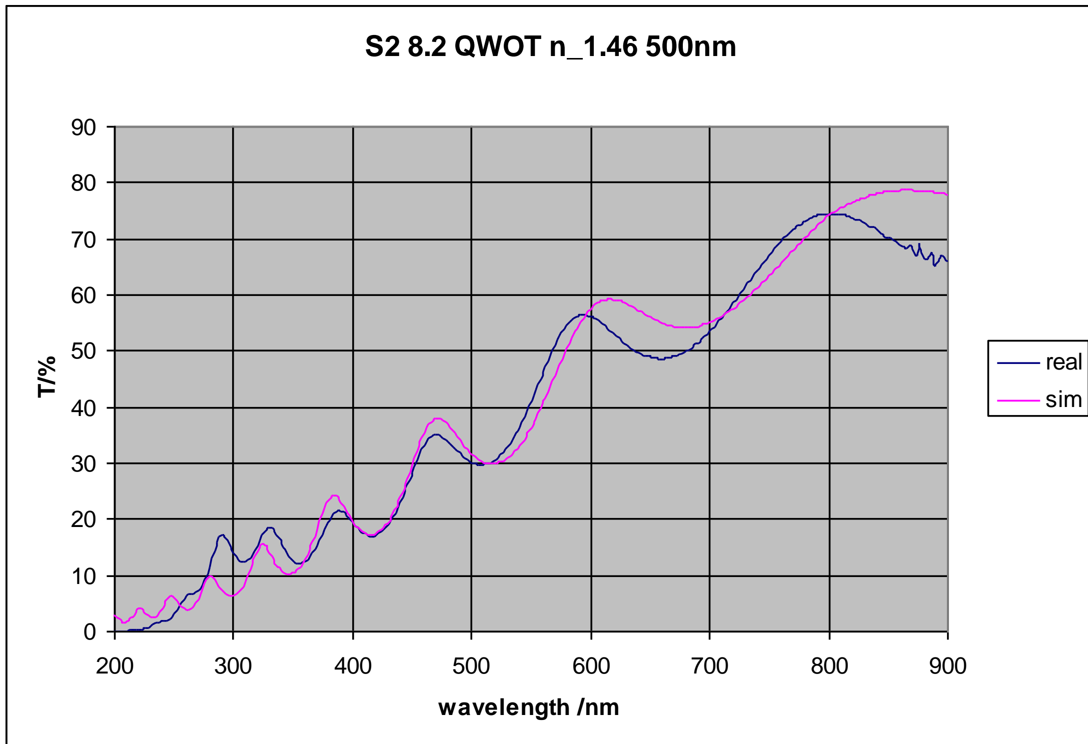

Figure A10 *S2 best fit.*

7.3 Solutions

Concentrations of some used chemicals:

HF titration with NaOH gave 23.92 M or 47.8%.

Note: in cases where 3% HF was used the calibrated value should be 3.6% but the difference is small and has little effect on the result. In all cases the same dilution was used.

H_2O_2 concentration was 10.137 M or 34.5% determined by permanganate titration.

NH_3 titration with 0.1M HCl gave concentration of. 12.38 M.

BHF was a pre-made mixture with 10 volume parts NH_4OH (40%) and 1 volume part HF (49%).